Microfluidic Columns with Nanotechnology-Enabled Stationary Phases for Gas Chromatography

HAMZA SHAKEEL

Dissertation submitted to the Faculty of the Virginia Polytechnic Institute and State University in partial fulfillment of the requirement for the degree of

Doctor of Philosophy

In

Electrical Engineering

Masoud Agah, Chair

Gary W. Rice

John R. Morris

Mantu K. Hudait

Scott M. Bailey

January 29, 2015

Blacksburg, Virginia

Keywords: micro gas chromatography, separation columns, stationary phases, nanoparticles, MEMS columns

Microfluidic Columns with Nanotechnology-Enabled Stationary Phases for Gas Chromatography

HAMZA SHAKEEL

Abstract

Advances in micro-electro-mechanical-systems (MEMS) along with nanotechnology based methods have enabled the miniaturization of analytical chemistry instrumentation. The broader aim is to provide a portable, low-cost, and low-power platform for the real-time detection and identification of organic compounds in a wide variety of applications. A benchtop gas chromatography (GC) system is considered a gold standard for chemical analysis by analytical chemists. Similarly, miniaturization of key GC components (preconcentrator, separation column, detector, and pumps) using micro- and nanotechnology based techniques is an on-going research field. This dissertation specifically deals with the design, fabrication, coating, and chromatographic testing of microfabricated separation columns for GC. This work can be broadly categorized into three research areas: design and development of new column designs, introduction of new stationary phases and the development of novel fabrication methodologies for integrating functionalized thin-film into microchannels for chromatographic separations. As a part of this research, two high performance new micro column designs namely width-modulated and high-density semi-packed columns are introduced for the first time. Similarly, two new types of functionalized stationary phases are also demonstrated i.e. a highly stable and homogenous silica nanoparticles coating deposited using a layer-by-layer self-assembly scheme and a highly conformal functionalized thin aluminum oxide film deposited using atomic layer deposition. Moreover, novel thin-film patterning methods using different microfabrication technologies are also demonstrated for high-aspect ratio multicapillary and semi-packed columns.

Preface

The journey of my PhD research started in January, 2011 as a collaborative effort between VTMEMS lab and research groups from the Department of Physics, Virginia Tech and the Department of Chemistry, College of William and Mary. During the course of these four years, I have gained a breadth of knowledge in various research fields. The level of experience that I take with me will be invaluable to me throughout my future career. First of all this work could not have been possible without the support, guidance and mentorship of my PhD adviser Dr Masoud Agah (Associate Professor, Electrical and Computer Engineering Department, Virginia Tech). Dr Agah did not only provide me with a great research opportunity but also gave me the resources and liberty to explore new research avenues. I also appreciate the guidance and technical feedback provided by Dr Gary Rice (Associate Professor and Dean of the Department Chemistry College of William and Mary, Williamsburg) and Dr Randy Heflin (Professor of the Department of Physics and Associate Dean Research, Virginia Tech). Moreover, I am also grateful to Dr John Morris (Professor, Department of Chemistry, Virginia Tech) for giving me the opportunity to work on challenging problems during the summer of 2014. I wish to express my warmest graditude to all of my PhD advisory committee members including Dr Masoud Agah, Dr Gary Rice, Dr John Morris, Dr Mantu Hudait (Associate Professor of the Electrical and Computer Engineering Department, Virginia Tech) and Dr Scott Bailey (Associate Professor of the Electrical and Computer Engineering Department, Virginia Tech) for their invaluable feedback.

Additionally, I would like to thank both current and former members of the VTMEMS lab, Mr. Muhammad Akbar, Dr Shree Narayanan (Intel), Mr. Apoorva Garg (Bloomberg), Mr. Michael Restaino, Dr. Phillip Zellner (Deparment of Defense), Mr. Alperen Ketene (Boeing), Mr. Yahya Hosseini, Mr. Mohammad Mehdi Alemi, Mr. Hesam Babahosseini, Ms. Sarah El-Helw, Ms. Vaishnavi Srinivasaraghavan, Ms. Diana Nakidde and Mr. Yahya Hosseini. I also wish to express my gratitude to Dr Dong Wang (currently a Postdoctoral Researcher at Virginia Tech), coauthor in two of my publications, for his great work.

Moreover, I am also grateful for the funding and grants provided by the National Science Foundation (NSF), the National Institute of Occupational Safety and Health (NIOSH), and the Institute of Critical Technology and Applied Science (ICTAS) at Virginia Tech.

I want to specially thank my amazing and beautiful wife Zara for her support and help during my PhD. I also want to acknowledge the continuous support of my parents, father-in-law, mother-in-law, my sisters and my brother-in-laws (Zane and Zakee). Last but not least, I want to thank my friends Dr Waseem

Ansar Malik, Mr. Tamoor Gandapur, Mr. Awais Khawar, Mr Shafiq Ur Rahman and Mr. Syed Ali Raza Zaidi.

This work resulted in a number of important contributions in the field of micro gas chromatography but there is so much more to explore. I wish the best of luck to all the incoming students who will be working on a challenging project to develop a handheld gas chromatography analyzer in the near future.

Hamza Shakeel

January 2015

Dedicated to my family, friends and students in Pakistan

Table of Contents

List of Figures

List of Tables

Abbreviations and Symbols

$\boldsymbol{A}$	eddy diffusion
$\boldsymbol{a}$	the front part of peak width and measured at 5% of the height for tailing factor (T_f).
AFM	atomic force microscope
ALD	atomic layer deposition
$\boldsymbol{B}$	longitudinal diffusion in mobile phase
$\boldsymbol{b}$	the back part of peak width and measured at 5% of the height for tailing factor (T_f).
BHF	buffered hydrofluoric acid
BLs	Bilayers
$\boldsymbol{C}$	mass transfer in and out of stationary phase
$\boldsymbol{C_M}$	resistance due to mass transfer in mobile phase
$\boldsymbol{C_S}$	resistance due to mass transfer in stationary phase
CNTs	carbon nanotubes
CVD	chemical vapor deposition
DDSP	double doped self-patterned
$\boldsymbol{d_f}$	average stationary phase thickness
$\boldsymbol{D_G}$	diffusion coefficient of solute in mobile
$\boldsymbol{D_S}$	diffusion coefficient of solute in stationary phases
DRIE	deep reactive ion etching
DI	deionized
DMMP	dimethyl methyl phosphate
$\lvert\Delta_r \boldsymbol{H^\theta}\rvert$	standard adsorption heat
EDP	ethylenediamine pyrocatechol
FID	flame ionization detector
$\boldsymbol{f_1}$	Giddings-Golay gas compression coefficients
$\boldsymbol{f_2}$	Martin-James gas compression coefficients
GC	gas chromatography
GLC	gas liquid chromatography
GNPs	gold nanoparticles
GSC	gas solid chromatography
HAR	high aspect ratio

HCl	hydrochloric acid
H or HETP	height-equivalent-to-a-theoretical-plate
H_{eff}	effective height-equivalent-to-a-theoretical-plate
$\overline{HETP}$	local plate height
HDSPC	high density semi-packed column
HMDS	hexamethyldisilizane
HPLC	high performance liquid chromatography
IC	integrated circuit
IL	ionic liquid
k or k'	retention or capacity factor
k_0	k_0 is the compound retention factor in a capillary with average cross-sectional area of $h_0 \times w_0$.
KOH	potassium hydroxide
L	length of the column
LbL	layer-by-layer
LVC	linearly-variable column
MA	mask aligner
MEMS	micro-electro-mechanical system
MPG	monolayer-protected-gold
μGC	micro gas chromatography
μMCC	micro multicapillary column
μSC	micro separation column
μTAS	micro total analysis system
μWMC	micro width modulated column
N	plate number
NaOH	sodium hydroxide
N_{eff}	effective plate number
ODTS	octadecyltrichlorosilane
OT	open tubular
OV1™	polydimethylsiloxane polymer
PAH	polycation polyallylamine hydrochloride
PDMS	dimethyl polysiloxane
PECVD	plasma-enhanced chemical vapor deposition

PR	photoresist
PVD	physical vapor deposition
r_C	internal column diameter
RIE	reactive ion etching
R_S	peak-to-peak resolution
SDSP	single-doped self-patterned
SEM	scanning electron microscope
SCC	single capillary column
SGC	step-gradient column
SPC	semi-packed column
SNPs	silica nanoparticles
$\left(\frac{\sigma_h}{h_0}\right)^2$	$(\sigma_h/h_0)^2$ represent the cross-sectional height deviations normalized by the average height.
$\left(\frac{\sigma_w}{w_0}\right)^2$	$(\sigma_w/w_0)^2$ cross-sectional width deviations normalized by the average width.
σ_0^2	peak variance of a single capillary
TMA	trimethylaluminum
TMAH	tetra methyl ammonium hydroxide
T_f	tailing factor
t_M	dead or hold-up time
t_r	retention time
t_{ri}	retention time of compound *i*
TCD	thermal conductivity detector
TZ	Trenzahl number
UV	ultra violet
$\bar{u}$	linear carrier gas velocity
u_0	average linear gas velocity
w_{ri}	peak width at base of compounds *i*
$w_{1/2}$	peak-width at half height

CHAPTER 1: Introduction

(Part of this chapter will appear as a book chapter "Chip Based GC", in Volume 3 Gas Chromatography, Sub- and Supercritical Chromatography, Chromatography, Wiley VCH, Editors: Jared l. Anderson, Verónica Pino)

I. Gas Chromatography

Gas chromatography (GC) is considered to be a mainstay for chemical analysis of volatile or semi-volatile organic mixtures. The applications of GC for chemical analysis has been increasing ever since its inception and includes the pharmaceutical industry, environmental monitoring, petrochemical analysis, biomedical and food processing.

A typical GC system consists of five main components: 1) carrier gas, 2) preconcentrator, 3) separation column, 4) detector, and 5) data analysis system as shown in Figure 1.1. The carrier gas (mobile phase) is a high purity gas (air, helium, nitrogen or hydrogen) that is used to transport gas mixture into the preconcentrator, separation column and detector. A preconcentrator unit is employed for increasing the detection limit of a GC system. A preconcentrator is a sample collection and concentration stage, it collects and thermally desorbs the sample as a concentrated narrow pulse. Subsequently, this concentrated peak is injected into the next stage for separation and identification purposes. A separation column, normally coated with a polymer (stationary phase), is considered to be the most important building block for the GC system, since it physically separates the constituents of a mixture into individual components based on their relative vapor pressures and affinities for the stationary phase. Afterwards the sample and carrier gas pass through a detector (typically flame ionization detector or thermal conductivity detector) where it converts a chemical signal into an equivalent analog electrical

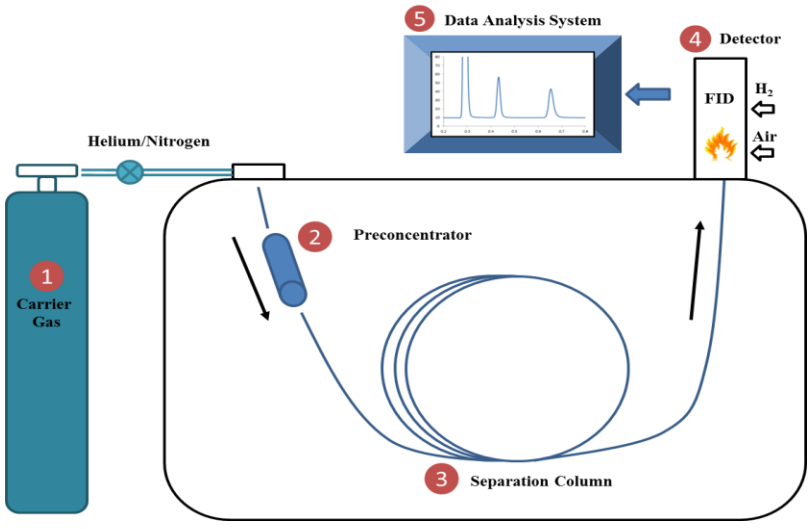

Figure 1.1: *Schematics of a typical conventional GC System*

output. Following signal conditioning circuitry, the signal is fed to a data analysis system. The data analysis system plots the detector response (y-axis) versus time (x-axis) on a graph known as a chromatogram. Typically each peak on the chromatogram corresponds to a separated compound in the sample mixture.

II. Separation Columns

Separation columns are considered to be an integral component of a GC system. Conventional separation columns are broadly categorized into three main types 1) packed columns, 2) open tubular columns, and 3) multicapillary columns (MCC) as shown in Figure 1.2. Initially GC columns were made from stainless steel, 1~5 m long with internal diameters between 1mm to 5mm [1], and packed with liquid coated solid-adsorbent particles (Figure 1.2 b). Although packed columns have high sample capacity but these columns suffer from low separation efficiencies and high pressure drops. Moreover, the metal surface is highly active and not suitable for analysis of polar compounds. Though, packed column are still preferred for trace analyses of gas samples and sample preparation. After the invention of inert fused silica based open tubular (OT) capillary columns (Figure 1.2 a) and highly sensitive detectors, the requirement for higher sample capacity is somewhat reduced and almost 90% of all GC analyses are now based on OT columns [1]. OT columns, affording longer column lengths (5 m~100 m) due to low

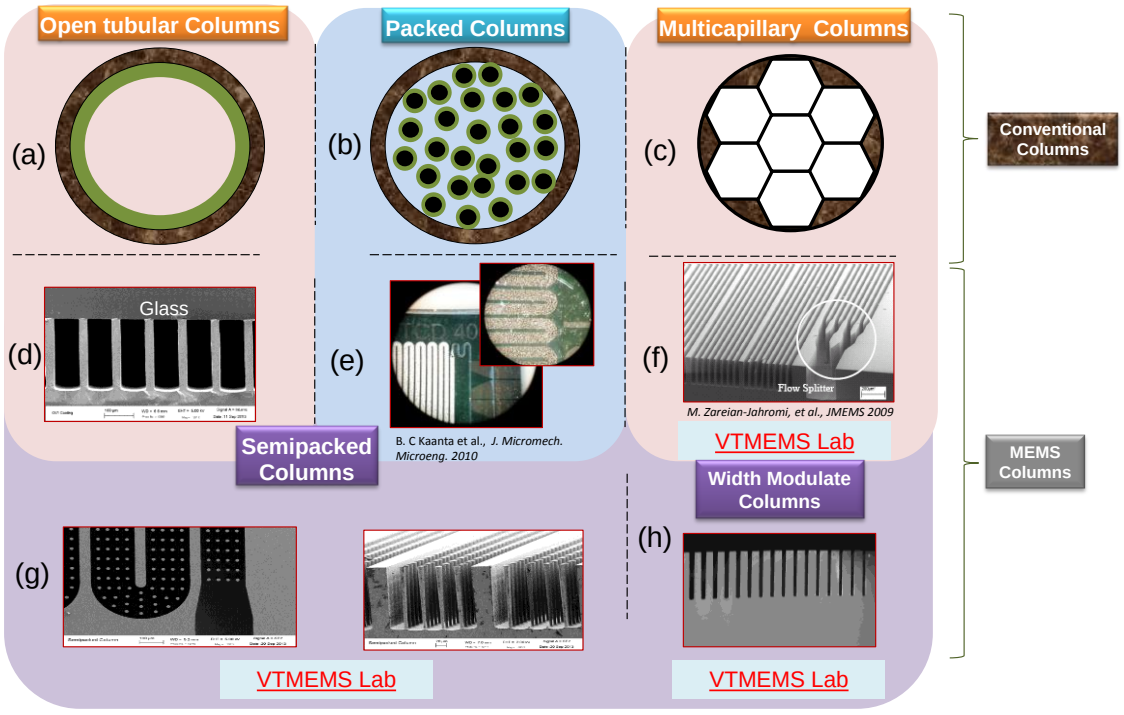

Figure 1.2: *Different types of conventional columns (a-c) and microfabricated columns (d-h).*

pressure drop requirements, have typically narrow diameters (0.1 mm~0.53 mm) and thin stationary phase films (typically 0.1~3 µm) uniformly coated on the column walls [1]. Additionally, OT columns provide narrow peaks leading to improvements in separation power and peak resolution. In order to realize the maximum separation performance, it is desirable to employ OT columns with very narrow internal diameters (5 µm to 50 µm). By reducing the internal diameter of single-bore OT columns, the sample capacity is reduced significantly and pressure drop also increases. In order to overcome these challenges MCC (Figure 1.2c), with a bundle of 1000~4000 parallel working capillaries (10 µm~40 µm I.D) having very short lengths (<0.5 m) [2, 3], were developed. With a higher cross-sectional area, the sample capacity of MCC is increased significantly compared to single-bore OT columns with similar channel dimensions. Additionally, with very narrow matched capillary diameters and a short column length of MCCs ensure fast chromatographic separations and provides higher separation efficiencies for a wide range of gas flow rates.

III. Stationary Phases

Gas chromatographic separations can be broadly categorized into two distinct types based on the stationary phase coating material. Chromatographic separations for columns coated with a liquid phase are termed as gas-liquid chromatography (GLC), while gas-solid chromatographic (GSC) columns have solid-adsorbent materials as a stationary phase.

A. Liquid Stationary Phases

Majority of capillary columns are coated with polymer based thin liquid stationary phases. Liquid stationary phases, with a range of polarities, present a wide spectrum for analytical applications. The main aim of the coating procedure is to get uniform, thermally stable and chemically selective phases. The liquid stationary phase coating of capillary columns consists of three main steps 1) surface treatment to deactivate active sites on the silica surface, 2) stationary phase coating and 3) cross-linking or chemical bonding to further improve the thermal stability of a liquid phase. Moreover, static and dynamic coating techniques are two of the most common methods utilized for coating columns.

1. Static Coating

In static coating method, the column is first filled with a known concentration of a polymer dissolved in a volatile solvent. One end of the column is sealed while vacuum pump is attached to the other end of the column. The solvent slowly evaporates when vacuum is turned on, leaving behind a known and uniform film thickness. In order to further improve the film quality the process is normally carried out at a constant temperature using water bath.

2. Dynamic Coating

The dynamic coating is a much simpler method compared to static coating. It is carried out by pushing a plug of known concentration of a polymer dissolved in a volatile solvent through the column at constant velocity using an inert gas supply. When the plug travels through the column length it leaves behind a very thin layer of polymer film. After dynamic coating, the column is continuously purged for around an hour to evaporate the residual solvent. The film thickness for this procedure is less controllable and non-uniform and normally a modified dynamic method is preferred.

B. **Gas-solid Stationary Phases**

The applications of GSC have been ever increasing due to its chemical selectivity and high thermal and chemical stabilities than those afforded by GLC. Solid-adsorbents can be employed either in a particulate form for adsorption based separations or act as a solid support-material for non-volatile liquid based phases. Alumina, silica gel and carbon [1] are the most common type of adsorbent materials employed for gas-solid separations. Moreover, the recent advancements in nanotechnology have also enabled the utilization of nontraditional adsorbents materials such as thiol-encapsulated gold nanoparticles [4], silica nanoparticles [5] and carbon nanotubes [6] for gas-solid separations.

IV. Column Efficiency

The quality of a column is normally quantified using parameters such as plate number (N) and plate height (H or HETP) [1]. The separation efficiency of a column for a certain compound is quantitatively expressed by the plate number and calculated directly from the chromatogram using equation (1.1)

$$N = 5.546 \times \left(\frac{t_r}{w_h}\right)^2 \qquad (1.1)$$

Where, t_r represents the retention time of a compound used as a probe and w_h stands for peak width calculated at half height. The column with higher N values has better efficiency and less peak band broadening. Moreover, the peak band-broadening is further characterized by height-equivalent-to-a-theoretical-plate (HETP) that takes into account the length (L) of the column (HETP=L/N). According to Van Deemter Equation [1], HETP is related to carrier gas velocity ($\bar{u}$) and given by

$$\mathrm{HETP} = \mathrm{A} + \frac{\mathrm{B}}{\bar{u}} + \mathrm{C}\bar{u} \qquad (1.2)$$

Where, A is eddy diffusion term resulting from multiple pathways encountered only in packed columns, B is longitudinal diffusion term in mobile phase and C represents mass transfer term in and out of stationary phase. Mass transfer term C is related to the diffusion of molecules perpendicular to the direction of flow. Since we want to minimize the band broadening (HETP), all A, B and C parameters

should also be as small as possible. In order to further analyze the effect of physical controllable parameters (film thickness, column diameter, carrier gas velocities and carrier gas choice) on peak band broadening, equation 1.2 is further expanded by Golay for OT columns [1].

$$\mathrm{HETP} = \frac{2D_G}{\bar{u}} + \left(\frac{2k\, d_f^2}{3(1+k^2)D_S} + \frac{(1+6k+11k^2) r_c^2}{24(1+k)^2 D_G} \right) \bar{u} \qquad (1.3)$$

Where, D_G and D_S represent the diffusion coefficient of solute in mobile and stationary phases respectively. Moreover, d_f is the average stationary phase thickness, r_C is the internal column diameter and k is the retention factor. It is clear from this equation that in order to minimize the band-broadening the columns with very narrow diameters and coated with very thin-films are desirable. Meanwhile, the stationary phase should be selected to provide large diffusion coefficient.

V. Micro Gas Chromatography (µGC)

Although a conventional GC system has numerous benefits but it is bulky, power-hungry and not suitable for field applications. Miniaturization of all three components and the GC system as a whole could enable a number of added advantages like low-power consumption, portability and real-time monitoring. The aim of miniaturizing analytical systems, such as GC, is to produce an integrated chip-based platform that provides all the required chemical analysis functions such as sampling, separation, detection, and subsequently identification. When this "micro total analysis system" (µTAS) platform is completely realized, it enables trace level analysis of the sample in a shorter time, significantly lowers the power consumption, offers higher throughput and portability, and reduces the use of reagents. Furthermore, a portable platform could open up new avenues for real-time and on-site monitoring of the analytes of interest.

The first true manifestation of a miniaturized analytical system for chemical analysis was developed in 1979 by Terry and colleagues [7]. This micro gas chromatograph (µGC), though ahead of its time, was realized by utilizing techniques (wet etching and photolithography) developed originally for an integrated circuit (IC) manufacturing. A brief overview of existing technologies is presented in the next section for readers who are unfamiliar with microfabrication technology.

VI. Microfabrication Techniques

The two most common substrate materials used in the development of µGC separation columns are silicon and glass. Some of the key features of single crystal silicon as a substrate material are its high thermal conductivity, mechanical rigidity, ready availability, and its ability to integrate electronic functionality into microfluidic devices. Similarly, optically transparent glass wafers normally used to seal silicon channels provide thermal insulation and chemical resistance. Although both silicon-silicon [8] and

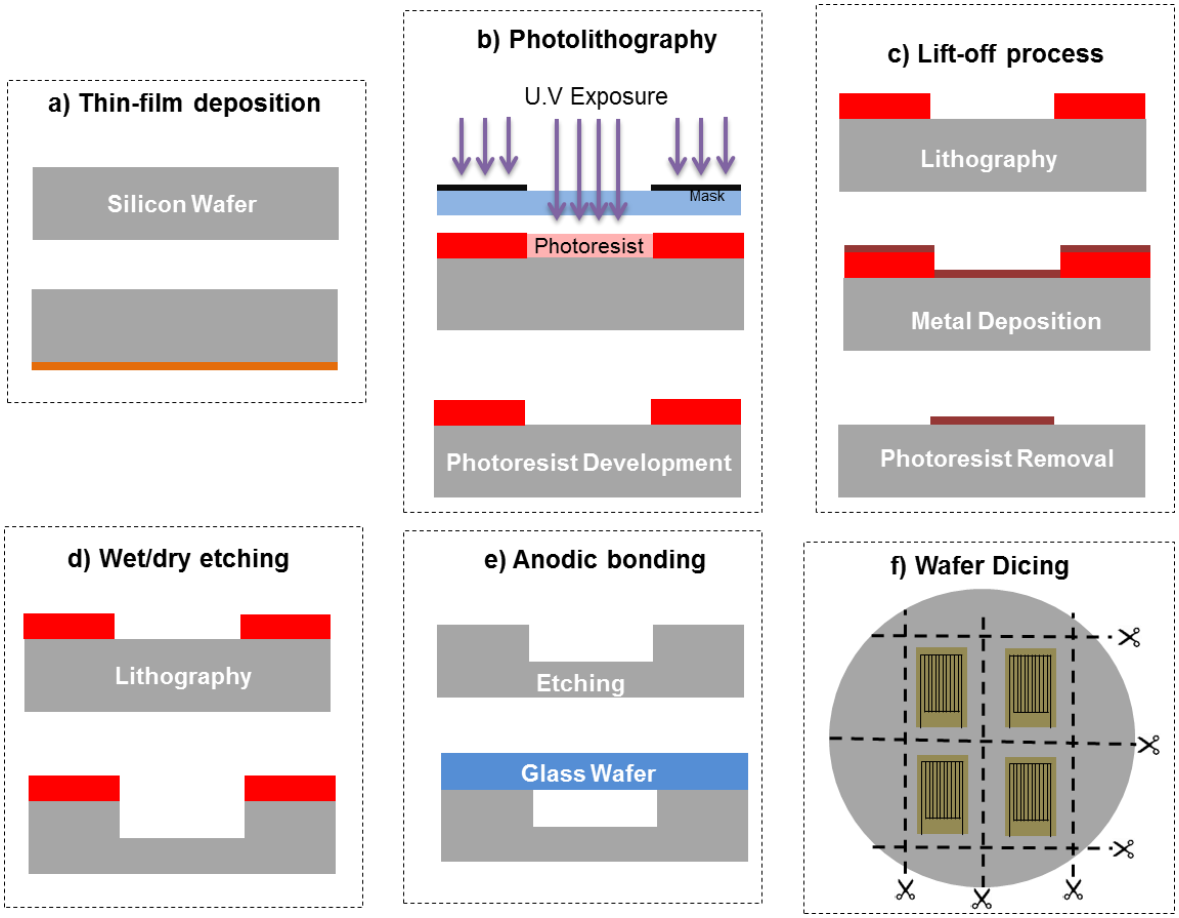

Figure 1.3: *Brief overview of most common microfabrication techniques used for producing µGC components.*

glass-glass [9] µGC components have been produced, the most common microfabrication methods of these devices involve silicon-glass combination.

Microfabrication technology can be broadly categorized into three main processes: 1) deposition, 2) patterning, and 3) selective etching of materials. Figure 1 represents the typical processing techniques utilized during the fabrication of silicon-glass micro devices. Microfabrication utilizes many techniques like oxidation, diffusion and thin-film deposition that were originally developed for IC domain. Thermal oxidation of a silicon surface, using either a dry or a wet technique, is normally performed at temperatures between 800 °C to 1200 °C and provides an insulating barrier. Furthermore, chemical vapor deposition (CVD) techniques are also used for dielectric film deposition at relatively low temperatures. These CVD methods involve plasma enhanced CVD, low pressure CVD and highly controllable atomic layer deposition [10]. Diffusion is the process of introducing dopants from Group III or Group V elements to silicon and is carried out at very high temperatures (>1000℃). For semiconductor industry, diffusion is used to make PN junctions for diodes and transistors, but for microfluidic applications, it can serve a

totally different purpose. For example, boron diffusion of silicon substrate at high concentrations is used as an etch stop for the realization of thin silicon membranes for sensing applications [11]. Similarly, phosphorous diffusion can be used for seedless metal deposition inside the etched silicon microchannels [12]. Different types of materials are deposited on to the substrate with varying thicknesses (Figure 1.3 a). This includes metal film deposition using both physical vapor (sputtering and electron-beam evaporation) and wet chemical deposition (electroplating). It is important to note that thin metal films are commonly used for on-chip resistive heaters and sensors elements while dielectric films are normally employed for providing an electrical isolation. Analogous to the IC industry, lithography is used to transfer the desired patterns from a mask onto an ultraviolet (UV) sensitive polymer (photoresist) spun on to the substrate (Figure 1.3 b). Lift-off process, as shown in Figure 1.3 c, is an additive metal patterning process that utilizes a sacrificial polymer (photoresist). The sacrificial photoresist layer is removed after the metal deposition to get the desired pattern on to the substrate. The development of micromachining techniques such as reactive ion etching (RIE) and especially deep reactive ion etching (DRIE) has revolutionized the microelectromechanical systems (MEMS) field in the last two decades [10]. The main purpose of DRIE is to achieve a highly anisotropic channel profile (Figure 1.3 d) exhibiting well-defined vertical-angles using either the Bosch or Cryogenic process [10]. Moreover, orientation dependent anisotropic etching of silicon could also be achieved using wet etching in potassium hydroxide (KOH), tetra methyl ammonium hydroxide (TMAH) and ethylenediamine pyrocatechol (EDP) [10]. A thick photoresist film can be utilized as a mask for very shallow etches but for deep etching a metal or a dielectric film is preferred as a hard mask. After anisotropic etching of the silicon wafer, the microchannel is sealed with a glass substrate using anodic bonding (Figure 1.3 e). Anodic bonding is typically done at a temperature between 200 ° C and 400 ° C and with an electrostatic voltage between 200 V and 1200 V [13]. Important things to consider during the selection of the glass substrate (Pyrex or Borosilicate) are the presence of sodium ions and the matching thermal expansion coefficients with a silicon wafer. After anodic bonding, the bonded-wafer is diced (Figure 1.3 f) into individual chips. In order to provide a chip-to-instrument interface for further analytical testing, capillary tubes are inserted into the inlet and outlet ports of each device.

VII. Micro GC: A Brief History

Advancements in microfabrication techniques especially bulk micromachining has enabled the miniaturization of transducers and analytical devices. The seminal work on miniaturized gas analysis systems, by Terry and Coworkers (Figure 1.4) [7, 14], utilized wet etching and standard photolithography techniques. Both the sample injection valve and the 1.5 m-long separation column (200 µm-wide and 30 µm-deep) were monolithically fabricated on a single silicon wafer. Thereafter, etched silicon channels were anodically bonded with a Pyrex wafer. The separation column was statically coated with a liquid

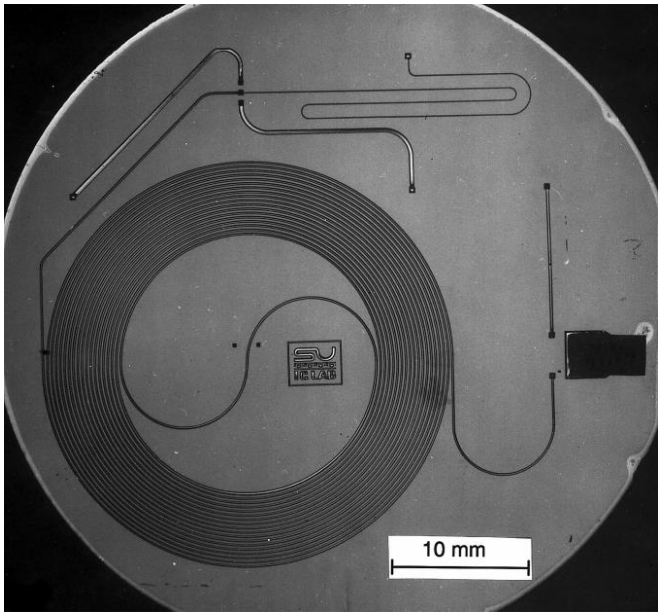

***Figure 1.4**: First miniaturized gas chromatograph system on a silicon substrate bonding with glass wafer (Reprinted with permission from A. d. Mello, Lab on a Chip, vol. 2, pp. 48N-54N, 2002. Copyright 2002, The Royal Society of Chemistry).*

stationary phase using OV-101. Meanwhile, a thermal conductivity detector (TCD) was separately batch fabricated using the standard IC processes. Although this hybrid µGC system was able to separate a simple hydrocarbon mixture in less than ten seconds, the resolving power of the first micromachined column was not comparable to a conventional capillary column of the time. The incorporation of a polymer based stationary phase into a sealed column produced a non-uniform film thickness especially at the corners and curves, resulting in a poor separation performance. Therefore, the main focus of µGC research has been towards the integration of novel and high-performing stationary phases into microchannels from the start.

Although Manz and colleagues realized the advantages of microfabricated system for analytical separations and started work on micro liquid chromatography columns in 1990 [15]. The research in µGC was revived later by Reston *et al.* in 1994 [16]. The spirally patterned rectangular-shaped separation column (0.9 m-long, 300 µm-wide and 10 µm-deep) and 10 µm-deep sample injection loop were microfabricated on a silicon wafer. In order to suppress the stationary phase condensation and non-uniformity, the authors utilized an evaporated copper phthalocyanin (0.2 µm) thin uniform film prior to bonding. Afterwards the deposited thin-film was selectively removed from the top channel surface using mechanical polishing followed by anodic bonding with a glass wafer. The authors also produced a TCD and chemiresistor-based sensors forming a dual detection mechanism. Although the coating method was limited by the channel depth, this hybrid µGC system was able to successfully separate ammonia and

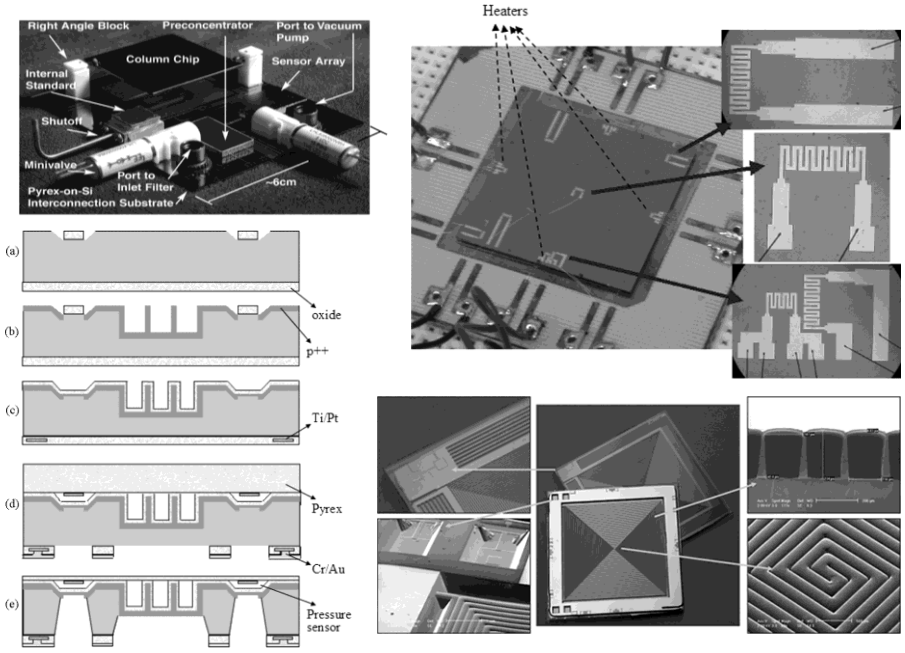

Figure 1.5: *First generation µGC system by WIMS2 center (top left). Process flow (bottom left) for fabrication of microcolumns with on-chip heaters, thermistors and pressure sensors. SEM images of heater and sensors (top right) and pressure sensor (bottom left). (Adapted with permission from Agah, M.; Potkay, J. A.; Lambertus, G.; Sacks, R.; Wise, K. D. , Journal of Microelectromechanical Systems 2005, 14, 1039-1050. Copyright 2005, IEEE).*

nitrogen dioxide with minimum detection limits in a parts-per-million range. Working in a similar manner, Uwe Lehmann *et al.* introduced a 500 nm thick uniform film of polymer-like-stationary phase using plasma-enhanced-CVD inside a reactive-ion-etched silicon substrate [17]. Additionally, TCD and silicon etched sample valves were utilized along with a micromachined column to show high-speed separation of hydrocarbon gases. In order to fully utilize the advantages of the micro analytical systems, Sandia National Laboratories initiated a micro-chemical sensors program called µChemLab^{TM} for in-situ monitoring of hazardous chemicals [18]. Under this program, microfabrication techniques were employed for producing novel sample pre-concentrators, separation columns, and detectors. This research led to the advancements in chemically selective chemiresistors and polymer-coated surface acoustic wave based miniaturized gas sensors. The birth of the Engineering Research Center for Wireless Integrated MicroSystems (WIMS ERC) in 2000 funded by the United States National Science Foundation and led by the University of Michigan has the most profound influence on advancing the field of µGC. Figure 1.5 [19] demonstrates one such effort, where the first generation µGC system equipped with a micromachined column, preconcentrator and sensor array units is shown. Moreover, different functionalities (temperature programming and flow control) are also integrated on a single microcolumn (Figure 1.5). This fabrication scheme establishes the true capabilities of MEMS technology for providing multiple functionalities on a

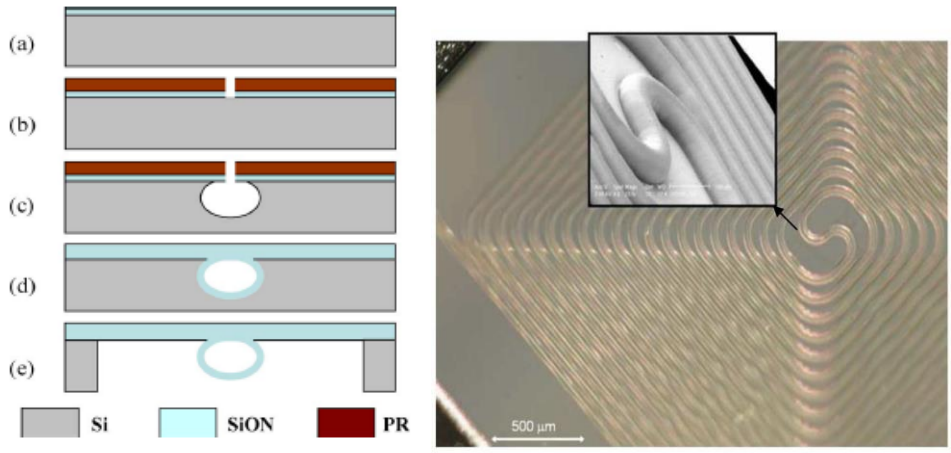

Figure 1.6: *Fabrication process flow and optical image of a released 25 cm long oxynitride column (Adapted with permission from Agah, M.; Wise, K. D. Journal of Microelectromechanical Systems, 2007, 16, 853-860. Copyright 2007, IEEE).*

single chip. The work on fabrication and integration [20] of µGC components (columns [21-25], valves [26], detectors [27, 28], and pumps [29, 30]) is an ongoing research area [31].

VIII. Microfabricated Separation Columns

Separation columns are an integral part of the GC system. The microfabricated columns are typically micromachined on a silicon substrate. Resistive heaters and temperature sensors can be integrated on the substrate to provide on-chip oven for column temperature programming with high rates thanks to the high thermal conductivity of silicon and the small chip size. There are three main types of conventional GC columns based on their geometrical design; open tubular, packed, and multicapillary as already shown in

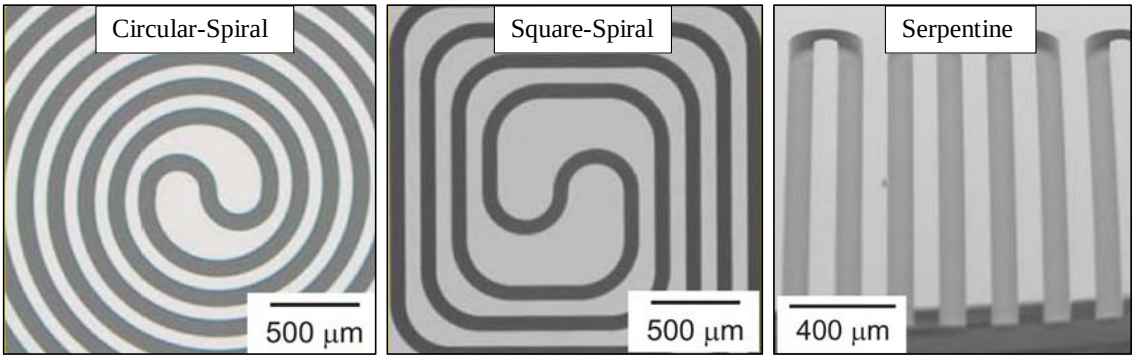

Figure 1.7: *SEM micrographs show different column layout configurations, each column is 3 meters with cross-sectional area of 100 µm x 100 µm (Adapted with permission from Radadia, A. D.; Salehi-Khojin, A.; Masel, R. I.; Shannon, M. A. Sens. Actuators, B-Chem 2010, 150, 456-464. Copyright 2010, Elsevier Limited).*

Figure 1.2.

Microfabricated GC separation columns were initially designed following the conventional open tubular columns and had either a semi-circular or a rectangular cross section profile. The first semi-circular/elliptical designs were realized with wet chemical etching processes. The introduction of DRIE enabled the realization of µGC columns with high-aspect-ratio rectangular channels. One of the design criteria is the selection of the channel layout configurations i.e. circular-spiral, square-spiral, and serpentine (Figure 1.6) for superior chromatographic performance. The group at the University of Illinois Urbana Champagne analyzed these three column geometries and designed 3 m long columns each with 100 µm x 100 µm square cross-sectional area [32]. It was experimentally demonstrated that amongst these designs, the serpentine layout is favored in velocity range of 15-40 cm/sec under both isothermal and temperature-programmed (mode of operations) runs. This was supported by its best peak-to-peak resolution for n-alkane mixture (n-C_7 to n-C_{13}). Furthermore the serpentine microcolumns produced 18,700 plates per meter compared to 11,000 plates per meter obtained for circular-spiral and 10,500 plates per meter for square-spiral microcolumns, respectively. The authors attributed the better performance of serpentine configuration to a uniform and thinner stationary phase film deposition. However, the authors did not provide any design rules for the optimization of turn geometry, cross-sectional area, and the number of channel windings.

Agah and Wise at the University of Michigan presented a semi-circular suspended separation channel enabled using low-stress oxynitride thin films (Figure 1.7) [33]. The suspended channels having a low-thermal mass resulted in a low-power dissipation (150 mW). Moreover, these 65 µm semi-circular channels afforded plate numbers close to 5,000 plates per meter, and separated a multicomponent gas

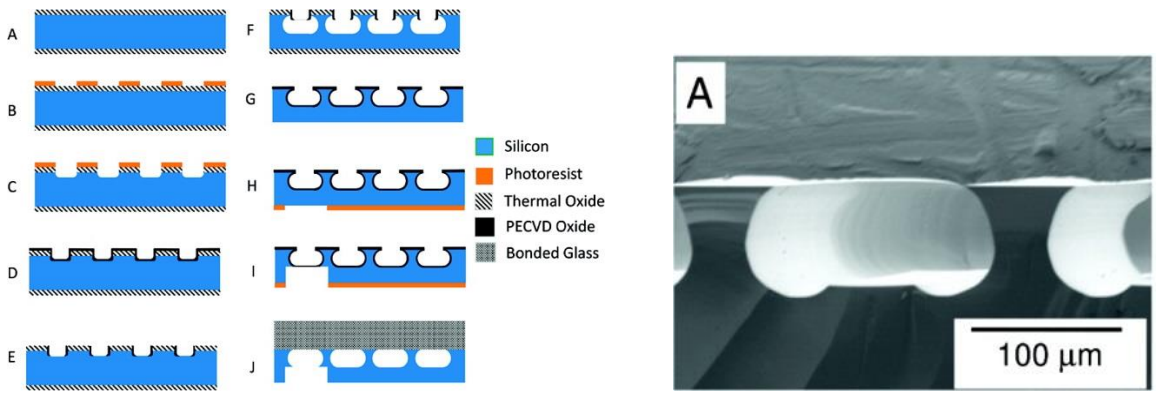

Figure 1.8: *Process flow for the realization of partially buried silicon micro columns (left image) and the corresponding SEM image of single channel (Adapted with permission from Radadia, A. D.; Morgan, R. D.; Masel, R. I.; Shannon, M. A. Anal. Chem. 2009, 81, 3471-3477. Copyright 2009, American Chemical Society).*

mixture. In order to improve the polymeric film deposition inside the microchannel, A. Radadia and M. Shannon at the University of Illinois Urbana Champagne introduced partially buried columns with a rounded channel profile (Figure 1.8) [34]. The fabrication of this novel design required multiple lithographic and microfabrication steps as shown in Figure 1.8. The chromatographic results demonstrated a uniform stationary phase deposition and a lower-dispersion wall profile. Therefore, these columns with partially buried channel provided superior chromatographic performance compared to the anisotropically etched square columns. Recently the theoretical model for optimizing the cross-sectional shapes for µGC columns has revealed that this arbitrary buried channel design indeed provides higher plate number values than the rectangular designs but at the cost of fabrication complexity [35].

Conventional multicapillary columns, with a number of parallel working (1000~2000) narrow width (10~ 50 µm) channels, have been characterized for fast-separations, high-sample capacity, and higher flow rates compared to a corresponding single channel narrow width column (Figure 1.2 c). Based on a similar principle, MEMS lab at Virginia Tech initially introduced microfabricated multicapillary columns (µMCC) with numerous parallel working rectangular 65 µm wide channels (Figure 1.9) [36]. The 4-channel µMCC statically coated with polymer-based polydimethylsiloxane (OV1) stationary phase showed high plate number values close to 12,500 plates/meter (Figure 1.10) and high sample capacity (200 ng). Comparatively 25 µm single channels columns produced only 2 ng sample capacity. Fundamentally, any variations in the cross-sectional dimensions (due to fabrication imperfections or stationary phase coating non-uniformity) between the channels results in solute band-broadening. The

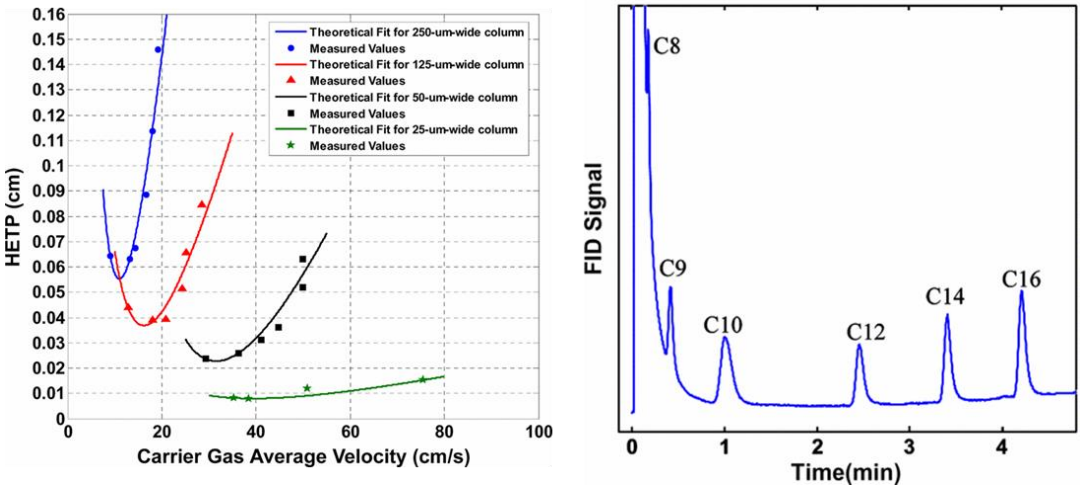

Figure 1.9 *Golay plots for OV-1 coated multicapillary and single capillary channels (left) and the corresponding separation performance of multicapillary column (right). (Adapted with permission from Zareian-Jahromi, M. A.; Ashraf-Khorassani, M.; Taylor, L. T.; Agah, M. Journal of Microelectromechanical Systems, 2009, 18, 28-37, Copyright 2009, IEEE).*

advancements in microtechnology enabled the fabrication of µMCCs with 0.5% dispersions in cross-sectional areas compared to 3~4% variations afforded by manufacturing techniques used in traditional multicapillary columns. The authors also acknowledged the challenges associated with the polymer coating of µMCCs with eight parallel channels and beyond, presenting an opportunity for the exploration of non-traditional stationary phase coating methods.

The researchers at MEMS lab, Virginia Tech also offered another innovative solution for improving the sample capacity and chromatographic efficiency. The group introduced a new class of microfabrication columns called "semi-packed" with an integrated array of micropillars inside the separation channel (Figure 1.11) [37]. These columns combined the properties of both packed (high sample capacity) and open capillary columns (high efficiency, speed of analysis and low pressure drop). The authors used a lithographic mask for the placement of micropillars and standard dry etching techniques for

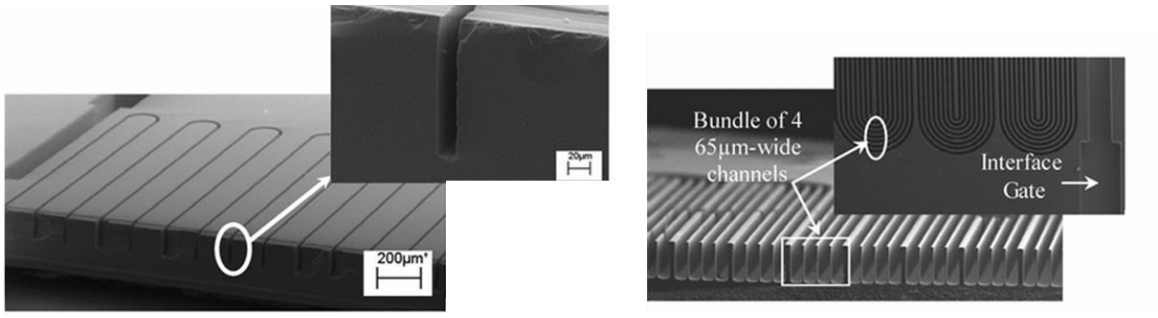

Figure 1.10: *SEM micrographs of a single capillary (left) and a 4 channel multicapillary separation column (right). (Adapted with permission from Zareian-Jahromi, M. A.; Ashraf-Khorassani, M.; Taylor, L. T.; Agah, M. Journal of Microelectromechanical Systems, 2009, 18, 28-37, Copyright 2009, IEEE).*

microfabrication. These columns were coated with a standard OV-1 polymer diluted in pentane using a well-established static coating procedure. The placement of micropillars provided multiple functions; 1) reduced the eddy diffusion and pressure drop 2) improved the sample capacity and 3) improved the separation efficiency by increasing solute-stationary phase interaction. The introduction of semipacked columns instigated great interest in µGC community and a number of research groups further explored different aspects of semipacked columns from the placement and optimization of micropillar geometries to integrating non-traditional stationary phases into these channel.

A. Stationary Phases for Microcolumns

It is relatively straightforward to fabricate etched microchannels using standard planar micromachining techniques. But the incorporation of stationary phase coatings, using either liquid or solid-adsorbent materials, into microcolumns is more challenging. Gas-liquid stationary phases for microcolumns have

been more prevalent from the start. Researchers have begun to look beyond the traditional methods and introduced nanotechnology and MEMS-compatible wafer level coating techniques.

1. **Gas Liquid-Stationary Phases**

   The polymer-based coating consists of three main steps, 1) deactivation of active sites on the channel surface, 2) chemical binding of polymer with column walls and 3) cross-linking of polymer film for temperature stability. There are essentially two liquid phase deposition methods described in literature; static coating and dynamic coating. In static coating, the entire column is first filled with a polymer solution (diluted in a suitable volatile solvent). Afterwards, one end of the column is sealed while the other end of the column is connected to the vacuum pump (Figure 1.12). The sealed column is placed inside a hot water bath to improve the film uniformity during deposition. The solvent slowly

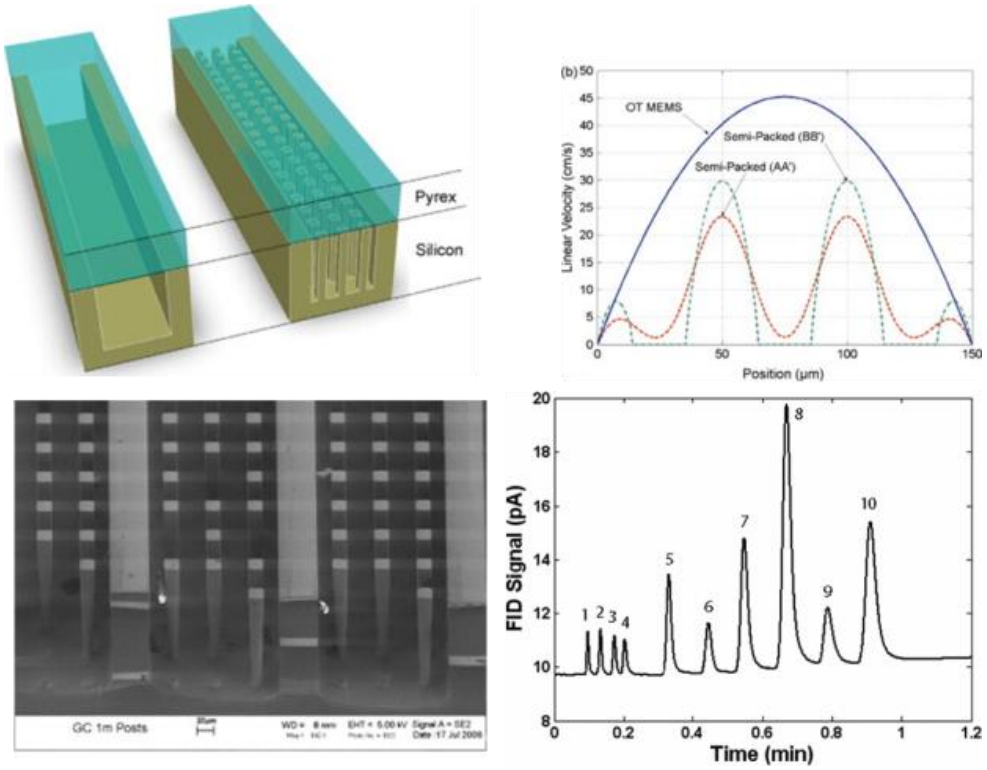

Figure 1.11: *Conceptual and SEM images of a first semipacked column. The corresponding velocity profile and the separation performance of OV-1 coated semipacked column (Adapted with permission from Ali, S.; Ashraf-Khorassani, M.; Taylor, L. T.; Agah, M. Sens. Actuators, B-Chem 2009, 141, 309-315. Copyright 2009, Elsevier Limited). Chromatogram reprinted with permission from Alfeeli, B.; Narayanan, S.; Moodie, D.; Zellner, P.; McMillan, M.; Hirtenstein, D.; Rice, G.; Agah, M. Sensors Journal, IEEE 2013, 13, 4312-4319. Copyright 2013,IEEE. (compound identification (1) dichloromethane, (2) chloroform (3) carbon tetrachloride (4) dibromomethane (5) toluene (6) tetrachloroethylene (7) chlorobenzene (8) p-xylene (9) 1,1,2,2-tetrachloroethane (10) bromobenzene).*

evaporates when the vacuum pump is turned on, leaving behind a thin layer of the polymer film. The thickness of the coated-film is proportional to the concentration of polymer in the solvent. This coating method, pictorially described in Figure 1.12, has been optimized by S. Reidy and R. Sacks at the University of Michigan [38]. The authors coated open rectangular silicon columns with different lengths (0.5 m, 1 m and 3 m) and incorporated deactivation and in-situ cross-linking steps. Moreover, these columns produced 4000 plates per meter and successfully separated a multicomponent hydrocarbon mixture as shown in Figure 1.13. For dynamic coating, a plug of polymer (with controlled plug-width), dissolved in an appropriate solvent, is slowly passed through the column using a non-reactive gas. The film thickness is controlled by the polymer concentration in the solvent and flow-rate through column. With dynamic coating, very thin polymer films are deposited resulting in a low sample capacity and a high separation performance. The separation performance of a dynamically coated (polydimethylsiloxane) semipacked column is shown in Figure 1.11 [39]. The inner surface of semipacked columns is first deactivated using hexamethyldisilazane at 140 °C followed by dynamic coating and cross-linking of polymer with azo-tert-butane vapor at 220 °C for 1 hour. The dynamically coated semipacked columns yielded very high separation performance and afforded 15,000 plates per meter. The above mentioned coating procedures are versatile and applicable to both polar and non-polar stationary phases without any modifications. Since the polymer-based stationary phase coating techniques were originally developed for fused silica capillary columns with round cross-sections, the integration of these conventional polymeric coatings into microcolumns has not been simple especially as the aspect ratio of the channel increases. It has been demonstrated that polymer coating of microfabricated columns result in a non-uniform film deposition especially at the corners (known as the pooling effect).

2. **Gas Solid stationary Phases**

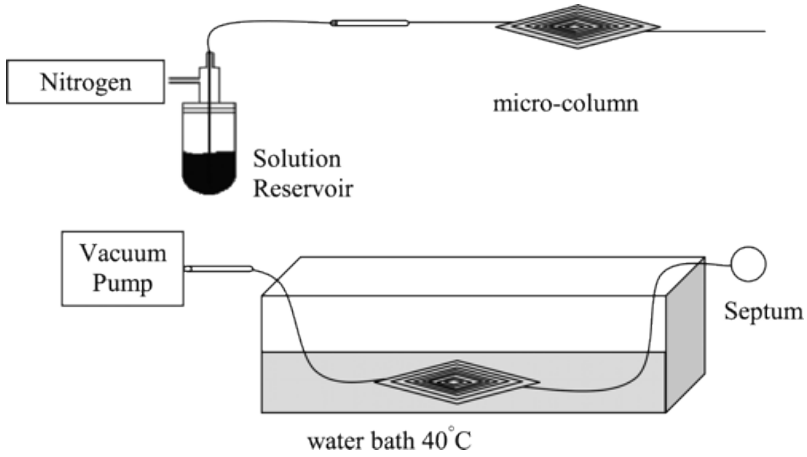

***Figure 1.12**: Optimized static stationary phase coating method for microfabricated columns. (Reprinted with permission from Reidy, S.; Lambertus, G.; Reece, J.; Sacks, R. Anal. Chem. 2006, 78, 2623-2630. Copyright 2006 American Chemical Society).*

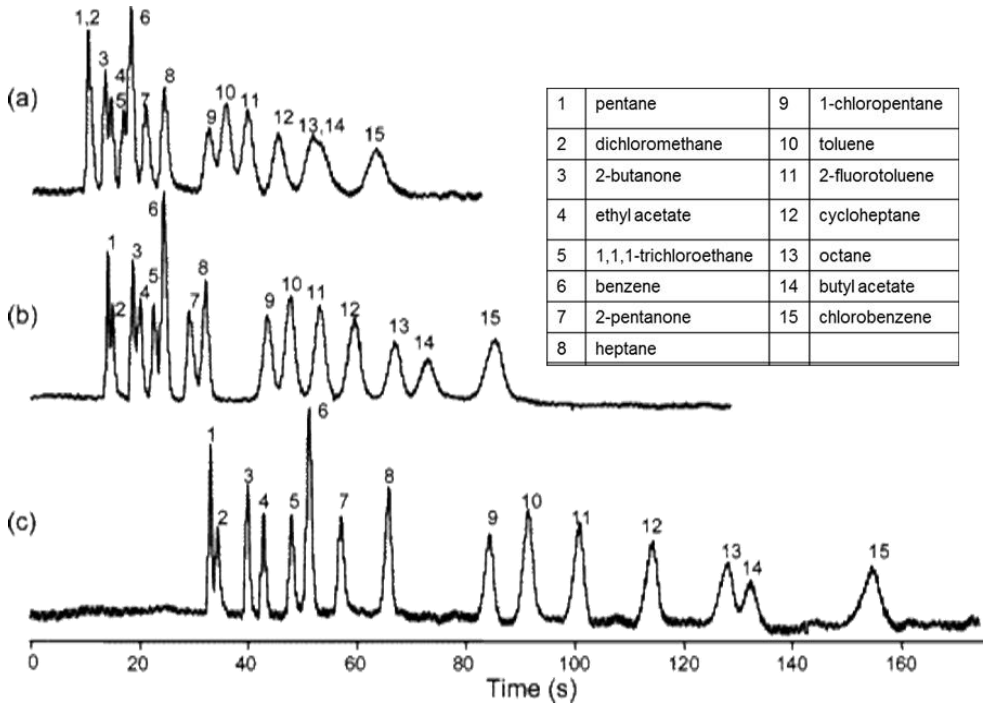

1	pentane	9	1-chloropentane
2	dichloromethane	10	toluene
3	2-butanone	11	2-fluorotoluene
4	ethyl acetate	12	cycloheptane
5	1,1,1-trichloroethane	13	octane
6	benzene	14	butyl acetate
7	2-pentanone	15	chlorobenzene
8	heptane		

Figure 1.13*: Separation performance of statically coated microcolumns with different lengths (a) 0.5 m (b) 1 m and (c) 3 m (Adapted with permission from Reidy, S.; Lambertus, G.; Reece, J.; Sacks, R. Anal. Chem. 2006, 78, 2623-2630. Copyright 2006 American Chemical Society).*

The research on non-traditional solid-adsorbent based stationary phases into µGC columns was first explored by Reston and Co [16] as described earlier. Different IC compatible microfabrication techniques have been employed for these depositions. Stadermann et al. utilized CVD for the integration of single-wall carbon nanotubes (SWCNTs) into a 50 cm long silicon channel with 100 µm x 100 µm cross-sectional area (Figure 1.14) [40]. The authors were able to demonstrate ultra-fast separations (less than 1 second) for a simple four compound mixture on SWCNTs coated micromachined columns with on-chip temperature programming capabilities.

Similarly, our group utilized non-traditional thiol-protected electroplated gold surfaces (Figure 1.15) for the separation of high boiling hydrocarbon mixtures [12]. By shifting the coating step before anodic bonding authors were able to coat separation columns with different configurations (single and 4-channel multicapillary columns). This new thiol-coated stationary phase was found to be stable at high GC operating temperature (350 °C) and flow conditions (1 mL/min). The application of this process is limited by the manual gold removal step from the top silicon surface and could not be applied to very narrow (less than 20 µm) and more complex channel geometries (16 channel multicapillary and semipacked columns). Later, we modified the fabrication process flow to improve the fabrication yield and eliminate the manual gold removal step. The end result showed a more universal applicability of monolayer-protected-gold layers into complex channel geometries (multicapillary and semipacked columns) [23].

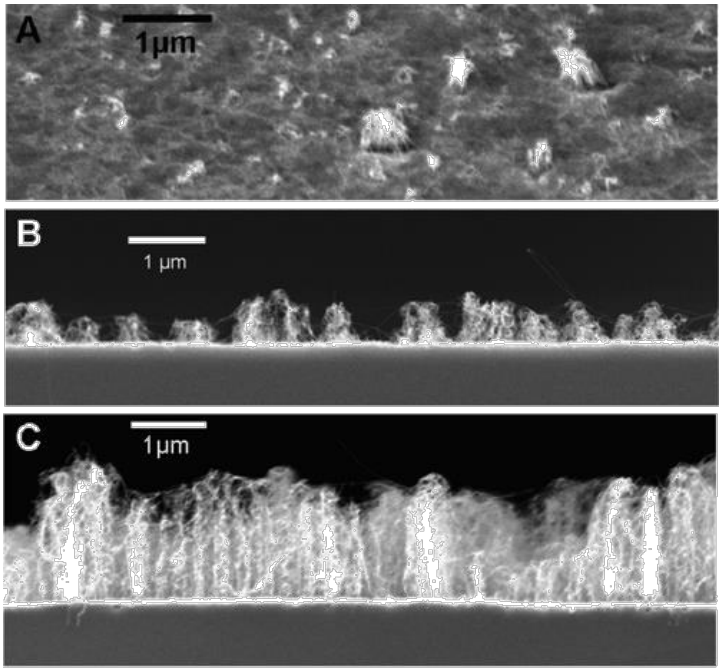

***Figure 1.14**: SEM micrographs of SWCNTs inside a 10 µm x 10 µm microchannel (Adapted with permission from Stadermann, M.; McBrady, A. D.; Dick, B.; Reid, V. R.; Noy, A.; Synovec, R. E.; Bakajin, O. Anal. Chem. 2006, 78, 5639-5644. Copyright 2006 American Chemical Society).*

Additionally, the chemical selectivity of thiol stationary phases was further tuned using thiols with different head-groups [41]. These thiol coated microcolumns produced separation efficiencies of ~7,000 plates per meter (16-channel µMCC) [23]. Chapter 2 and 3 describe modified gold self-patterning fabrication schemes for thiol self-assembly inside both µMCC and semi-packed columns.

J. Vial and colleagues presented a novel wafer level stationary phase deposition method using a sputtering technique [24, 25]. In the microelectronics industry, sputtering is utilized for the deposition of dielectric and metal films. Similar to most common conventional solid-adsorbent materials used for gas chromatographic separations, the research group employed silica, graphite and alumina thin films for light-hydrocarbon separations. This new MEMS compatible deposition method was employed for both open-rectangular and semipacked separation columns (5000 plates per meter). Additionally, the effect of film thickness on chromatographic efficiency and separation performance was also studied and optimized. By integrating an on-chip heater and sensors, fast and efficient separation of the hydrocarbon mixture was achieved for petrochemical applications. The classical sputtering method is typically employed for thin-film deposition on flat substrates and results in the variation of thickness for high aspect-ratio microstructures. It was demonstrated by the authors that for an aspect ratio close to one, the deviation in film thickness was 25% measured at the top and the bottom of the microchannel [25].

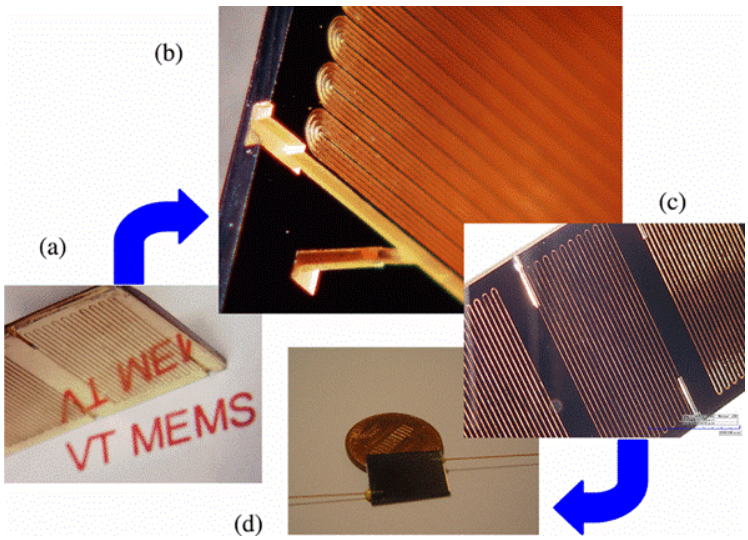

Figure 1.15: *Optical images of gold electroplated separation columns. (Reprinted with permission from Zareian-Jahromi, M. A.; Agah, M., Journal of Microelectromechanical Systems 2010, 19, 294-304. Copyright 2010, IEEE).*

Nanoparticles due to their thermal stability, chemical selectivity, high surface area and small size present a promising solution for chromatographic separations. Different nanoparticles have played a key role in showing gas separation capabilities. Silica nanoparticles are also likely candidates for gas chromatography applications. By employing a well-established layer-by-layer ionic self-assembly method, our group successfully coated different column designs with silica nanoparticles [22]. Both open-rectangular channels (1 m-long, 150 µm-wide and 250 µm-deep) and 16-channel µMCC (25 cm-long, 20 µm-wide and 220 µm-deep) were coated with optimized film thickness in the range of 400~490 nm (Chapter 4). This new methodology used for MEMS columns produced a stationary phase with a high thermal stability and reproducibility. Silica nanoparticles as a stationary phase showed successful separation of both straight chain alkanes and aromatic hydrocarbons. More recently our group has also demonstrated the capabilities of atomic layer deposited thin alumina film as a stationary phase medium inside a semipacked column [42] as described in detail in Chapter 6 and 7.

The chromatographic results of all microcolumns, presented in the subsequent chapters, are generated using a conventional GC system equipped with a FID. The peak identification is carried out by first separately injecting each compound (diluted in a solvent). Afterwards a sample mixture is prepared and the recorded retention time for each separately injected compound is used for assigning the peaks.

CHAPTER 2: Self-Patterned Gold Electroplated Multicapillary Gas Separation Columns with MPG Stationary Phases

(Part of this chapter reproduced from [23] with permission from IEEE JMEMS)
H. Shakeel and M. Agah, "Self-Patterned Gold-Electroplated Multicapillary Gas Separation Columns with MPG Stationary Phases," Microelectromechanical Systems, Journal of, vol. 22, pp. 62-70, 2013.

Gas Chromatography (GC) is one of the primary analytical techniques used for the analysis of unknown volatile or semi-volatile organic compounds. Introduced in 1950, GC has broad range of applications that includes forensic analysis, pharmaceutical industry, petrochemical industry, food processing, environmental monitoring, and biomedicines. A typical GC system consists of a carrier gas cylinder, injector, separation column, detector, data acquisition system, and GC oven. As shown in Fig. 2.1, after injection of an unknown sample into a GC oven, the sample is first vaporized and then carried into the column by the carrier gas. Separation column is considered to be the heart of the GC system; it is coated with a polymer known as a stationary phase and physically separates compounds into distinct components in the time domain. This separation is based on the mass transfer between the stationary phase and the mobile phase (carrier gas). In the next step, these separated components are fed to a detector such as a flame ionization detector (FID) or a thermal conductivity detector (TCD) to generate chromatograms according to the compound retention time in the column. Advances in the technology of microelectromechanical systems (MEMS) has enabled the realization of micro gas chromatography (µGC) with improved features such as better portability, less power consumption, and faster analysis time when

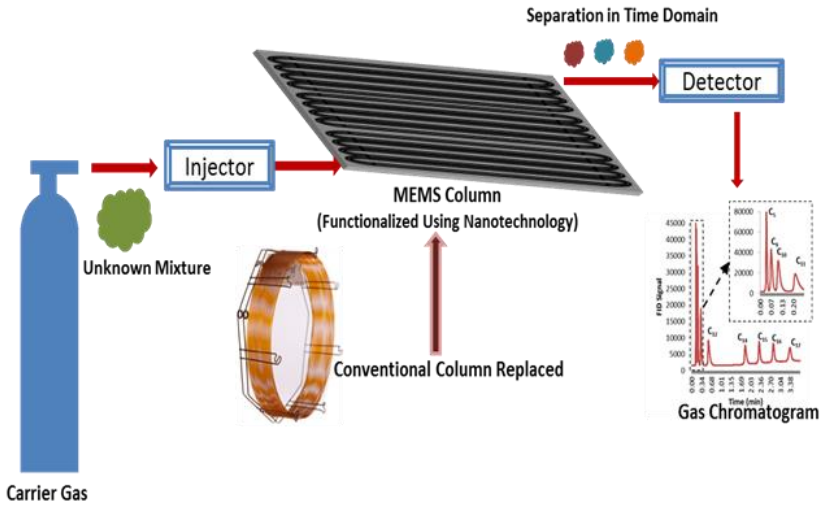

***Figure 2.1**: Schematic view of a gas chromatography system.*

compared to conventional bulky GC systems [19, 25, 37, 43-49].

In recent years, there has been growing interest among the MEMS community to miniaturize and improve the chromatographic performance of separation columns by employing novel fabrication techniques and stationary phase coating procedures [50-58]. In order to reduce the analysis time, improve sample capacity and separation efficiency of µGC columns, our group has earlier introduced [36] µMCC consisting of a bundle of high-aspect-ratio (HAR) channels working in parallel. The benchmark for calculating separation efficiency of columns is considered to be the height-equivalent-to-a-theoretical-plate (HETP). It has been shown that HETP of an MCC can be defined in terms of its single capillary separation performance, properties of stationary phase, and the degree of geometrical homogeneity of the individual rectangular channels. The simplified HETP for MCCs [59] can be represented by (2.1)

$$HETP = \frac{u_0^2}{L(1+k_0)^2}{\sigma_0}^2 + L\left(\frac{\sigma_h}{h_0}\right)^2 + L\left(\frac{\sigma_w}{w_0}\right)^2 \qquad (2.1)$$

where u_0 is the average linear gas velocity, L is the length of column, σ_0^2 is the peak variance of a single capillary (calculated from Golay equation) and k_0 is the compound retention factor in a capillary with average cross-sectional area of $h_0 \times w_0$. While, $(\sigma_h/h_0)^2$ and $(\sigma_w/w_0)^2$ represent the cross-sectional height and width deviations normalized by the average height and width, respectively. The first term in (2.1) shows HETP of a single capillary whose dimensions are average of dimensions of all multi-capillaries. The second and third terms deal with band broadening caused due to inhomogeneity between channel dimensions. From (2.1), if the height and width dispersions of MCCs ($\sigma_h = \sigma_w \sim 0$) are close to zero- provided all channels are coated uniformly with a stationary phase- HETP of MCCs becomes (2.2).

$$HETP = \frac{u_0^2}{L(1+k_0)^2}{\sigma_0}^2 \qquad (2.2)$$

From standard GC equations for a single capillary column, plate number (N) and retention time (t_r) are defined as (2.3) and (2.4) respectively

$$N = \left(\frac{t_r}{\sigma_0}\right)^2 \qquad (2.3)$$

$$t_r = \frac{L}{u_0} \times (1+k_o) \qquad (2.4)$$

Substituting equation 2.4 into 2.3

$$N = \frac{L^2 \times (1 + k_o)^2}{u_o^2 \times {\sigma_0}^2} \qquad (2.5)$$

Substituting equation 2.5 into 2.2

$$HETP = \frac{L}{N} \qquad (2.6)$$

Therefore, $HETP$ of multicapillary approaches that of a single capillary column provided there are no dispersions in height and width of channels ($\sigma_h = \sigma_w \sim 0$). Moreover, its sample capacity is increased by the number of capillaries working in parallel. In practice, however, dispersions in the width and length of individual channels as well as non-uniformities in stationary phase coating thickness reduce the separation efficiency of the MCC. This is because slight dimensional variations of individual capillaries result in different flow rates of the sample through each capillary (capillaries with larger cross section have high volumetric flow rates and the smaller ones low flow rates). This also causes deviations in the thickness of stationary phase between each channel during coating process, increasing band broadening of the chromatographic peaks. Therefore, very tight tolerance bound is placed on the precision of individual capillary dimensions for higher chromatographic resolution of MCC [2, 60-63]. Utilization of MEMS technology has facilitated the realization of very narrow-width capillaries with appreciable reduction in

Table 2.1 *Pulse electroplating conditions for gold deposition on MEMS GC columns.*

ELECTROPLATING CONDITIONS	**PARAMETERS**	
	SDSP (Plating time =90 min)	**DDSP (Plating time =15 min)**
Forward Current Density (J_f)	1mA/cm^2	7mA/cm^2
Reverse Current Density (J_r)	3mA/cm^2	1mA/cm^2
Forward Current Time	τ = 100ms	T- τ = 3s
Reverse Current Time	T- τ =3s	τ = 100ms

area dispersion. Our group, in the first reported MEMS-based MCC, has shown [36] that both average width and height dispersion of µMCC can be as small as 1%. As a result, the deviation of MEMS-based MCCs from their theoretical performance is mainly attributed to the inhomogeneity of the stationary phase coating.

Limitations in getting uniform coating inside rectangular µMCCs using conventional static or dynamic coating techniques present a major hindrance towards their full utilization. When these classical coating methods, developed for circular silica capillary columns, are used for microfabricated rectangular columns, they cause problems like non-conformal deposition, column clogging and pooling of stationary phase at the corners [36, 38, 64, 65], ultimately leading to the loss of column efficiency. Therefore, getting reproducible, homogenous and stable stationary phase is often considered to be crucial step towards the realization of a complete µGC system. Accordingly, there is a critical need to develop alternative stationary phase deposition techniques which are more compatible with the fabrication processes for MEMS-based GC columns, examples of which are recently reported silica deposition using sputter coating [25] and carbon nanotubes grown by chemical vapor deposition [40]. Our group in

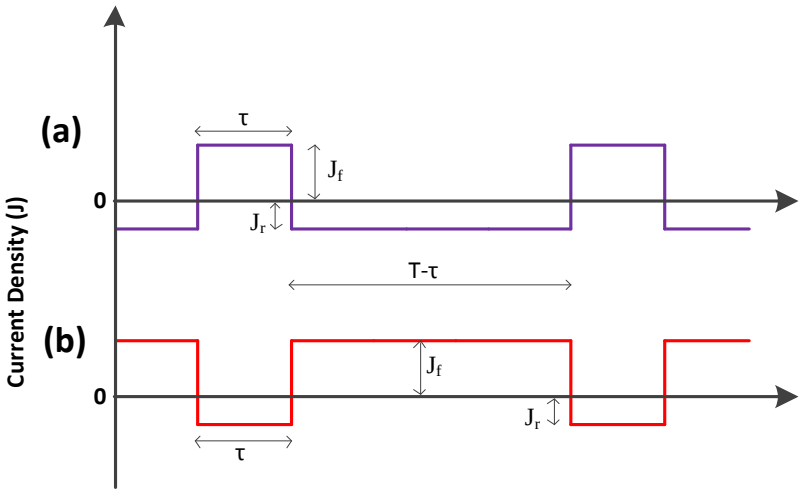

***Figure 2.2**: Pulse electroplating waveforms for (a) SDSP and (b) DDSP. J_f is the forward current density and J_r is the reverse current density.*

previous work [12] pioneered a unique stationary phase deposition technique by combining gold electroplating followed by thiol self-assembly. While reporting promising results, our fabrication process required mechanically removing gold from the top surface due to non-selective deposition. This step was a limiting factor in achieving a high-yield process since it could damage the µMCCs comprising very thin walls and narrow fluidic channels. Additionally, incomplete removal from the top surface could result in anodic bonding degradation and failure.

This paper resolves the aforementioned issue and takes a major step forward by presenting two different highly reproducible single-step selective deposition approaches to deposit the target layer inside the HAR microstructures. These deposition methods that eliminate the need for mechanical polishing or post-

deposition patterning steps are categorized as single-doped self-patterned (SDSP) and double-doped self-patterned (DDSP) processes. SDSP method uses novel geometry-dependent tuned electroplating conditions to self-pattern gold only on vertical sidewalls leaving the horizontal surfaces intact, while DDSP relies on the fabrication process to completely cover the interior surfaces of the microchannels. By utilizing self-patterned deposition techniques and thiol self-assembly, we have been able to uniformly coat for the first time 16-channels μMCCs and achieve the highest reported separation efficiency on this promising class of μGC columns.

I. Fabrication

The proposed fabrication methods are schematically shown in Fig. 2.3 (SDSP) and Fig.2. 4 (DDSP). These can be broadly divided into four major steps, which includes anisotropic etching of micro channels, thin film deposition using electroplating, anodic bonding (and *in situ* gold annealing), and functionalizing the gold layer with a thiol functional group to serve as the stationary phase. Complete description of each step is explained below.

A. Column Fabrication and Thin Film Deposition

The column fabrication starts with anisotropic etching of a 4" silicon (p-type, <100>, 0-100Ω-cm) wafer. Thin film deposition inside highly conductive microfluidic channels is done using pulse electroplating as it is shown to improve current distribution and mass transport conditions [66, 67]. The pulse plating waveforms for both SDSP and DDSP methods are shown in Fig. 2.2. The detailed description of column fabrication and thin film deposition of each method is explained below.

1. Single-Doped Self-Patterned (SDSP) Method

In order to evaluate the proposed SDSP technique, μMCC with 25cm-long 16 channels are fabricated. First AZ9260 photoresist is spin coated at 3000 rpm to get a thickness of ~8μm. Secondly, the photoresist is patterned and the wafer is etched using deep reactive ion etching (DRIE) to get 250μm-deep and 30 μm-wide microchannels (Fig.2.3b). In the next step, photoresist from the etched wafer is cleaned using acetone while oxygen plasma is used to ensure the complete removal of residual polymers deposited during DRIE etching.

Next, the solid source phosphorous diffusion of the etched wafer is accomplished at 950˚C for 10 hours (Fig. 2.3c). This step reduces the silicon resistivity, thereby providing a conductive path between the electrode and microchannels during electroplating and eliminating the need for seed layer deposition. After dicing the wafer, buffered hydrofluoric (BHF) acid is used to remove native oxide on each individual chip. Each device is then dipped in methanol for 2 minutes to wet the surface. Platinized Ti electrode grid placed at 2cm from each doped device is used as anode and cathode, respectively, for seedless gold

electroplating deposition. Gold electroplating solution (TG-25 RTU, Technic Inc USA) is kept at 55°C and stirred at 300rpm to obtain uniform distribution of gold ions in the bath. Selective electroplating conditions (Table 2.1) are used to deposit gold along the vertical walls of the channels (Fig. 2.3d). Relying on channel geometry and pulse electroplating conditions, this technique presents a unique phenomenon by selectively depositing gold only along the vertical sidewalls inside 3D microchannels. This can be explained by the fact that during electroplating, gold is being deposited during forward time period (τ) or the positive cycle, while the concentration of the ions on the flat surface depletes during the reverse time period (T-τ) or the negative cycle. If negative cycle is much greater than the corresponding positive cycle, then the ions deposited on horizontal surfaces start to get removed during this reverse time period. If the reverse time is large enough, then no gold deposition occurs on these horizontal surfaces. The relative reverse and forward time periods are geometry dependent and are experimentally found for different channel dimensions. For our selected µMCC geometry, extended characterization was performed to find the tuned electroplating conditions mentioned in Table-2.1. The selective deposition along the vertical sidewalls is seen from SEM images (Fig.2.6a-f). Fig. 2.6a-b confirm the absence of gold at top and bottom horizontal surfaces, respectively, for our tuned conditions. Reverse and forward time periods play an important role in achieving our selective plating conditions. The effect of changing reverse time on gold deposition on horizontal top surfaces can be seen from Fig. 2.6g-h. Forward time period of τ=150ms is used for both depositions. The first scenario (Fig. 2.6g) shows that for a given forward pulse duration, reverse time is not enough (T- τ = 1s) and results in gold deposition on top of the channel walls. Fig. 2.6h reveals that increasing the reverse time (T- τ = 3s) further results in removing gold from the top surface. Comparatively, gold particulate density for the first scenario (Fig. 2.6g) on the top channel walls is much

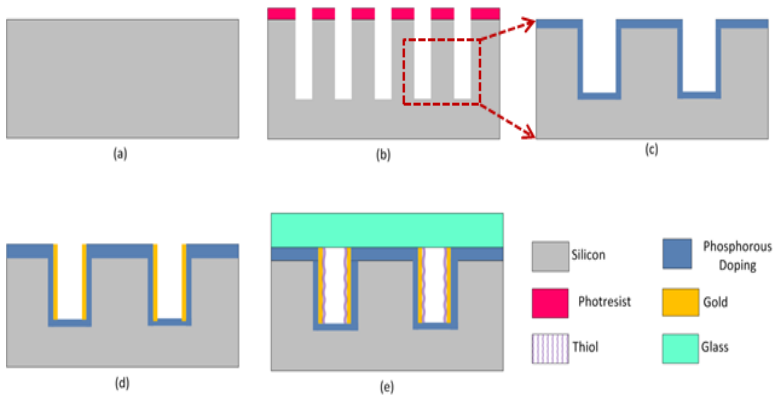

***Figure 2.3**: Process flow for the fabrication of µMCCs using SDSP(a) Silicon (b) Deep Reactive Ion Etching (c) Phosphorous diffusion (d) Seedless gold electroplating (e) Anodic bonding and thiol deposition*

higher than the second case (Fig. 2.6h); this was also confirmed by performing SEM-EDS analysis on both chips. To achieve the selective electroplating conditions, forward time is further reduced to 100ms, while reverse current duration is kept at 3 seconds (Fig. 2.6a-b). The thin gold layer alongside the vertical walls (Fig. 2.6a-b) enables the functionalization through self-assembly. Under the given conditions (Table 2.1), a gold film thickness of around 310nm is observed. The surface thickness of this deposited gold layer can be adjusted further by changing the electroplating time. The applied current density, topography, and dimensions of the channels are the most important factors that affect the electrodeposition of metal ions inside these HAR microstructures. We hypothesize that traditional methods like stirring for improving ion transport inside the HAR microstructure become inefficient as electrolyte remains stagnant deep inside the microtrench, leading to insufficient supply of metal ions for deposition along the depth of channel [68-70]. This results in a gradual decrease of the gold thickness along the channel sidewalls as revealed in SEM images in Fig. 2.6c-f and eventually causes negligible gold deposition on the channel bottom. For top planar surfaces with convection dominated mass transport deposition, our geometry-dependent tuned electroplating conditions with higher reverse current time (3s) depletes most of the gold ions deposited during a very short positive current cycle (100ms). This causes insignificant deposition on the top planar surfaces of the channel walls. This was confirmed by electroplating gold on flat doped silicon surface with the same area as the actual device under identical conditions. This interesting phenomenon could be subject of further investigation.

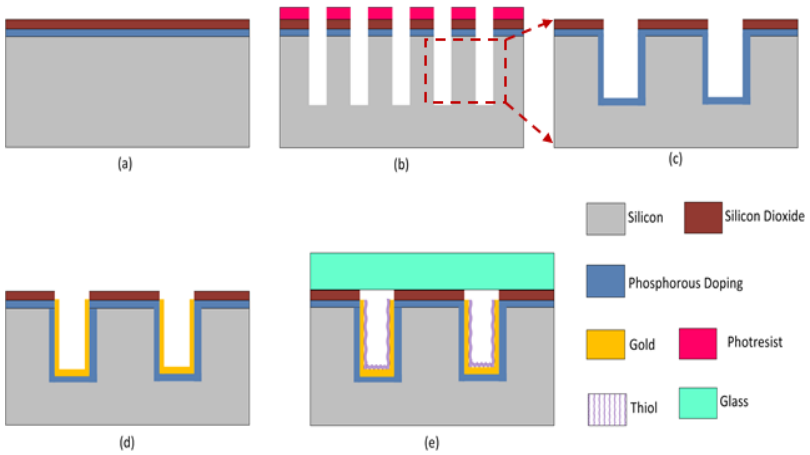

Figure 2.4: *Process flow for the fabrication of µMCC-16 using DDSP (a) Phosphorous diffusion and PECVD oxide deposition (b) Deep Reactive Ion Etching (c) Second phosphorous diffusion (d) Seedless gold electroplating (e) Anodic bonding and thiol deposition*

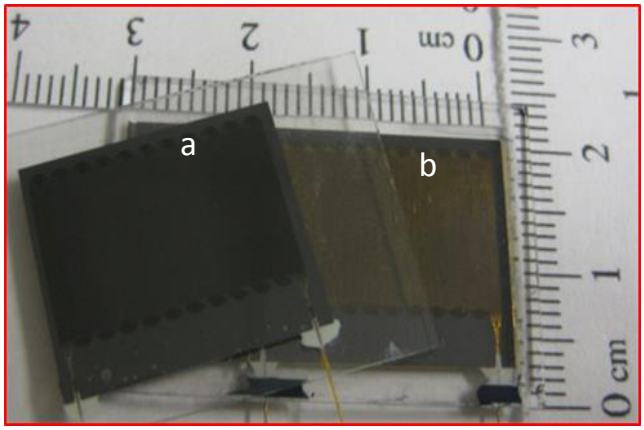

***Figure 2.5**: Optical Image of electroplated devices a) SDSP column and b) DDSP column.*

2. Double-Doped Self-Patterned (DDSP) Method

The proposed fabrication of DDSP-based µMCCs starts with solid source phosphorous doping of a plain silicon wafer (950˚C, 10 hours). Next, on the top of this doped wafer, silicon dioxide with a thickness around 220 nm is deposited using Plasma Enhanced Chemical Vapor Deposition (PECVD) at 350˚C (Fig. 2.4a). This thin layer of oxide acts as a mask for top horizontal surface of the device during electroplating and does not affect the formation of the depletion layer at the glass-silicon interface during anodic bonding. After oxide deposition, photoresist is spin coated, exposed, and developed. DRIE is used to first anisotropically etch silicon dioxide and then to form 250µm-deep, 30µm-wide, 25cm-long channels (Fig. 2.4b).

After RCA cleaning, the etched wafer is subjected to a second phosphorous doping process at 950˚C for 10 hours (Fig. 2.4c). This step enhances the surface conductivity inside microchannels and enables performing seedless gold deposition. It is notable that the first doping step provides the conductive path between the electrode and these highly conductive n-type channels. Subsequently, each wafer is diced into individual devices. Before placing each device in a gold bath, native oxide is removed by dipping the chip in BHF for 30 seconds. Then, a small oxide portion on the chip periphery outside the microchannel area is etched for 3 minutes using BHF in order to provide electrical connection for electroplating between the electrode and the doped channels. Afterwards, each device is dipped in methanol for 2 minutes to wet the surface. Using the same setup mentioned for SDSP deposition, pulse electroplating conditions (Table 2.1) are used to deposit gold inside HAR microstructures (Fig. 2.4d).Under these conditions the thickness of deposited gold layer is found to be approximately 830nm (Fig. 2.7e). Due to the presence of the thin oxide masking layer, no deposition occurs on the top horizontal surfaces of the chip. This was also confirmed from SEM-EDS analysis of DDSP fabricated devices. This is confirmed in the optical (Fig. 2.5b) and SEM (Fig. 2.7a-d) images. In our DDSP method, complete coverage of gold on all interior surfaces of the

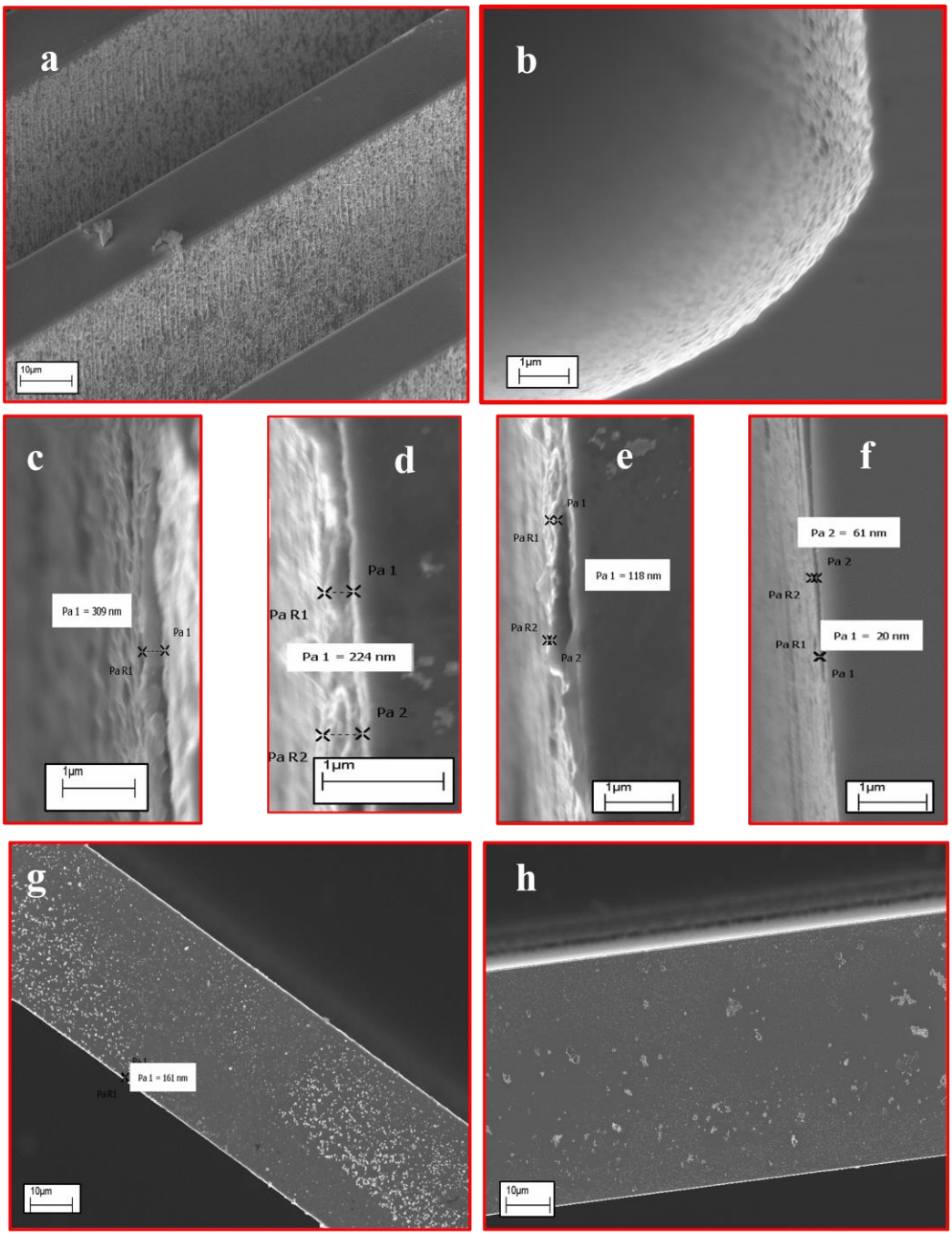

***Figure 2.6**: Selective gold deposition achieved by SDSP under tuned plating conditions confirmed by SEM images (a) top-view of channel (b) crosssectional bottom-view of channel (c-f) gradual reduction in gold thickness along the depth of the microtrench from the top to the bottom, effect of changing electroplating conditions with Jf=3mA/cm2, Jr=1mA/cm2, τ=150ms for (g) T-τ =1s and (h) T-τ =3s.*

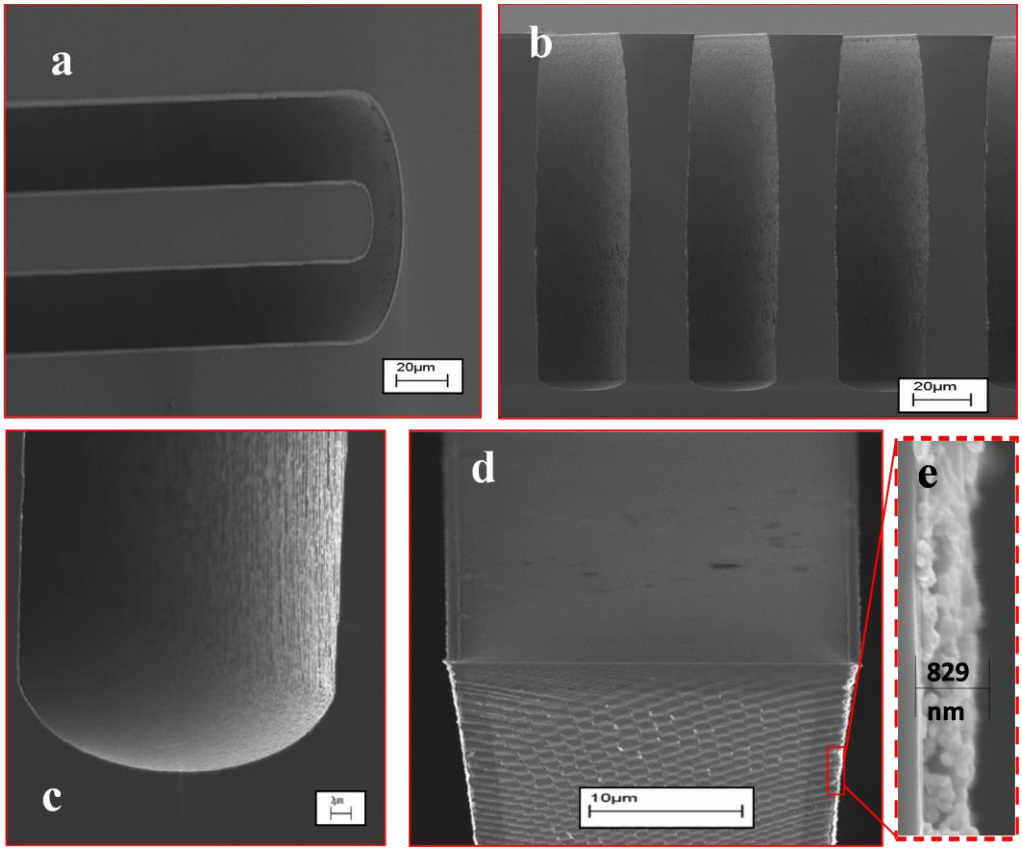

***Figure 2.7**: Selective and conformal gold deposition using DDSP scheme confirmed by SEM micrographs a) top view of the channel, (b-c) conformal deposition inside the channel (d) cross-sectional view of a single sidewall (e) film thickness.*

microchannels are achieved regardless of the duration of reverse and forward times. Similar to SDSP, the thickness of the deposited layer can be varied by changing the plating time and current density.

B. Anodic Bonding and Stabilization

Both types of fabricated devices are then bonded with Pyrex using anodic bonding at 350°C and 1250V (Fig. 2.3e and Fig. 2.4e). The high temperature during bonding improves the adhesion between the electroplated gold layer and doped silicon [71]. Following bonding, deactivated fused silica capillary tubes (outer diameter 220µm, internal diameter 100µm and length of 25 cm) are attached to the inlet and outlet ports using epoxy (Epoxy 907, Miller-Stephenson Co, USA).

C. Functionalization

Finally, the fabricated columns are coated with 2mM of Octadecanethiol ($C_{18}H_{37}SH$) diluted in hexane for 40 hours. This process attaches the alkane group to the electroplated gold surface by self-assembly (Fig. 2.3e and Fig. 2.4e); this monolayer protected gold layer (MPG) acts as a stationary phase [4, 72, 73].

$$C_{18}H_{37}SH + Au^0 \xrightarrow{SAM} [C_{18}H_{37}S^- + Au^+] + {}^1/_2\, H_2$$

II. Chromatographic Results and Discussion

A. Experimental Setup

To evaluate the separation efficiency of the functionalized columns, a conventional GC oven (GC HP 5890 series II) with an FID, auto sampler (7673B, Hewlett Packard), and electronic pressure controller is used. The conventional column in the GC oven is replaced with the MEMS column. The injector and FID temperatures are maintained at 280˚C. Dry nitrogen is used as the carrier gas for all the experiments. All the chemicals used for testing are of HPLC grade and purchased from Sigma Aldrich.

B. Conditioning

Before using functionalized columns, they are first purged with constant stream of dry nitrogen at room temperature for 15 minutes to remove any air trapped within the column [1]. In the second step, each column is conditioned for 1 hour in the GC oven which is temperature programmed at a rate of 1.5˚C/min from room temperature to 120˚C at a constant inlet pressure of 2.5psi. Column conditioning is important particularly for removal of any loosely connected thiol monolayer or any contaminant present inside the column. The stabilized baseline observed after conditioning ensures the stability of the stationary phase for the operating temperature being used for column testing [1].

C. Separation Results

Before functionalizing gold plated columns with thiol, these devices are first tested to check the capability and contribution of gold layer towards chromatographic separation. Chromatogram obtained

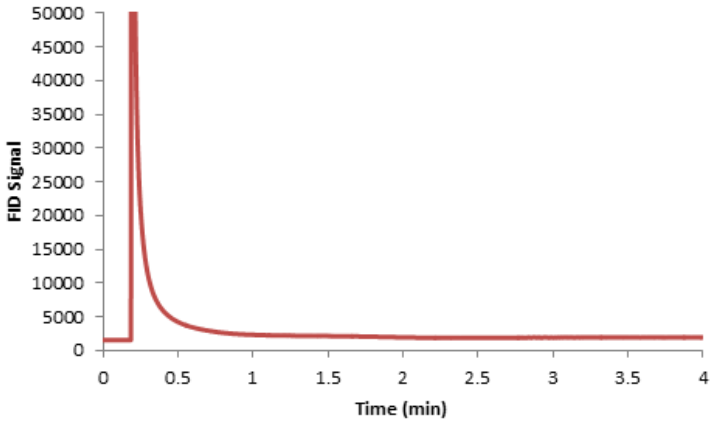

Figure 2.8: *Chromatogram of the n-alkanes sample mixture for the gold-plated µMCC-16 without functionalization.*

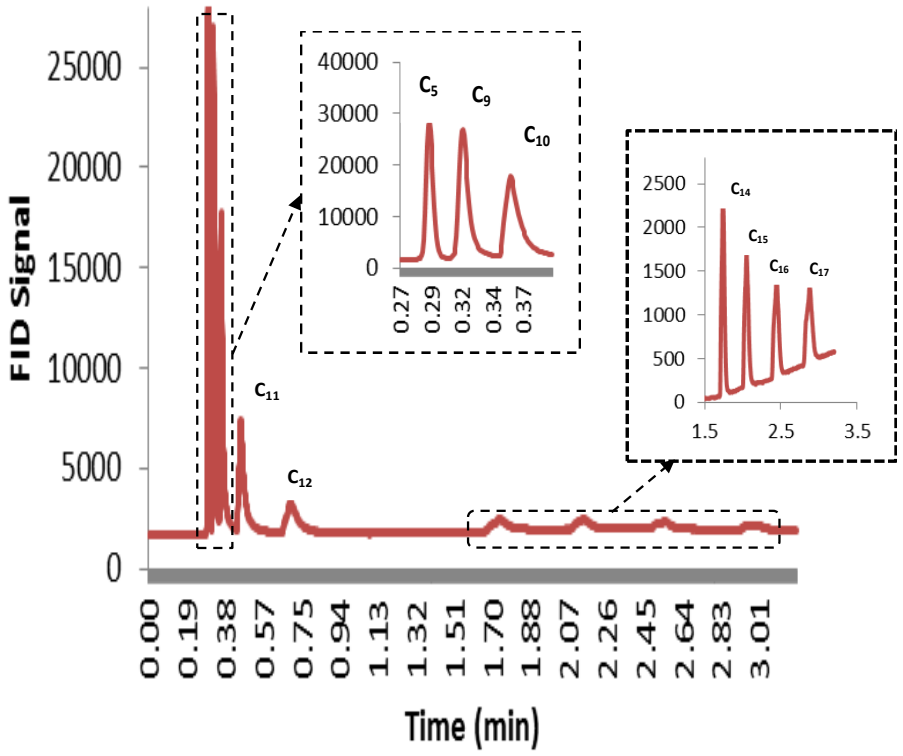

***Figure 2.9**: Chromatogram of nine alkanes using SDSP scheme (initial temperature= 50°C for 0.7 min, final temperature= 120°C, temperature rate of 70°C/min, inlet pressure= 10psi for 1.7 min, pressure program rate=15psi/min after 1.7min , split ratio= 100:1)*

after injection of sample containing alkane mixture (Fig. 2.8) clearly shows the inability of the gold surface to separate the constituents of the sample mixture and its inadequacy as a stationary phase. Afterwards; both types of columns are first functionalized and then tested for separation ability by injection of a 0.3µL sample containing nine alkanes (n-pentane, n-nonane, n-decane, n-undecane, n-tetradecane, n-dodecane, n-pentadecane, n-hexadecane and n-heptadecane). Fig. 2.9 (SDSP) and Fig. 2.10 (DDSP) show chromatograms obtained from both MPG coated columns by temperature programming the columns from 50˚C to 120˚C at a rate of 70˚C/min with 100:1 split ratio. All the constituents (boiling points ranging from 36.5˚C to 302˚C) of the mixture are separated successfully by both columns with reasonable resolution in less than 4 minutes.

The performance of GC columns is gauged by the number of theoretical plates (N), as well as the HETP. N/HETP is equal to the length of the column (L). The efficiency (HETP) of each µMCC is graphically characterized by the following formula [1]:

$$HETP = \frac{L}{5.54} \times \left(\frac{w_h}{t_r}\right)^2 \qquad (2.7)$$

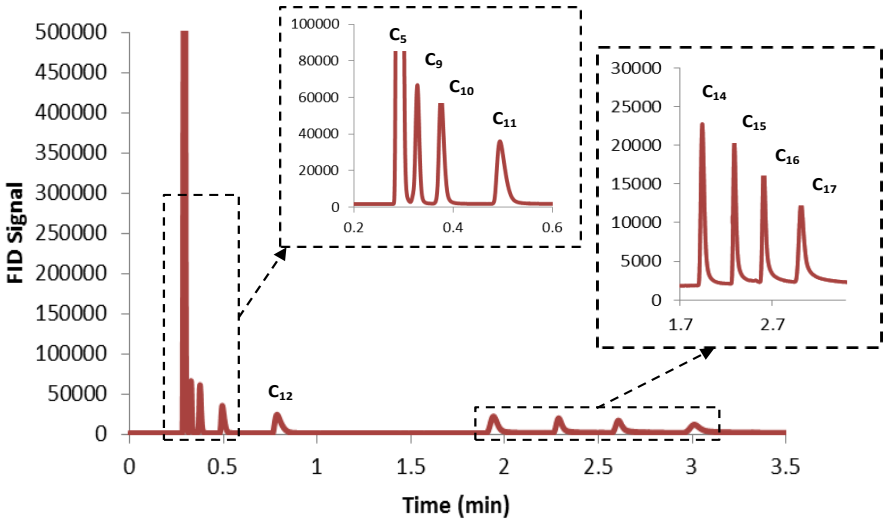

***Figure 2.10**: Chromatogram of nine alkanes using DDSP scheme (initial temperature= 50°C for 0.7 min, final temperature= 120°C, temperature rate of 70°C/min, inlet pressure= 10psi for 1.7 min, pressure program rate=15psi/min after 1.7min, split ratio= 100:1).*

where w_h is the peak width at half height, t_r is compound retention time, and L is the column length.

For HETP analysis, inlet pressure is varied from 2.5 psi to 20 psi under isothermal conditions (50˚C). Auto sampler is used to inject 1µL of the sample containing small amount of n-dodecane ($C_{12}H_{26}$) diluted in dichloromethane (CH_2Cl_2) with a split ratio of 150:1. Fig. 2.11 shows the equivalent-plate-number as a function of pressure (Golay Plot) for the 16-channel µMCCs fabricated using both schemes. The maximum plate number of 5400 plates/m at 7.5psi is calculated for SDSP fabricated columns. While, the columns produced using DDSP technique show a plate number of 7300 plates/m under the same optimum pressure.

III. Discussion

To check the reproducibility and robustness of the fabrication methods for µGC development, multiple devices were produced from different wafers and checked for chromatographic performance. The chromatographic data obtained from these columns show successful separation of nine alkane mixture with qualitatively similar resolution under similar testing conditions. Similarly, the effect of variations in coating uniformity and dispersions in dimension of column on chromatographic efficiency is also evaluated. The conditions for electroplating for SDSP devices need to be tightly controlled to ensure nonappearance of gold on the top surface and subsequent high quality anodic bonding. Out of six devices, only three showed good performance and their separation efficiency was characterized. The average of the maximum plate numbers at optimal flow velocity for these three columns was about 4600 plates/m. DDSP

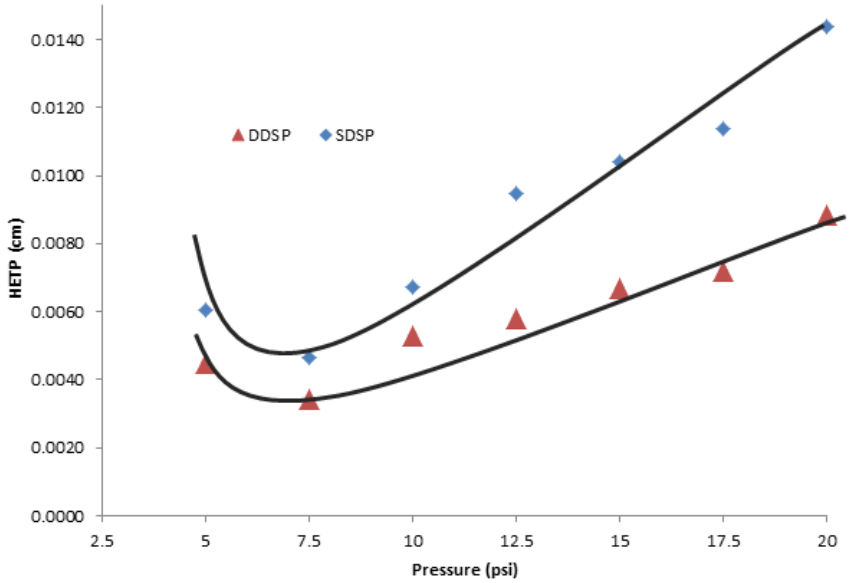

***Figure 2.11**: The golay plot for n-dodecane under isothermal (50º C) condition and 1µL injection for µMCC-16 (SDSP and DDSP).*

columns did not have the aforementioned issue and their fabrication yield was close to 80%. We tested seven µGC column chips fabricated using this technique. These columns were able to achieve an average maximum plate number of 6100 plates/m.

Our proposed SDSP method, which deposits gold only on vertical sidewalls, is a novel and promising electrodeposition technique that can find its applications in a wide range of areas, including electrochemical sensing, biomedical applications, and physical sensors. However, its utilization in GC, apart from requiring extended characterizations and longer plating times, suffers from the fact that it does not cover the bottom of the silicon channel with gold, and hence, it provides less surface area for thiol self-assembly. This results in less retention of the sample by the stationary phase. In comparison, devices fabricated at the expense of extra fabrication steps using DDSP method do not require extensive electroplating characterization, result in conformal gold deposition across the channel and expose more surface area for thiol self-assembly. This results in stationary phase coating that effectively increases sample retention. Comparing Fig. 2.9, Fig. 2.10 and Fig. 2.11 also show that columns fabricated using SDSP method retain less amount of sample, but at the expense of lower chromatographic resolution. Since devices produced using DDSP scheme provide high fabrication yield and better chromatographic resolution, DDSP is the preferred self-patterned fabrication method for µGC applications.

IV. Conclusion

In this report, two different self-patterned gold electrodeposition approaches have been evaluated for HAR microstructures. Both techniques afford film deposition with varying thickness inside the three dimensional micro channels without any deposition on the top horizontal surfaces, thus eliminating the requirement of post-deposition patterning steps. The first presented scheme, SDSP, is very promising and unique but its application in µGC suffers from incomplete coverage of microchannels. In contrast, DDSP leads to complete gold coverage of the interior surfaces and also removes the need for costly characterizations. The chromatographic performance of each technique is demonstrated by exploiting the self-assembly of thiol on gold surface that is used as a stationary phase. This leads to improvements in resolving power of the columns, observed from theoretical plate number study. The effect of plating thickness on chromatographic efficiency and performance will be studied in future work. It is also envisaged that a wide variety of available thiol-based organic compounds can be self-assembled to achieve chemical selectivity of MPG stationary phases.

CHAPTER 3: Improved Self-Assembled Thiol Stationary Phases in Microfluidic Gas Separation Columns

The miniaturization of different GC components, such as pre-concentrators/injectors [74-80], separation columns [81-86], and detectors [27, 55, 87-90], enables the realization of a field portable system [20, 91-98] for real-time sample analysis. Chip-based GC separation columns, realized through planar microfabrication of silicon-glass substrates, have been the main subject of several recent research studies. Apart from separation capabilities, certain critical GC functionalities such as temperature programming [24, 99] and flow rate sensing [86] have also been integrated on the same silicon-glass chip. The high thermal conductivity of silicon (149 W/ m•K) [100], shorter column lengths (0.25 m to 3 m) [38, 40, 101], and smaller chip sizes (typically 2 cm x 2 cm) [85, 102] along with new stationary phase coating materials result in low-power consumption (<100 mW) [85] and rapid temperature programming rates (60 ℃/s) [40] enabling faster (less than a minute) as well as efficient (>10,000 plates/m) separations [102, 103]. Moreover, the use of standard cleanroom fabrication processes, mainly lithography and plasma based dry etching, has also enabled the realization of producing separation channels with arbitrary shapes and geometrical patterns. This is not possible with the conventional manufacturing techniques employed for glass capillary columns. These innovative designs include partially buried micro-columns [34], low-

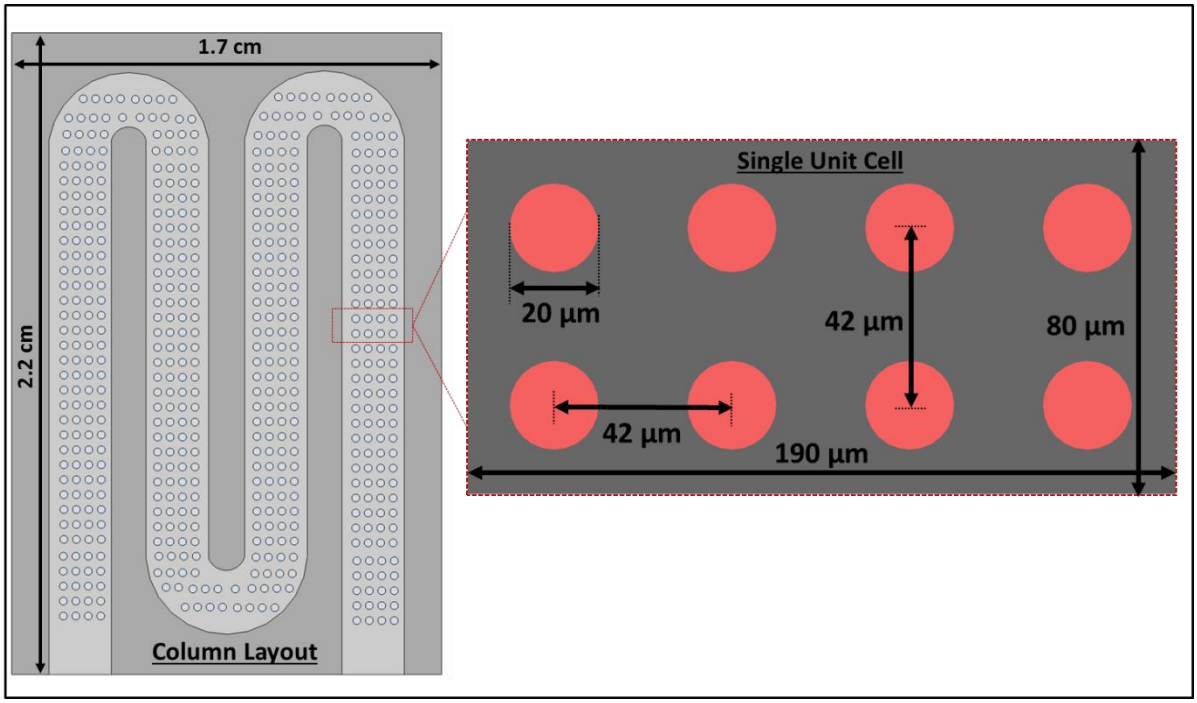

Figure 3.1: *Layout (top view) of a 1 m-long semipacked column showing critical dimensions.*

mass oxy-nitride semi-circular suspended columns [104], width-modulated rectangular columns [105], and SPCs with embedded micron-sized pillars [25, 37, 42, 99, 102, 106-108]. Among these designs SPCs, invented at Virginia Tech MEMS lab [37], have attracted considerable attention due to their improved separation efficiency, sample capacity, and speed of analysis compared to regular open channel columns.

Both static and dynamic gas-liquid phase coating methods [38, 51, 102], specifically tailored for microchip coating, have been successfully employed for silicon-glass microchannels. The work on micro-electro-mechanical-systems (MEMS) compatible gas-solid stationary phase coating methods has been the focus of continuous research during the last decade. Different research studies have demonstrated the separation capabilities of carbon nanotubes (CNTs) [40], sputtered oxides [24, 25, 106], atomic layer deposited alumina [42], silica nanoparticles (SNPs) [109, 110], and monolayer-protected-gold (MPG) [101, 103] based solid adsorbent films for silicon microcolumns. Briefly, Stadermann *et al*. [40], using chemical vapor deposition, integrated single-walled CNTs into a 100 µm x 100 µm channel to achieve ultrafast separation of four compounds in 1 second using fast temperature ramp rates. R. Haudebourg *et al*. [24] employed a wafer-level sputtering mechanism to coat thin films of different adsorbent materials (silica and graphite) into SPCs (100 µm-deep channel and 10 µm x 10 µm square micropillars) for oilfield applications. Similarly, our research group has previously shown the separation capabilities of SNPs (coated using layer-by-layer self-assembly) [109] and wafer-level atomic layer deposited/silane functionalized alumina thin films [25] for different channel geometries. Furthermore, we have shown different microfabrication methodologies for depositing thin layers of gold inside high-aspect-ratio (HAR) microcolumns followed by a thiol functionalization step. In this article, we introduce a new high-yield metal patterning process for HAR structures, using a single layer positive photoresist (PR) and a three stage (anisotropic, plasma clean and isotropic) etching process to generate an undercut profile. Therefore, when metal is deposited, the film is discontinuous over the deep etched (>200 µm) micron-sized features enabling easy removal of PR and leaving behind a well-defined metal thin film. Two different gold deposition techniques are successfully demonstrated for 220 µm-deep SPCs, 1) a wafer-level electron-beam evaporation (physical vapor deposition), and 2) a LbL self-assembly of gold nanoparticles (GNPs). Compared to our previous effort for coating functionalized GNPs [111], this new LbL coating scheme was found to be highly stable under GC testing conditions mainly due to shorter coating steps (~3 min) and calcination at higher temperature. Moreover, comparatively our earlier work on self-patterned gold-electroplated columns with MPG phases required very high processing temperature (950 °C) and also afforded high fabrication complexity [41, 101]. The separation capabilities of the proposed gold coated/thiol functionalized SPCs are demonstrated with high-speed separation of an alkane

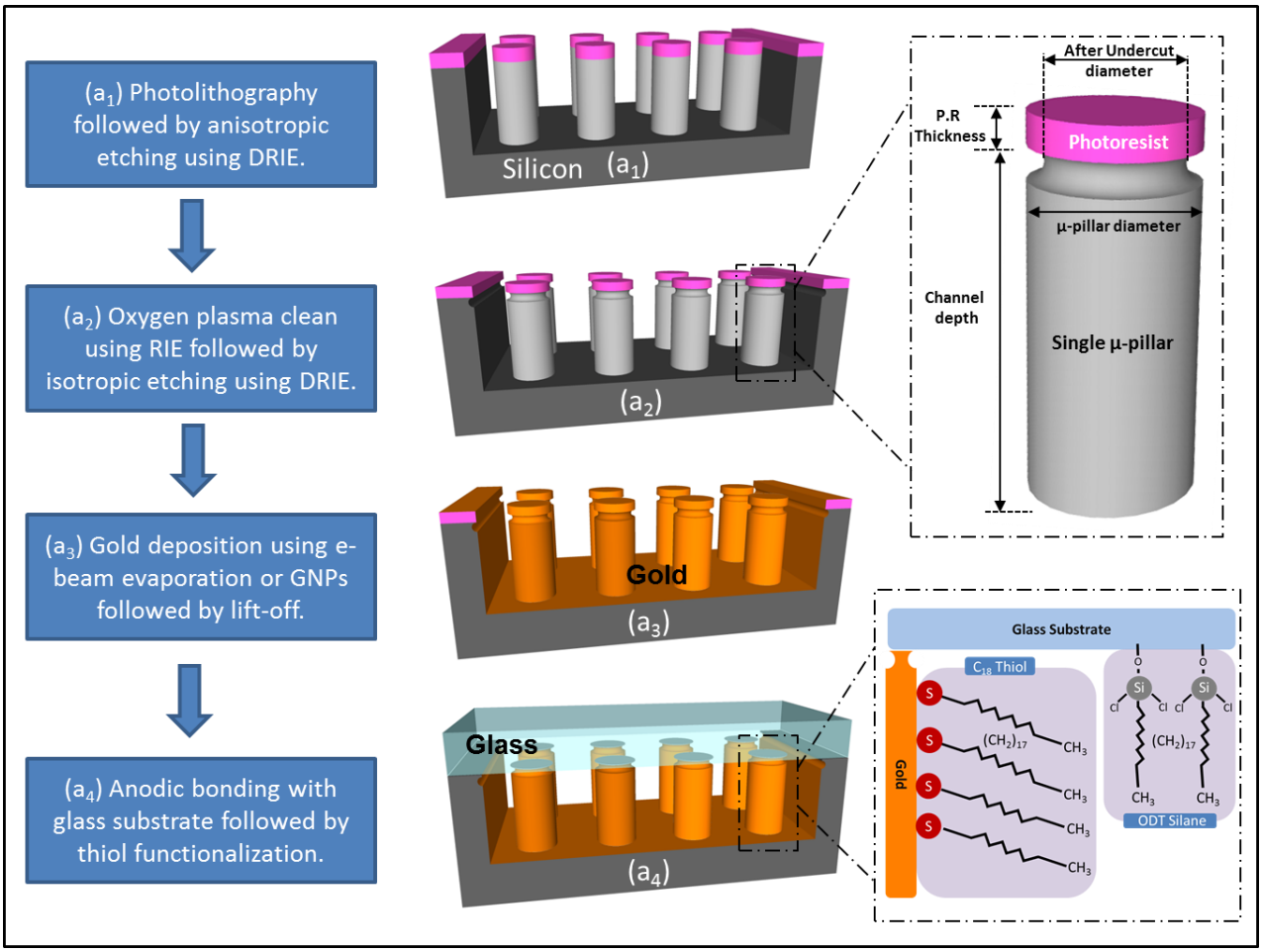

***Figure 3.2**: Process flow for the fabrication of semipacked columns with a three-step etching technique to produce undercut profile.*

mixture. Figure 3.1 shows the detailed column and microchannel layout profile of 1 m-long SPCs utilized for validating our newly proposed fabrication method.

I. Experimental

A. Materials and Regeants

Microcolumn fabrication took place on 4" silicon (500 µm thick, p-type, <100>, 0-100Ω-cm) and Borofloat® glass (700 µm thick ± 7 µm) wafers purchased from University Wafers and Corsix Precision Glass, respectively. Deactivated fuse silica glass capillary tubing (outer diameter 200 µm and internal diameter 100 µm), was obtained from Polymicro Technologies. A two part epoxy adhesive (MS-907) was purchased from Miller Stephson. All the chemicals used for GC testing (analytical standard with ≥ 99.8% purity), LbL coating (polycation polyallylamine hydrochloride (PAH), self-assembly (octadecanethiol) and glass surface deactivation (octadecyltrichlorosilane (ODTS) were obtained directly from Sigma-

Aldrich. Ultrahigh pure helium (>99.99%) was used as the carrier gas for all GC experiments and purchased from Air Gas Ltd, USA. Methane gas (99% grade) used for calculating column dead time,

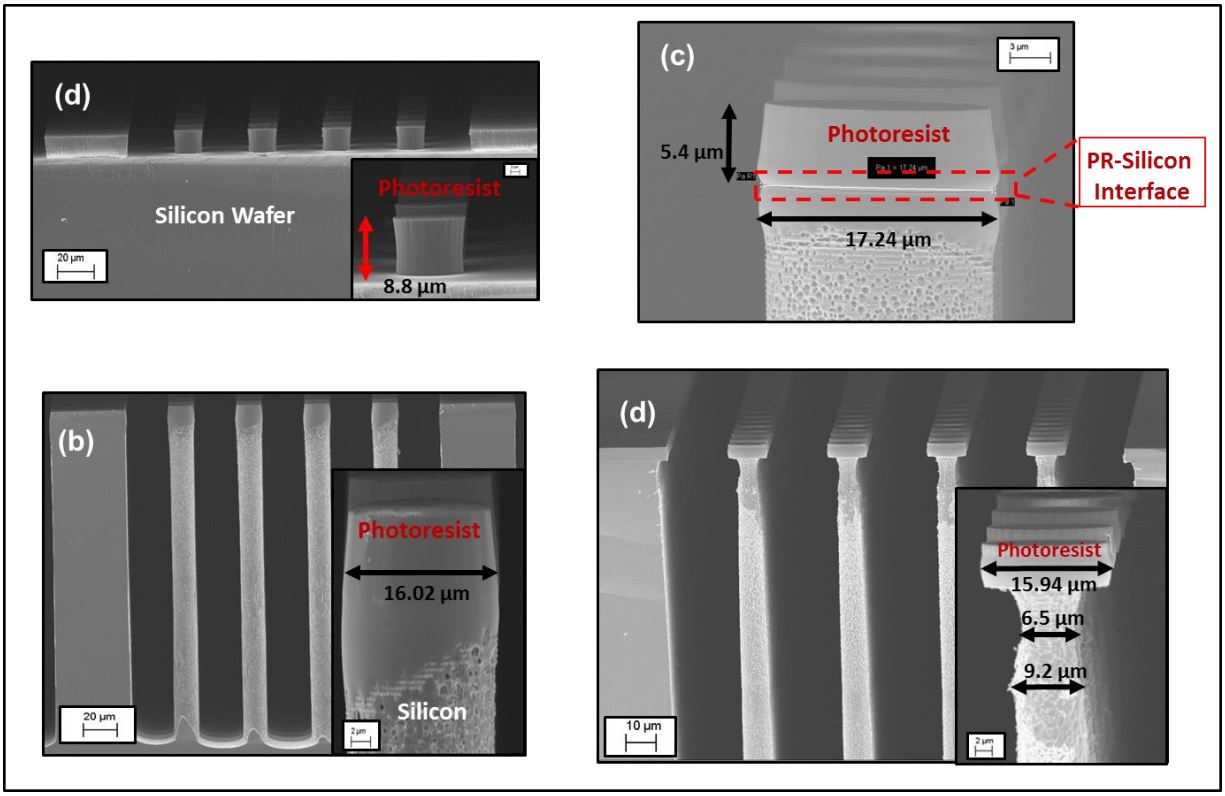

***Figure 3.3**: SEM micrographs of a device during different fabrication steps: (a) after lithography, (b) after anisotropic etching using DRIE, (c) O_2 plasma etch of passivation polymer in Trion RIE, and (d) under-etching of high-aspect ratio micropillars in DRIE using isotropic etching. Insets show the images at magnified scale.*

linear velocity, and capacity factors (k') was acquired from Matheson Trigas, Ohio. Gold nanoparticle suspension (MesoGold™, 3.2 nm average diameter and 20 ppm concentration in pure water) was purchased from Purest Colloid Inc.

B. Instrumention and testing

A bench-top Agilent GC system (7890) equipped with an autosampler (7359A), an electronic pressure controller, and a flame ionization detector (FID) was used for performing all the chromatographic tests. Both inlet and detector temperatures were maintained at 280 °C for all the tests.

C. Fabrication

The fabrication of a modified lift-off process for metal deposition and surface functionalization requires multiple stages and is illustrated step-by-step in Figure 3.2. This process can be broadly

categorized into column fabrication, thin gold film deposition (either e-beam or LbL), anodic bonding, and column functionalization.

1. Column Fabrication

The fabrication of microcolumns starts with a silicon wafer priming step using hexamethyldisilazane (HMDS); an adhesion promoter for the photoresist (PR), followed by substrate heating at 110 °C for 5 minutes. After which the HMDS-primed wafer is spin coated with a positive AZ® 9260 PR (i-line broadband PR by AZ Electronic Materials) at 500 rpm for 15 seconds and 2000 rpm for 1 minute. Following this, the PR-coated wafer is soft-baked at 110 ˚C for 90 seconds. This process is conducted to reduce the solvent content in the PR and further improve wafer adhesion with PR. Next the soft-baked wafer is exposed for 55 seconds using an ultra-violet light source with a mask aligner (Karl Suss, MA-6) system followed by development in an aqueous AZ400K (3:1) developer solution. In the proceeding step, the thickness of PR (~8.8 µm) is characterized with a surface profilometer (DekTak) and further verified through SEM imaging (Figure 3.3a). It is important to note that the wafer is not hard-baked after PR development; this is found to further improve the metal lift-off process. The three-step dry etching of SPCs is explained in detail below.

Table 3.1 *DRIE Etch Parameters (Anisotropic Etching at 0 °C)*

Gas flow rates	SF_6 = 300 sccm, C_4F_8 = 150 sccm
Gas pulse duration	SF_6 = 5 s, C_4F_8 = 2.2 s
Chamber pressure	$4.5x10^{-2}$ mbar
Source power	1800 W
Substrate holder (SH) generated power pulse	70 W (20 ms) 0 W (80 ms)

Anisotropic Etching*:* First, the PR-patterned wafer is anisotropically etched for 48 minutes at 0 °C in a deep reactive ion etching (DRIE) system (Alcatel AMS-100). This is conducted using a sequential flow of etch (SF_6) and passivation (C_4F_8) gases; known as a standard Bosch™ process under conditions mentioned in Table 3.1. Although the micropillars (µ-pillars) are designed with 20 µm-diameters (Figure 3.1), anisotropic etching results in a ~3 µm lateral etching eventually producing ~17 µm µ-pillars (Figure 3.3b).

Table 3.2 *RIE Oxygen Plasma Parameters*

Chamber Pressure	500 mT
Oxygen Plasma flow	98 sccm
ICP RF	250 W
RIE RF	50 W

Oxygen Plasma Etch*:* In the second step, the anisotropically etched silicon wafer is etched for 2 minutes (O_2 plasma, conditions mentioned in Table 3.2) using a Trion reactive ion etching (RIE) system to remove the passivation layer deposited on the etched surfaces during Bosch™ process. It is important to note that without this step, undercutting of silicon is not possible since all the vertical surfaces are covered with passivated polymer from the first step. Similarly, a low-powered RIE system is found to be more suitable compared to DRIE system for this step. Moreover, it has also been found during SEM imaging that the interface between PR and the top silicon surface is also cleared from residual PR/passivation polymer as shown in Figure 3.3c. This helps in achieving the required undercut. It is important to mention here that a single wafer was also fabricated by terminating the process at this point but no improvement in metal lift-off was observed.

Table 3.3 *DRIE Etch Parameters (Isotropic Etching at 0 °C)*

Flow rate SF_6	300 sccm
Chamber pressure	$4.5x10^{-2}$ mbar
Source power	1800 W
SH generated power pulse	50 W (10 ms) 0 W (90 ms)
SH Position from the source	200

Isotropic Etching: In the last step, the undercutting of HAR microstructures is carried out using an isotropic etch recipe with a fluorine based chemistry (SF_6) at 0 °C inside a DRIE chamber for 2 minutes. Table 3.3 shows etch conditions utilized for achieving the desired undercut. The overall thickness of the µ-pillar is further reduced by ~3 µm due to isotropic etching. The detailed etch profile after 3-dimensional undercutting is shown in the Figure 3.3d. Keeping the PR intact, thin gold film deposition is carried out in the next steps.

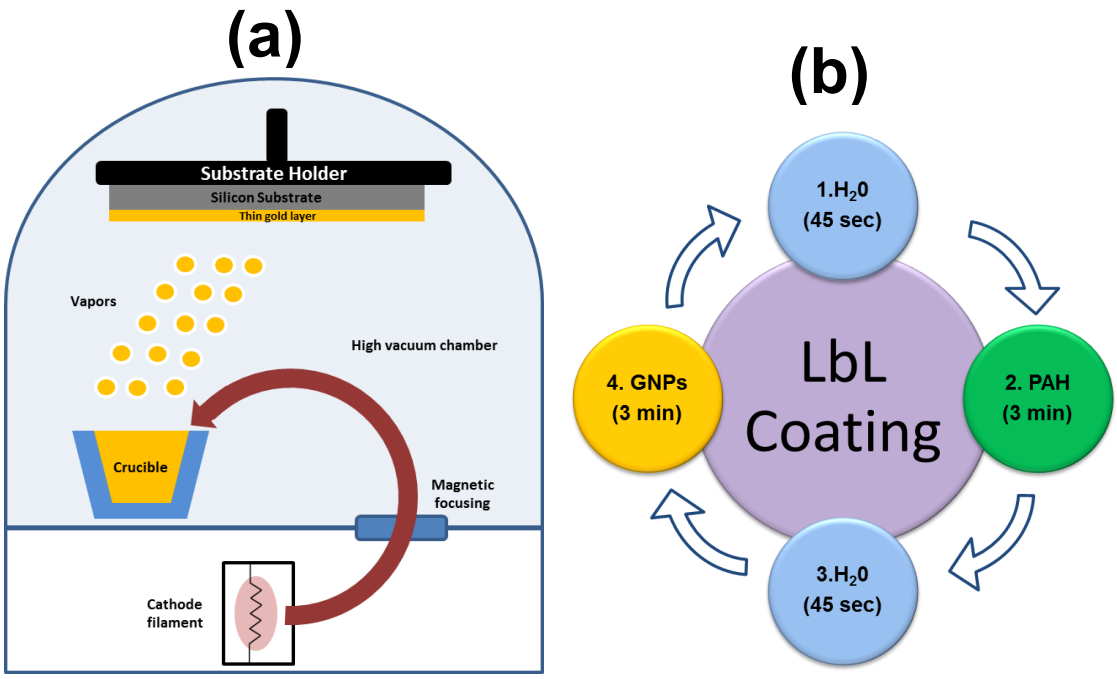

***Figure 3.4**: Schematics of (a) an e-beam evaporation system during wafer coating and (b) a LbL coating scheme for thin-gold film deposition using GNPs and PAH.*

2. Gold Film Deposition

The self-patterning of thin gold layers inside the etched SPCs is achieved by two methods, 1) a wafer-level physical vapor deposition (PVD) using an e-beam evaporation source, and 2) a device level LbL method using GNPs suspension (Figure 3.4). The details of each gold deposition method are provided below

E-beam Evaporation: The PVD deposition of the thin film starts with placing an etched silicon wafer on a rotating platen inside the PVD-250 (Kurt Lesker) chamber as shown in Figure 3.4a. In short, the chamber is pumped down to a base pressure of $3x10^{-6}$ torr. Then, an e-beam power source is turned-on and is directed towards the target (anode) with the help of magnetic deflectors. The high energy e-beam bombards the surface of the target material causing it to transform into a gaseous phase. This gaseous anode material nucleates on the surface of the wafer forming a thin film with the desired thickness. Since the adhesion of the gold layer to silicon is poor, a thin layer (~25 nm) of chrome is first deposited on the surface followed by 240 nm thin gold film deposition (1 Å /sec rate). After gold deposition, the metal lift-off process is accomplished by immersing the wafer into acetone followed by a short agitation (5 minutes) in a sonication bath. The average film thickness of the gold layer was found to be 239 nm (Figure 3.5).

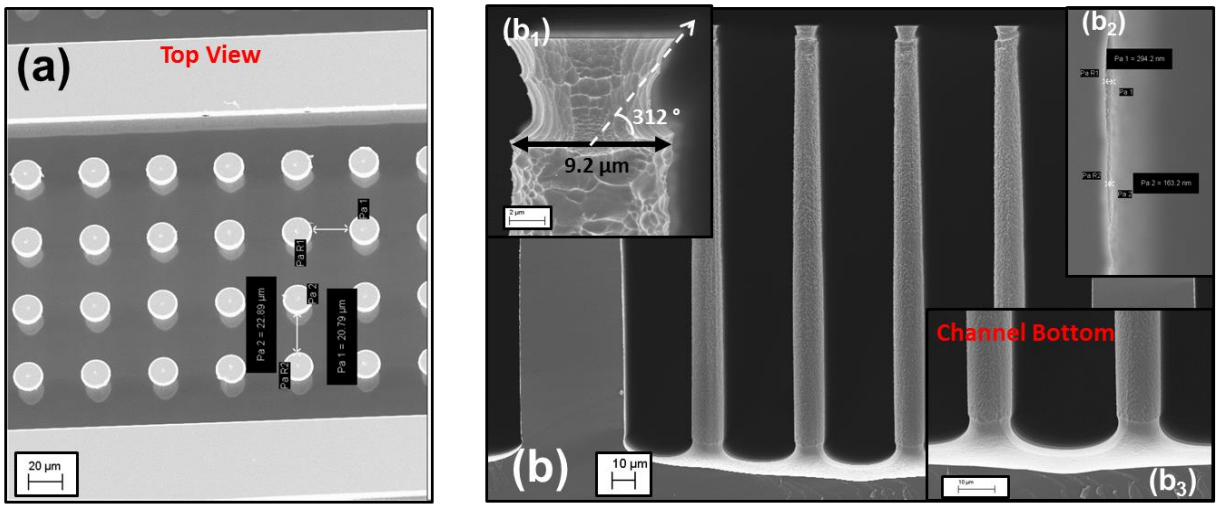

***Figure 3.5**: SEM micrographs of a microchannel after photoresist removal in acetone (a) top view and (b) channel cross-section. Inset (b_1) shows pillar-top at magnified scale, (b_2) shows gold thickness on sidewall and (b_3) shows slight undercut at the bottom of microchannel.*

LbL self-assembly of GNPs: For LbL deposition, the etched silicon wafer, with PR intact, is first diced into the individual devices. The GNP thin film is deposited via the LbL ionic self-assembly method recently demonstrated/optimized for µGC by our group with SNPs [109]. Each device is first attached to a glass microscope slide with a double-sided scotch tape and placed in an automatic dipping system (StratoSequence VI Robot, nanoStrata, Inc.). In the current scheme, the LbL coating starts by alternately immersing each device into an aqueous 10 mM PAH (pH= 4.0 ±0.1, stirred overnight) and GNPs colloid (used as received) solution for 3 minutes. Each coating cycle results in a single bilayer (BL) and is formed by an attractive electrostatic bonding of a positively-charged PAH layer and a negatively-charged GNP (-40 mV zeta potential) layer. A single 3 minute coating cycle of PAH or GNPs is followed by three 45 seconds rinsing steps in between using deionized (DI) water to remove any excess material coated during the prior step (Figure 3.4b). The process is terminated after the desired number of BLs are deposited inside the microchannel. In the current work, SPCs are coated with 30, 50 and 100 bilayers. After LbL coating, each device is first dried with a low flux nitrogen gas and dipped in acetone followed by sonication for 5 minutes to achieve the metal lift-off. Similar to our earlier studies, the devices were placed in an oven at 500℃ for 4 hours to burn the PAH, leaving behind only the evenly distributed GNPs coating with nanoscale roughness on the desired microsurfaces. The robustness of the newly developed scheme is validated by fabricating 12 gold-coated columns across different wafers producing a fabrication yield of ~91%.

3. Anodic Bonding and Functionalization

Following thin gold film deposition, each micro column is sealed with a Borofloat® glass substrate (400 ˚C, 1250 V, 45 minutes) using a custom made anodic bonding station. Approximately 30 cm-long glass capillary tubing is glued using Epoxy-907 to each port of the silicon-glass chip, providing a fluidic interface between the chip and GC oven.

Surface deactivation using silylating agents improves the inertness of the glass substrate and limits the residual activity of surface silanol (hydroxyl) groups to reduce the peak deformation/tailing during chromatographic separation. Similar to our previous findings to improve the peak symmetry, each microcolumn is first treated with a 10 mM octadecyltrichlorosilane (diluted in toluene) for 12 hours at room temperature [41]. Following glass deactivation, the self-assembly of octadecanethiol thiol on a gold surface is exploited to create a gas-solid stationary phase [72].

$$C_{18}H_{37}SH + Au^0 \xrightarrow{SAM} [C_{18}H_{37}S^- + Au^+] + {}^1/_2\, H_2$$

For thiol self-assembly, each column is filled with a 2 mM octadecanethiol ($C_{18}H_{37}SH$) in hexane, sealed at both ends using septa (made of high grade silicone) and kept at room temperature for 6 hours. Fig. 2 shows the chemical structure of both self-assembled C_{18} thiol on gold and ODTS on glass surfaces.

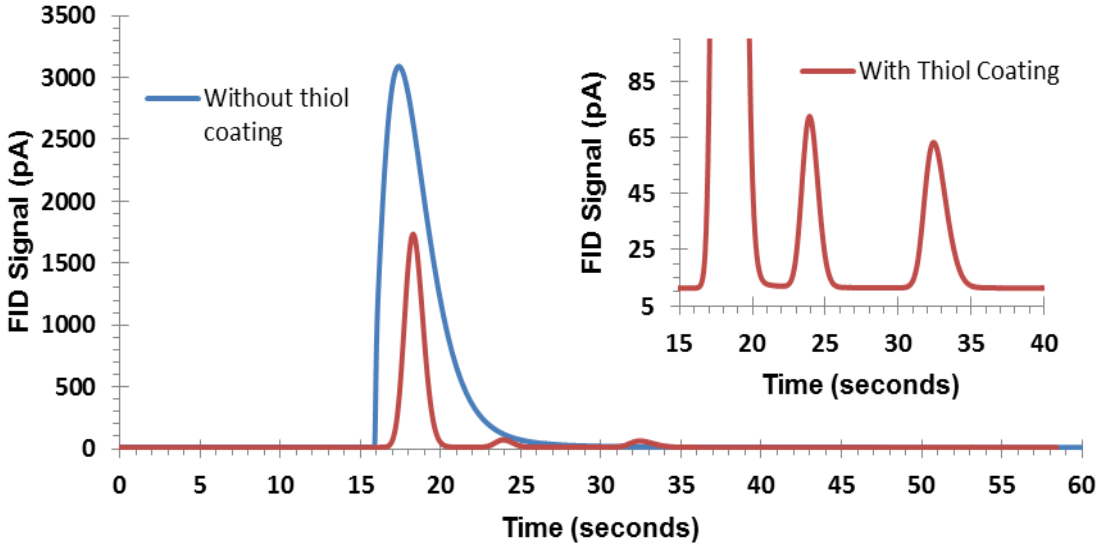

***Figure 3.6**: Separation performance of an uncoated and a thiol-coated GNPs column using n-nonane and n-decane (diluted in dichloromethane) as probes. Column tested at 50 ˚C, 5 psi head pressure, 200:1 split ratio, and 0.1 µL sample injection.*

II. Results And Discussion

The contribution of the gold films deposited using methods described in the last section is first tested before any functionalization steps. Figure 3.6 clearly demonstrates that GNP layer alone (evaporated gold film shows similar behavior but not shown) is inadequate for GC separations. Before performing any chromatographic separations on functionalized columns, each device is first purged with a constant flow of dry nitrogen for 30 minutes. Each chip is then connected to a conventional GC oven and slowly heated from room temperature to 150 ℃ (2 ℃/min) with a constant inlet pressure of 7.5 psi until a stable signal baseline is observed. Figure 3.6 also shows that SPCs with thiol functionalized GNPs (100 BLs) are able to separate a simple alkane mixture. It is important to note that 30 and 50 BL GNP columns performed poorly in comparison to those having 100 BLs due to incomplete coverage of the etched channels with nanoparticles. Therefore, only columns coated with 100 BL GNP were used for further GC analysis in addition to evaporated gold columns. The thickness of 100 BLs was measured to be ~300 nm using SEM

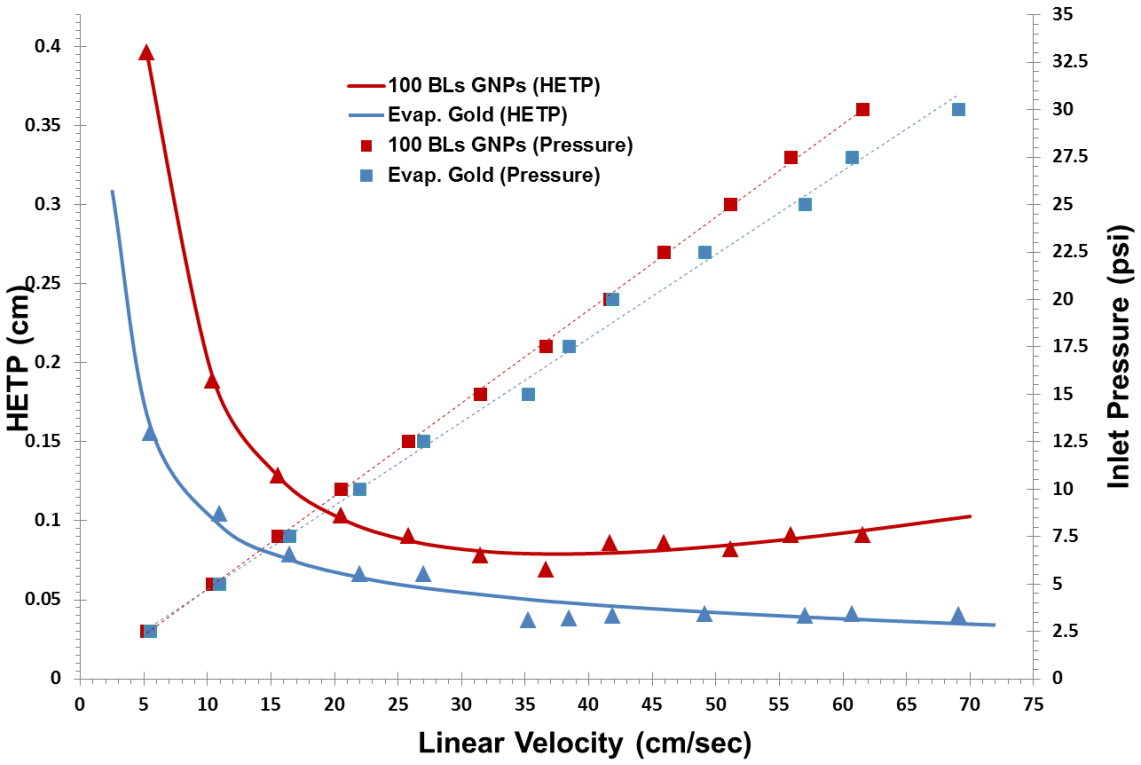

***Figure 3.7**: Golay plots of evaporated gold (blue) and GNPs (red) based SPCs using n-decane as a marker at isothermal condition with 0.1 µL sample injection and 200:1 split ratio (head pressure varied from 2.5 psi to 30 psi). Triangular markers represent HETP (solid lines) values, while square markers represent pressure (dotted lines). The error bars in the plot are smaller than symbols therefore they are omitted (sample size 3).*

(not shown).

A. Column Performance

In this work, both kinetic and thermodynamic properties of microfabricated columns with thiol phases are evaluated using Golay and Van't Hoff plots. The kinetic performance of the separation columns is typically evaluated using a metric known as a height-equivalent-to-a-theoretical-plate (HETP). The Van Deemeter equation (1) theoretically relates different sources of column peak band broadening to HETP (cm) [112].

$$HETP = A + \frac{B}{\bar{u}} + (C_s + C_M).\bar{u} \qquad (3.1)$$

Here, $\bar{u}$ (cm/sec) is the average linear carrier gas velocity. The A (cm) term, arising due to eddy diffusion or multiple paths, is only significant in packed columns and has minimal effect for SPCs properly designed with uniform gas flow paths [37]. The B (cm^2. sec^{-1}) term reflects the molecular diffusion of solute molecules in the carrier gas. The C_S and C_M (sec) terms represent the resistance due to mass transfer in stationary and mobile phases respectively. The HETP is typically calculated experimentally from a chromatogram using relationships (3.2) and (3.3) [112]

$$HETP_{eff} = \frac{L}{N_{eff}} \qquad (3.2)$$

where, L is the length of the column and N_{eff} is the effective plate number, taking into account dead volume in the column and evaluated using [112]

$$N_{eff} = 5.546 \times \left(\frac{t_r - t_M}{w_{1/2}}\right)^2 \qquad (3.3)$$

where t_M is known as the dead or hold-up time calculated from an unretained methane peak, t_r is the retention time and $w_{1/2}$ is the peak width at half the height of a selected solute probe, typically a straight chain alkane. It is necessary to account for the dead time in calculating efficiency (plate number) for microcolumns, especially with very narrow widths and comparable lengths of interfacing capillary tubing resulting in a large dead volume. Figure 3.7 shows Golay plots of both GNPs and evaporated gold SPCs, generated using n-decane as a probe under isothermal conditions (35 °C, 0.1 µL injection volume, split ratio 200:1). The optimum linear carrier gas velocity of 37 cm/sec is calculated providing a minimum

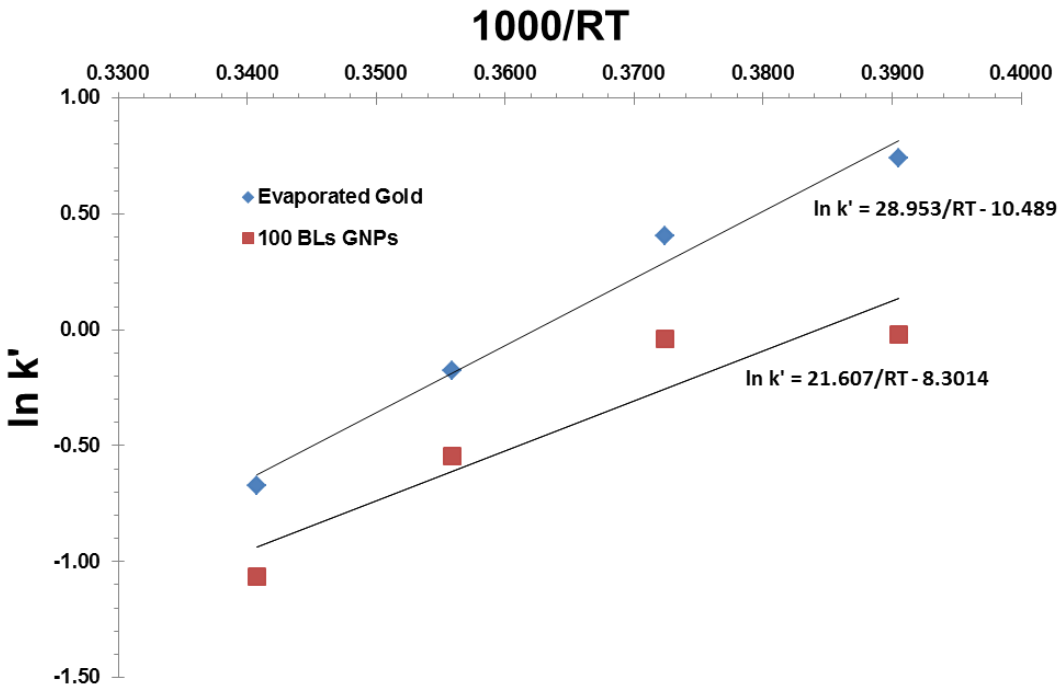

***Figure 3.8**: Thermodynamic properties of thiol functionalized evaporated gold and GNPs coated SPCs using Van't Hoff plots. n-decane is used as a probe with each column tested from 35˚C to 80˚C at 7.5 psi head pressure. Methane vapor is used to calculate the dead times/capacity factors (k') corresponding to different temperatures with $R = 8.314\ J/K \bullet mol$. The error bars in the plot are smaller than symbols therefore they are omitted (sample size 3).*

$HETP_{eff}$ value of 0.0376 cm (evaporated gold). It is desirable to operate columns above optimum linear velocities in order to reduce the analysis time. The flatness of the HETP curve above optimum linear velocities, a characteristic of SPCs, shows that there is small loss in separation efficiencies when operating the columns at high velocities. Moreover, the flatness of the curve at higher velocities demonstrates that the effect of mass transfer terms (C_s and C_M) is smaller than the B term, which is desirable for high speed operations. Figure 3.7 also shows a linear correlation between the inlet/head pressure and the corresponding calculated linear carrier gas velocity. Both gold-thiol coatings were found to be highly stable under GC testing conditions (maximum pressure of 30 psi and temperature up to 175 °C) and after multiple sample injections (200).

Thermodynamic properties of thiol functionalized gold films were evaluated using Van't Hoff plots (Figure 3.8) and equation 3.4

$$\ln k' = -\frac{\Delta_r H^\theta}{RT} + \frac{\Delta_r S^\theta}{R} \qquad (3.4)$$

Where k' is the capacity factor (retention factor), $|\Delta_r H^\theta|$ is the standard adsorption heat, R is the gas constant, T is temperature, and $|\Delta_r S^\theta|$ is the standard entropy term. The plots, generally linear ($R^2 > 0.87$ and R^2>0.96), are generated between 35 ℃ to 80 ℃ using n-decane (diluted in dichloromethane) as a probe and dead-time is yet again calculated from an unretained methane vapor. From the Van't Hoff plots, the values of the standard adsorption heat for evaporated gold ($|\Delta_r H^\theta| = 28.95\ k \bullet J/mol$) column is close to that of a 100 BLs GNPs ($|\Delta_r H^\theta| = 21.60\ \ k \bullet J/mol$) coated SPCs meaning evaporated gold coated columns retain slightly better than GNPs and thermodynamically very similar. It is important to note that the adsorption forces such as Van der Waal forces associated with $|\Delta_r H^\theta|$ are dominated gas separations compared to the entropic forces. These values are lower than that calculated for CNTs ($|\Delta_r H^\theta| = 46.2\ k.J/mol$) [40] based coating also using n-decane as a marker. This means that the retention of gold-thiol based stationary phases is lower than that of CNTs based phases. The higher retention of CNTs could be attributed to the higher surface area of nanotubes due to the height (1.7 µm) of a nanotube mat. The retention of gold-thiol coating could also be improved further by increasing the thiol coating time from 6 hours to 12 hours or more. The evaluation of thermodynamic properties of a newly developed stationary phase film is critical especially to compare its adsorption properties with already developed coatings. The outcome of this study could also be used for optimizing the ramp rate during temperature program runs [40].

B. Chromatographic Separations

The separation capability of both functionalized gold phases is evaluated using a simple straight chain alkane mixture. Since the separation behavior of both phases are very similar, only results of evaporated gold coated SPCs, showing better rentention than GNPs coated devices, are presented here. It has earlier been reported that C_{18}-thiol based phases are able to only selectively resolve straight chain alkane based mixtures [41]. Threfore, only straight-chain alkanes are used for GC separations. In order to show the significance of using SPCs, the mixture is tested at three different carrier gas velocities (16 cm/sec, 37 cm/sec and 70 cm/sec) as shown in Figure 3.9. Moreover, the peak-to-peak resolution (R_S) between adjacent analyte peaks is also evaluated using [112]

$$R_S = 2 \times \left(\frac{t_{rb} - t_{ra}}{w_{rb} + w_{ra}}\right) \qquad (3.4)$$

where, t_{ra} and t_{rb} correspond to retention times and w_{ra} and w_{rb} represent the peak widths at base of corresponding compounds a and b. From Figure 3.9, it is clear that SPCs operating below optimum carrier

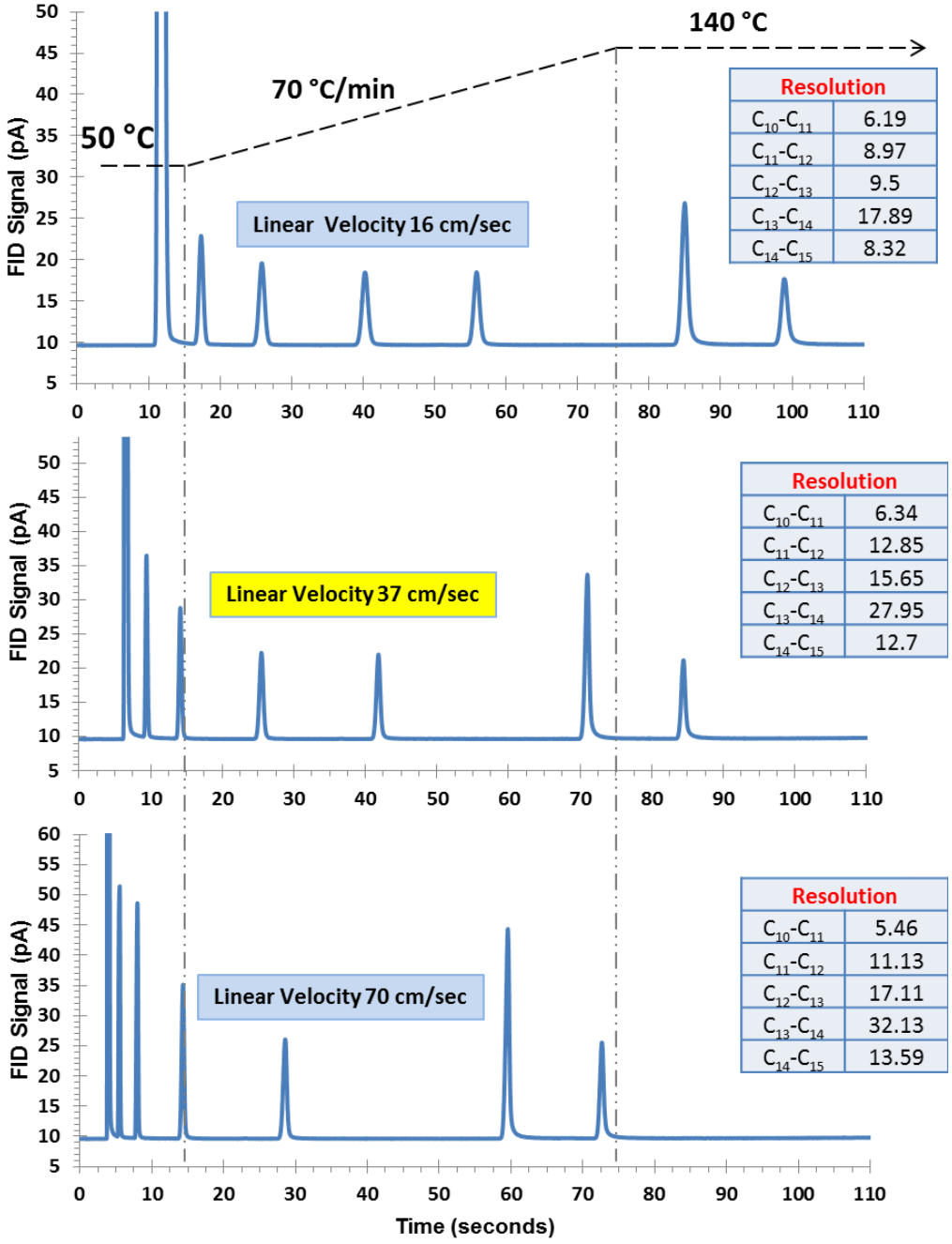

***Figure 3.9**: Separation performance of an evaporated gold coated/thiol functionalized column at three different linear velocities, 37 cm/sec (optimum), 17 cm/sec (below optimum) and 70 cm/sec (above optimum). Compound indentification (in order of elution), dicholoromethane, n-decane, n-undecane, n-dodecane,n-tridecane, n-tetradecane and n-pentadecane. Temperature programming curves are superimposed on each chromatogram. GC testing performed under a constant flow mode.*

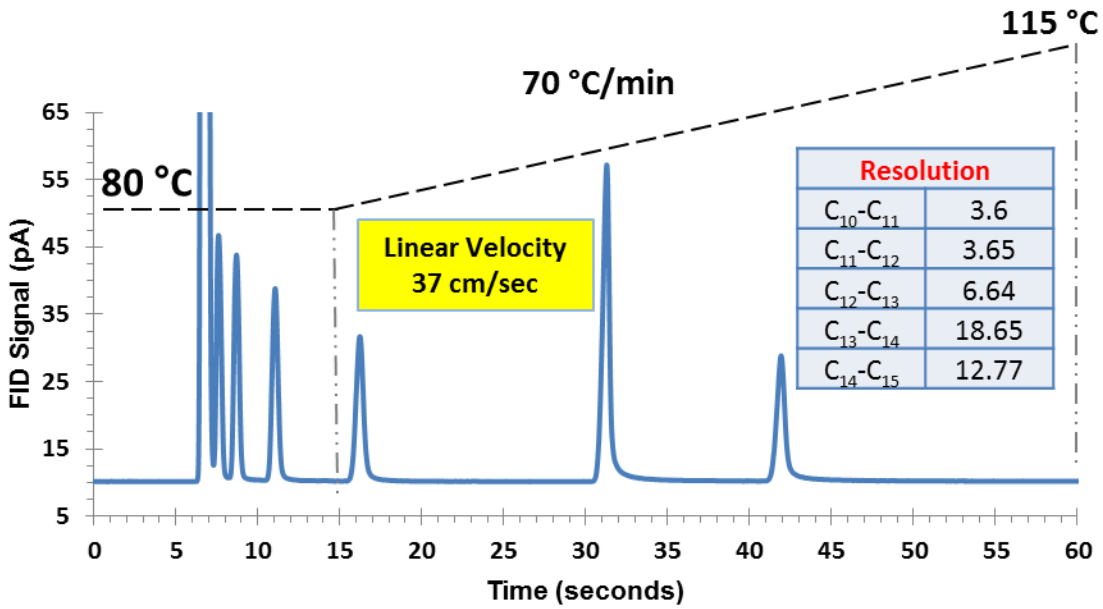

***Figure 3.10**: Separation performance of an evaporated gold coated/thiol functionalized column at optimum linear velocity (37 cm/sec) at higher initial temperature 80 ˚C. GC testing performed under constant flow mode.*

gas velocity take 100 seconds to complete the separation, while at higher linear velocity (70 cm/sec) the separation is completed within 75 seconds. Moreover, all the peaks are baseline separated ($R_S > 1.5$) with loss of resolution between the first few peaks being relatively small. In order to further reduce the analysis time, without significantly effecting peak-to-peak resolution, the initial operating temperature of SPCs is increased from 50 ˚C to 80 ˚C. Figure 3.10 shows that the separation of the same mixture could be achieved within 45 seconds with baseline resolution, thus significantly reducing the total analysis time.

III. Conclusion

In conclusion, we present improved gold-thiol coating schemes for SPCs. The proposed fabrication method is validated for both evaporated gold and thin GNPs films (deposited using LbL self-assembly). The chromatographic performance of thiol functionalized evaporated gold and 100 BLs of GNPs thin films is found to be comparable, with evaporated gold coated columns demonstrating slightly better separation efficiencies. Moreover, thermodynamically both phases show similar behavior with evaporated gold film showing slightly better retention. Fast analysis (45 seconds) for high boilers is achieved utilizing the proposed scheme for evaporated gold SPCs. We envision that this newly developed method could also be employed for patterning thicker stationary phase films (up to 1 µm) inside deep channels (≤ 250 µm).

Chapter 4: Highly Stable Surface Functionalization of Microgas Chromatography Columns Using Layer-by-Layer Self-Assembly of Silica Nanoparticles

(Part of this chapter reproduced from [22] with permission from ACS Analytical Chemistry)
D. Wang, H. Shakeel, J. Lovette, G. W. Rice, J. R. Heflin, and M. Agah, "Highly Stable Surface Functionalization of Microgas Chromatography Columns Using Layer-by-Layer Self-Assembly of Silica Nanoparticles," Analytical Chemistry, vol. 85, pp. 8135-8141, 2013.

Due to recent advancements and emergence of microelectromechanical systems (MEMS), energy-efficient integrated micro gas chromatography (μGC) systems have attracted considerable attention. This system upon complete realization could expand the range of applications for real-time and rapid on-site analysis at a lower cost [51, 53, 55, 113-119]. As a key component in μGC systems, conventional meters-long separation columns are necessarily replaced with microfabricated silicon columns on the order of a few cm^2. The separation ability and efficiency of the columns are directly related to the quality of the stationary phase. Using conventional coating techniques on microfabricated columns (e.g. dynamic or static coatings of functionalized polysiloxane polymers), especially for high-aspect-ratio (HAR) rectangular-shaped capillary channels, present major challenges towards obtaining stable, reproducible and uniform coatings [120].

There have been progressive research efforts toward the development of coating techniques that yield chemically inert, thermally stable1, selective and robust stationary phases. Specifically, nanotechnology based phases have opened up countless prospects for applications in conventional as well as microfabricated separation columns with nano-scale controllability, simplicity and flexibility [121, 122]. Recently, carbon nano-tubes [123, 124] and thiol-encapsulated gold nano-particles [4] have been utilized for gas chromatography (GC) separations. Our group has reported on the capability of thiol monolayers on electrodeposited gold surfaces as a stationary phase for microfabricated columns by combining nano and micro fabrication techniques [101, 103].

The excellent adsorption properties of silica for organics has long been demonstrated as a stationary phase medium for conventional columns (silica gel, celite) [125] and more recently by employing the MEMS compatible sputtering technique for microfabricated columns [25]. SNPs, due to their small and uniform size, high surface area, chemical inertness and thermal stability, are excellent candidates for stationary phases. SNPs have also been dispersed separately in ethanol and ionic liquid (IL) solutions for conventional capillary columns using static coating methods [5]. The SNPs-IL phase was reported to offer superior separation capability due to complete coverage of the inner capillary wall surface.

Developed first in 1991 [126, 127], the LbL method was used to fabricate ionic self-assembled multilayers thin films, which have been used in a wide range of applications including electromechanical

actuators [128-132], chemical and biological sensors [133-139], optical [5, 140-143] and electrochromic devices [144-150]. In short, by alternately immersing the substrate into two aqueous solutions of oppositely-charged materials, LbL thin films of the two materials are electrostatically bound together and can be built up to very large numbers of multilayers (a pair of such layers is referred to as one bilayer). Thorough rinsing in between each deposition step washes away excess material from the previous stage while leaving enough surface charge for the next material to be electrostatically deposited. Thus, uniform, dense, and robust stacks of layers can be deposited on the surface of the substrate with a wide variety of configurations. A desired film thickness can be achieved by simply terminating the procedure after a certain number of bilayers (BLs). Carbon nanotubes [151, 152], gold nanoparticles [153] and SNPs [154, 155] have been deposited via LbL assembly on flat as well as etched microfluidic surfaces [156, 157] for diverse nanotechnology-driven applications.

We present here the utilization of SNP-based stationary phases for µGC columns using LbL self-assembly that affords homogeneous and controllable film thickness. Both 1m-long micro single capillary columns (µSCC) and 25-cm long micro multi-capillary columns (µMCC) can be coated with ease. It is important to note that µMCC with very narrow widths and parallel channels provide high sample capacity, high separation efficiencies and rapid analysis times [2, 158]. Moreover, with the relatively simple concept and straightforward process, LbL assembly could be conveniently incorporated into the parallel manufacturing of silicon-based µGC devices.

I. Materials and Reagents

Single side polished silicon wafers (4 inch, 500 µm thick n-type) and double side polished (4 inch, 500

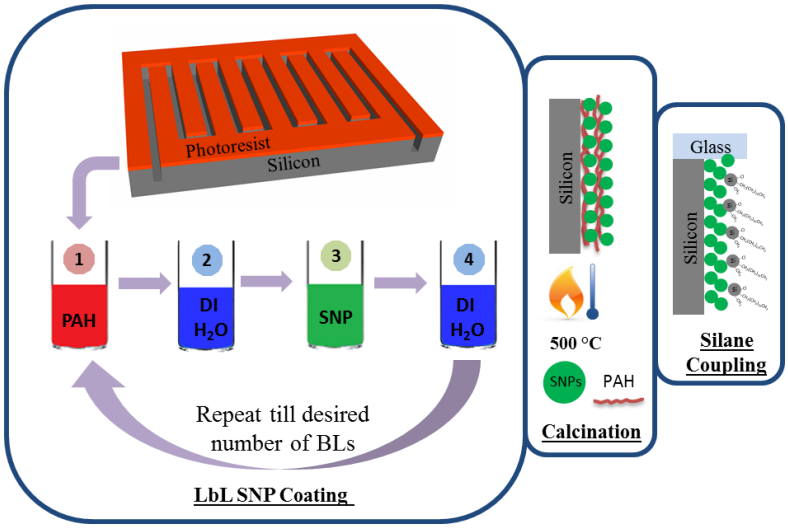

Figure 4.1. *Schematic process flow of SNPs coating using layer-by-layer self-assembly technique in the silicon channel.*

µm thick) Pyrex wafers used for sealing the microchannels were purchased from University Wafers. Fused silica capillary tubing (220 µm outer diameter, 100 µm inner diameter, Polymicro Technologies) was used for the microfluidic interface. SNPs suspension (45 nm average diameter, 20-21 wt. % in water) was purchased from Nissan Chemical. All chemicals including those used for chromatographic testing were of HPLC standard grade and purchased directly from Sigma-Aldrich. Ultrapure gases (>99.99%) including nitrogen and air were obtained from Airgas.

II. Fabrication

The fabrication scheme incorporating LbL self-assembled SNPs schematically shown in Figure 4.1 can be divided into four major steps, which include column fabrication, LBL deposition of SNPs, calcination and anodic bonding of the silicon substrate with Pyrex followed by deactivation of the silica surface.

A. Column fabrication

The fabrication of HAR 1 m-long, 150 µm-wide, 240 µm-deep µSCC and 25 cm-long, 30 µm-wide, 240 µm-deep µMCC with an array of 16 channels working in parallel start with anisotropic etching of plain silicon wafers using standard MEMS processes. In the first step, wafers are spin coated with AZ9260 photoresist at 3000 rpm, soft-baked at 110 ˚C for 1 minute and exposed for 45 seconds using a mask aligner (Karl Suss MA-6). After development using AZ400K, wafers are hard-baked at 110 ˚C for 2 minutes. Deep reactive ion etching (DRIE, Alcatel) with photoresist as the etch mask is used to etch the wafers in order to get the desired channel dimensions. Afterwards, the wafer is diced into individual devices. Selective deposition of nanoparticles inside the channels is achieved by using a liftoff procedure explained in the next section.

B. LbL deposition of SNPs

Keeping the photoresist intact, the LbL deposition of SNPs inside the HAR microfluidic channels starts with alternately dipping each device into a positively charged long-chain polymeric aqueous solution (10 mM polyallylamine hydrochloride, PAH), and then the negatively charged SNPs suspension. Because of the very narrow channels, the µMCC column deposition was performed using the SNPs suspension at one third of the original concentration (7 wt %) to prevent the formation of bulky nanoparticle structures between the channel walls. Following our earlier reported findings [159], the pH value of the PAH solution and SNPs suspension were adjusted to 7.0 (±0.1) and 9.0 (±0.1) respectively, by adding HCl and NaOH solutions to guarantee excellent PAH/SNPs LbL coating uniformity. The LbL coating is performed in an automatic dipping system (StratoSequence VI Robot, nanoStrata Inc.) in which every 2.5 minutes coating step with PAH and SNPs is followed by three 1 minute DI water rinsing steps (Figure 4.1). The attractive electrostatic interactions between negatively charged SNPs and positively charged PAH layer results in the formation of each bilayer. The LbL deposition scheme presented here affords a homogenous

SNPs coverage both on the interior microchannel surfaces and on the photoresist at the top of chip. After coating, the samples are rinsed thoroughly with deionized (DI) water and dried with low flux nitrogen. After deposition of the desired number of bilayers, the devices are then dipped in acetone and sonicated for 12 minutes. This liftoff procedure removes the SNPs deposited on the photoresist on top of the channel walls without removing the coating inside the channels. This is especially important for microfluidic applications in which the SNPs coated silicon channels are to be sealed with a glass substrate.

C. Calcination

Before anodic bonding with the pyrex cover plate, the devices are first calcinated (Figure 4.1) in a furnace

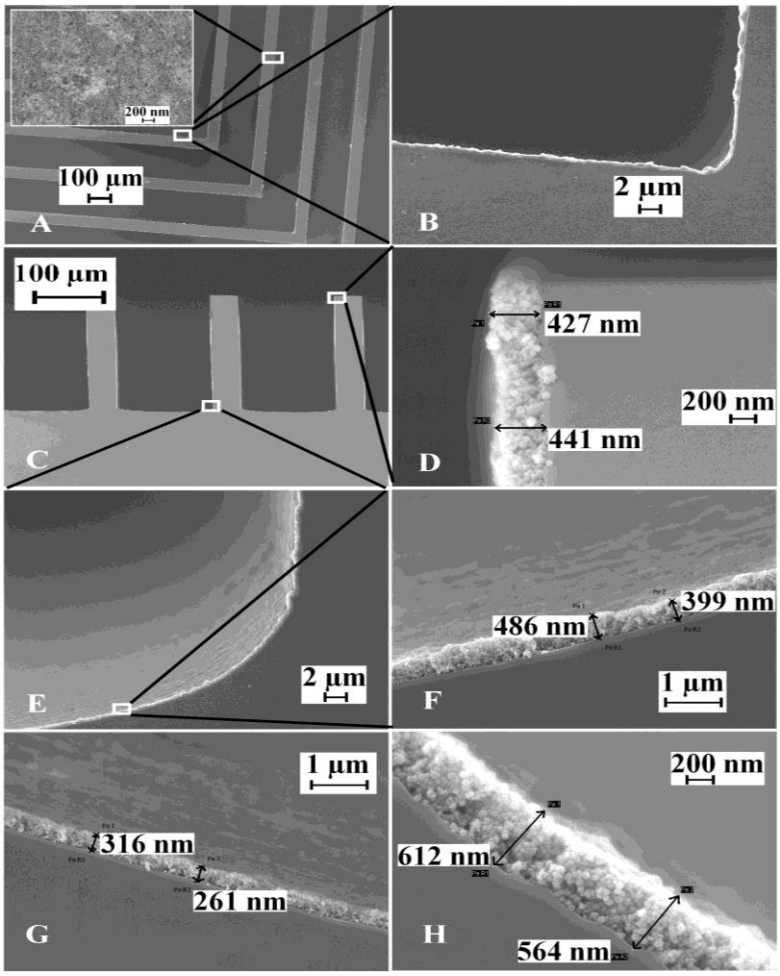

***Figure 4.2**. SEM images of the 10 BLs SNPs coated µSCC, top view and inset shows the coating on the bottom of the channel (A), coating on the sidewall viewed from top (B), cross-sectional view of channel with 10 BLs SNPs on the inner surfaces (C-F), top of the sidewall (D), bottom corner (E-F); 10 (F), 5 (G) and 15 (H) BLs SNPs coating with thickness value.*

at a high temperature (500 ˚C) for 4 hours to slightly fuse the SNPs together to ensure the stability of the coating during temperature programming of the GC columns while keeping the spherical shape of the SNPs intact. It has been reported that calcination of SNPs at higher temperatures can eliminate the binding polymer (PAH) and/or fuse SNPs together [160], resulting in a packed homogenous film.

D. Anodic bonding and silane-coupling

After calcination, SNPs coated silicon columns are sealed to a Pyrex wafer using anodic bonding at 400 ˚C and 1250 V. Deactivated capillary tubes are then installed at the inlet and outlet ports using epoxy. The presence of active silanol (hydroxyl) groups on the surface of silica and SNPs has been widely reported in the literature and are known to be detrimental to chromatographic performance. Deactivation of these groups using chlorosilanes has been shown to reduce peak broadening considerably. In this study, a 10 mM chlorodimethyloctadecyl silane **(**CDOS) solution in toluene was pumped into the chip by nitrogen (Figure 4.1) and allowed to sit overnight to deactivate the nanoparticles and glass surface [51]. The solvent was then removed by nitrogen prior to using the device for chromatographic analysis.

III. Characterization of SNPs Coating

To validate the simplicity, repeatability and robustness of the proposed stationary phase deposition technique, different HAR µGC column configurations (µSCC and µMCC-16) were coated using SNPs. The effect of the SNPs coating thickness on chromatographic separations was also evaluated by coating µSCC devices with 5, 10 and 15 BLs, respectively. The SEM micrographs (Figure 4.2 A-F) for the devices after calcination clearly show that the bottom and sidewalls of the trenches of µSCC are completely covered by SNPs of uniform film thickness. Moreover, the lift-off procedure successfully removed the SNPs from the top surface. The controllability of film thickness using the LbL approach is demonstrated by SEM micrographs of 5, 10 and 15 bilayers (Figure 4.2 G, F, H) deposited inside the silicon trenches, respectively. The thickness range measured on the surface inside the channel directly from the SEM at different locations were ~260 - 320 nm, ~400 - 490 nm, and ~560 - 610 nm for 5, 10, and 15 bilayers respectively. The range of each thickness (as high as a 20% deviation from the average thickness) is somewhat broader than what is typical for a commercial GC capillary coating (<5%). Nevertheless, this clearly demonstrates that film thicknesses are proportional to the number of coating steps and that the combination of microlithography and LbL self-assembly for selective SNPs deposition on the interior surfaces of µGC columns can readily be achieved.

In addition to wide channel (150 µm) µSCC, the LbL coating method was used on very narrow width channels (20 µm) inside µMCC configurations. It was observed that the original concentration used for µSCC (20-21 wt.% in water) resulted in bulky nanoparticle “bridges” between the sidewalls due to the narrow channel widths in µMCC, resulting in channel clogging (Figure 4.3C). The nanoparticle bridges

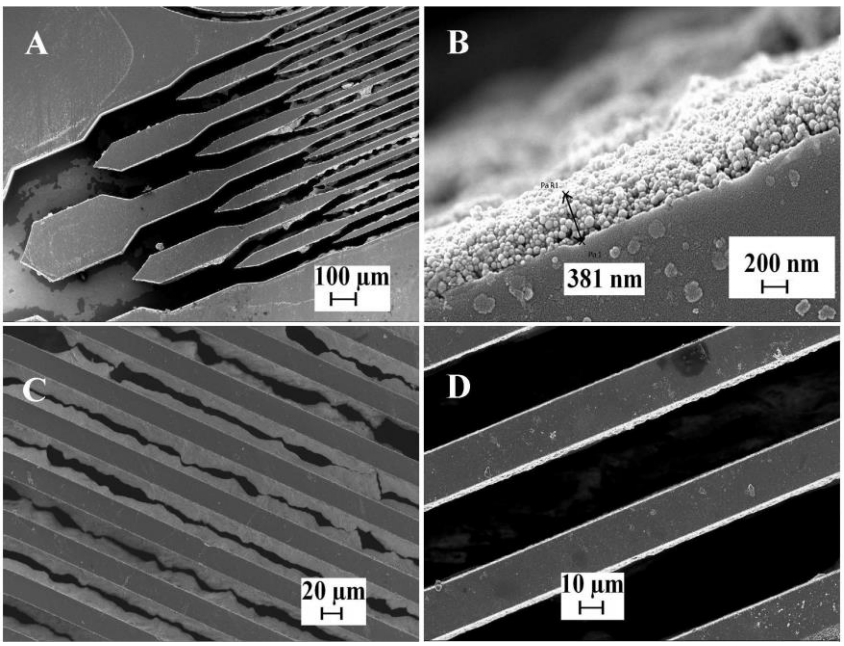

Figure 4.3. *SEM image of the inlet and 16 parallel channels of µMCC (A), and its cross-section with 10 BLs SNPs coating on the sidewall of silicon channel with thickness value (B). Coatings on the sidewall of multi-capillary µGC column using SNPs suspension with original (C) and 7 wt% concentration (D).*

were eliminated by reducing the original concentration of the SNPs suspension (Figure 4.3D) to 7 wt% relative to that used for the µSCC. Although a lower concentration of SNPs suspension was used, the 10 bilayers coating inside the microfluidic channels was approximately the same thickness (380 nm, Figure 4.3B) as the 10 bilayers coating inside the µSCC (Figure. 4.2F). This implies that the coating in SNPs suspensions at a lower concentration is sufficient to deposit a layer of SNPs over the previous PAH layer to neutralize and reverse the surface charge, while the excess SNPs during the µSCC coating with the higher concentration suspension are most likely washed off during the rinsing steps.

IV. Results and Discussion

A commercial GC system (HP 5890 Series II) equipped with an autosampler, electronic pressure controller, and flame ionization detector (FID) was used for characterizing the separation ability of the µGC columns coated with SNPs stationary phase. Highly purified nitrogen was used as the carrier gas. Inlet and detector temperatures were maintained at 280 ˚C with a split ratio set to 100:1. In order to evaluate the chromatographic performance, the functionalized µGC columns were placed in a conventional GC oven. All of the columns were first purged with dry nitrogen to remove any trapped oxygen in the system. Columns were conditioned gradually from ambient temperature to slightly above

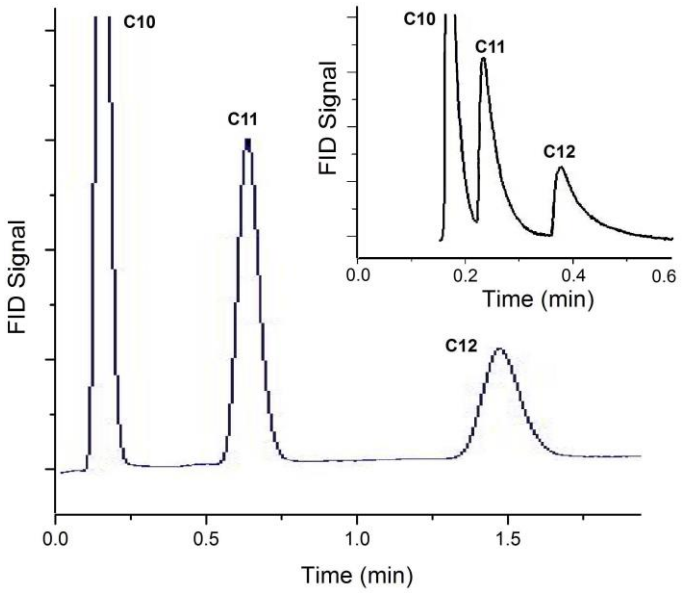

Figure 4.4. *Improvement in separation performance after silane deactivation of 10 BLs µSCC, inset shows column without silane treatment. Chromatographic conditions: 10 psi with 100:1 split injection ratio and 80 ˚C isothermal temperature.*

the maximum operating temperature (250 ˚C) of the column at a rate of 1 ˚C /min and a constant carrier gas flow of 7.5 psi until a constant baseline was observed. The maximum operating temperature of our microfabricated devices is simply limited by the epoxy seals currently used for the capillary connections.

A. Silane deactivation

The improvement in the separation performance from CDOS deactivation is illustrated in Figure 4.4, where a mixture of C_{10}, C_{11} and C_{12} was used to test the µSCC before and after silane-coupling. The µGC column treated with silane clearly generated sharper and more symmetric peaks. The CDOS was specifically chosen for the deactivation since the chlorinated end group readily reacts with active silanol groups on the SiO_2 surface to produce a covalent bond. The long non-polar octadecyl chain can also

Table 4. 1 Comparison of retention times (minutes) for three alkanes for 5, 10, 15 BLs SNPs coated µSCCs, and the same 10 BLs µSCC after conditioning.

	C 10	C 12	C14
5 BLs	0.01	0.05	0.92
10 BLs	0.07	0.46	1.48
15 BLs	0.11	0.68	1.65
2nd 10 BLs	0.08	0.49	1.55
Conditioned 10 BLs	0.05	0.30	1.40

enhance the column performance through interactions with the compounds being separated. Improvements in both chromatographic peak symmetry and baseline are also observed for columns subjected to the calcination process.

B. Separation Results

As a first step, the coating thickness for the reported µSCC was optimized using peak tailing/symmetry as a figure of merit. As discussed earlier, columns coated with 5, 10 and 15 BLs of nanoparticles provide different phase thicknesses (Figure 4.2). All three columns were able to successfully resolve alkane test mixtures. Table 4.1 illustrates retention times for three alkanes on each device. As expected, the thickest phase (15 BLs) provided the highest retention times. However, 5 and 15 BLs coated columns showed highly unsymmetric peaks, while the µSCC with 10 BLs had highly symmetric peaks. Additional characterizations from this point for deviations due to variations in fabrication processes, coating stability and separation capabilities were made with columns coated with 10 BLs SNPs. Deviations in fabrication processes were first considered, with ~10% variation in retention times observed for µSCC columns produced on two different wafers and coated with 10 BLs of SNPs (Table 4.1). The separation results of both devices closely resembled each other and had excellent peak symmetry. Similarly, the long-term stability of the SNPs coating under GC testing conditions was monitored by subjecting a 10 BLs coated µSCC to a conditioning process (constant flow at 7.5 psi at 160 ˚C for 24 hours). The SNPs based coating

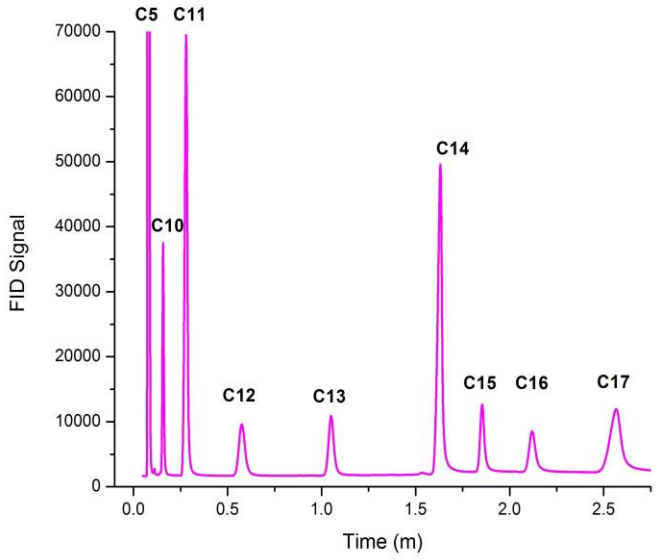

Figure 4.5*. Separation of nine straight chain alkanes using a 10BLs SNP µSCC. Chromatographic conditions: 10 psi with 100:1 split injection ratio and temperature* program (50 ˚C~120 ˚C at 70 ˚C/min).

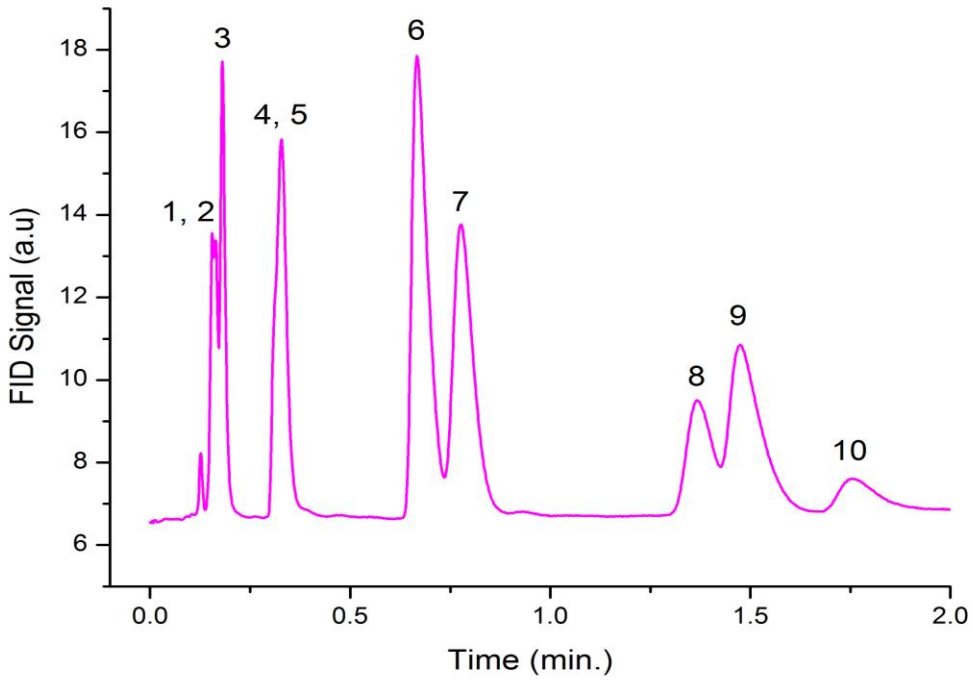

***Figure 4.6**. Separation of a ten component VOC mixture using a μSCC 10BLs SNP column. Chromatographic conditions: 10 psi with a 10:1 split injection ratio and temperature programing (30˚C-50˚C at 10˚C/min). Compound identification: 1. dichloromethane; 2. chloroform; 3. carbon tetrachloride; 4. dibromomethane; 5. tetrachloroethylene; 6. toluene; 7. chlorobenzene; 8. bromobenzene; 9. p-xylene; 10. 1, 1, 2, 2-tetrachloroethane.*

was found to have a good stable baseline after this accelerated testing with only modest differences in peak quality and retention times. This demonstrates the ability to produce stable, consistent and robust stationary phases with small deviations in column performance.

The separation capability of SNPs coating with 10 BLs for μSCC is successfully demonstrated using a series of alkanes (Figure 4.5) and a ten compound standard test mixture (Figure 4.6) containing a variety of commonly found volatile organic compounds (VOCs) to evaluate the resolving power of the SNPs columns. The chromatograms obtained from these columns had excellent reproducibility from multiple injections.

In order to validate our proposed scheme using narrow channel dimensions, the LbL fabricated SNPs coating was also used to functionalize a μMCC with modified SNP concentrations as previously described. Figure 4.7 shows a chromatogram obtained from the alkane test mix using a 10 BLs SNPs coated 16 channel μMCC that was also silane treated. The reason for the shift in baseline has not been determined, but it is clear that retention times are markedly longer and potentially provide for greater

separating capabilities. These results also indicate that these newly developed SNPs coating schemes should be applicable to other channel geometries and column configurations.

The figure of merit commonly used for column performance is height equivalent to a theoretical plate (HETP), where HETP=L/N, $N = 5.54 \times \left(\frac{t_r}{w_{1/2}}\right)^2$ (L being length of the column and N the number of plates in the column as determined experimentally from peak retention times (t_r) and widths at half the peak height ($w_{1/2}$)). To evaluate the efficiency of the SNPs functionalized µGC columns, the theoretical plate numbers were obtained over a range of column pressures using dodecane diluted in dichloromethane at 65 °C. The maximum plate numbers for the meter long µSCC and 25 cm-long µMCC columns were experimentally calculated to be 930/m and 4750/m respectively. The much larger plate number for the multi-capillary column is best explained by the narrower channels, which enhances interactions with the analytes and improves the overall capacity of the column. Plots showing the correlation of the inlet pressure to gas velocity and HETP versus gas velocity are shown in Figure 4.8. The linear velocity of the mobile phase was estimated from correlating the inlet pressure to the retention time obtained from methane injections, which was assumed to essentially be unretained. In addition to the much lower HETP values, the narrower channel µMCC provide relatively flat Golay plots over a broader range of flow rates compared to µSCC.

The static coating of SNPs in ethanol suspension, reported earlier for capillary columns [5], resulted in

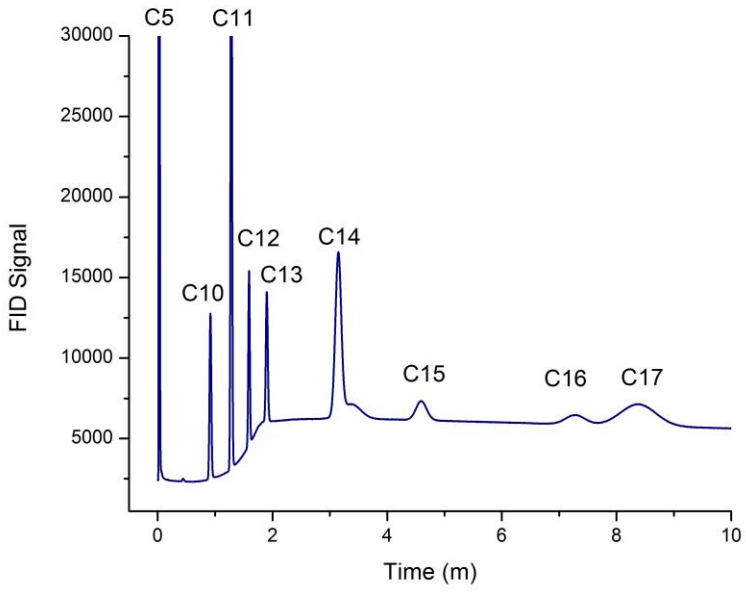

Figure 4.7*. Separation performance of a 16 channel µMCC functionalized with 10 BLs SNPs using the alkane test mixture. Chromatographic conditions: 10 psi with 100:1 split injection ratio and temperature program (50˚C-120˚C at 70˚C/min).*

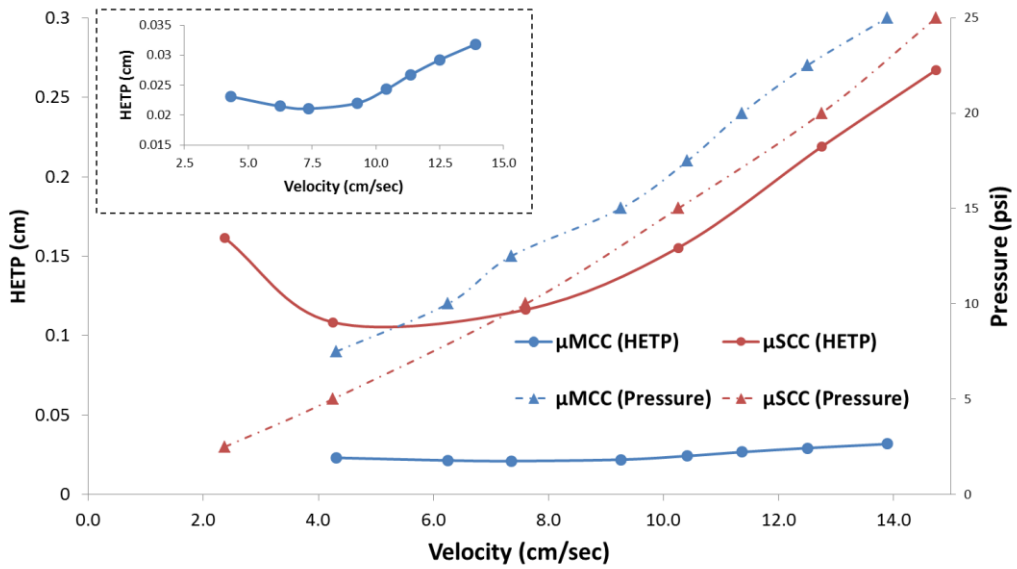

Figure 4.8. *HETP-gas velocity-pressure plots for µSCC and µMCC with 10 BLs SNPs coating. The dashed lines with triangle marker are plots of inlet pressure against gas velocity using methane vapor as an unretained marker. The solid lines with circular marker are Golay plots (HETP versus gas velocity). Inset represents the µMCC results at zoomed in scale.*

agglomeration of nanoparticles affording a non-uniform film. The effect of this non-uniformity was also demonstrated in poor chromatographic performance. In the same article, the authors integrated IL with SNPs to develop a uniform stationary phase (0.4 µm ~ 0.6 µm) with improved separation characteristics. Comparatively, our proposed 10 BLs SNPs coating scheme with a similar film thickness (0.4 µm ~ 0.5 µm) enables a homogeneous, stable, controllable and conformal stationary phase bed. Moreover, by incorporating calcination and silane deactivation, the chromatographic performance (especially peak symmetry) of our LbL technique is superior compared to reported static coating methods [5].

V. Conclusion

Homogeneous SNPs coatings of highly controlled thickness fabricated by the LbL technique have been incorporated into µGC separation columns and utilized as a stationary phase. With simple and parallel fabrication procedures, the LbL technique has shown the ability to generate a homogenous conformal SNPs coating with good nanoscale thickness control inside the µGC columns with different configurations. The µGC columns (both regular and multicapillary) with this stationary phase show good separation for alkanes with a wide range of boiling points with excellent consistency and repeatability. A more complex standard test mixture with ten VOCs was also successfully separated. This production

scheme results in high-yield and can be easily integrated into standard MEMS based fabrication processes. Moreover, the combination of unique properties of SNPs and facile coating procedures could also be applied to conventional GC columns. The next logical steps are to determine methods to reduce variations in the coating thicknesses as well as study the effect of size and shape of the SNPs on the chromatographic separations coupled with various chlorosilane functionalities.

CHAPTER 5: Width-modulated Microfluidic Columns for Gas Separations

(Part of this chapter reproduced from [105] with permission from IEEE Sensors Journal)
H. Shakeel, D. Wang, J. R. Heflin, and M. Agah, "Width-Modulated Microfluidic Columns for Gas Separations," IEEE Sensors Journal, vol. 14, pp. 3352-3357, 2014.

Gas chromatography (GC) is a versatile and widely acceptable chemical analysis technique based on the distribution of a sample between two immiscible phases (a stationary phase and a mobile phase). A typical GC system consists of a carrier gas (mobile phase), an injector, a separation column (with a fixed cross-sectional area) coated with a thin film (stationary phase), a detector, and a data acquisition system. Figure 5.1 shows the schematic representation of a bench-top GC system. The sample mixture is first introduced as a concentrated plug into the instrument (GC oven) through a heated injection port and carried through the separation column by an inert carrier gas (mobile phase). Afterwards the components of a

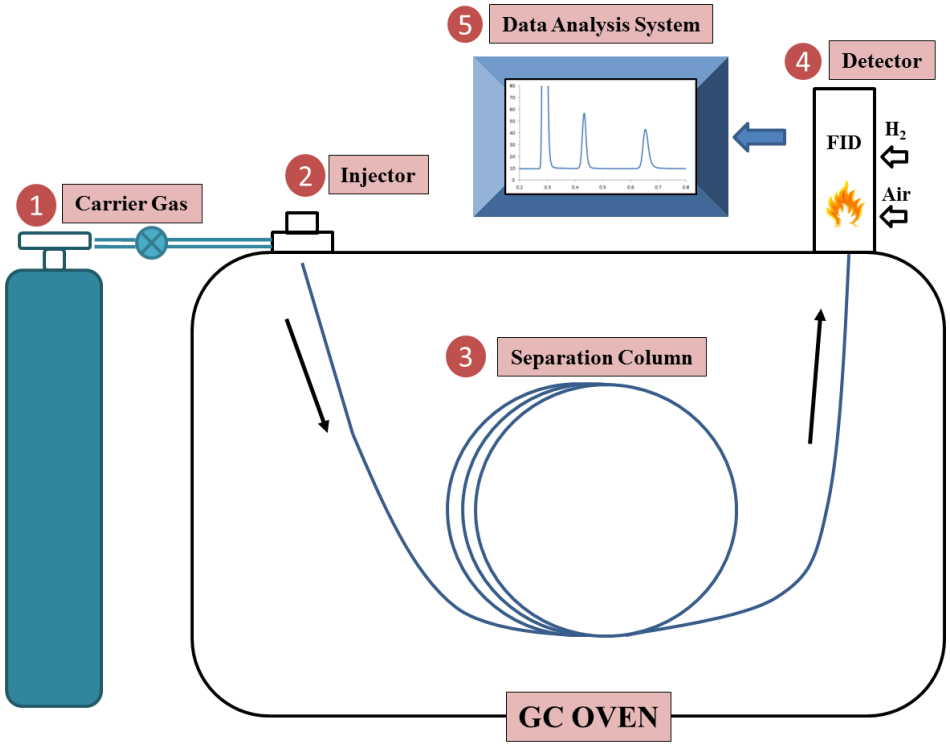

***Figure 5.1**: Schematic representation of a bench-top gas chromatograph.*

mixture are physically separated from one another by the separation column based on their interaction with the stationary phase bed. Next, the separated gas mixture along with a carrier gas enters the detector; that converts the chemical signal to an equivalent analog electrical output for measurements. Subsequently the data acquisition system plots the detector response against the time axis on a graph known as a

chromatograph. For a well-separated gas mixture each peak on the chromatograph corresponds to an individual constituent of a mixture.

Due to its reliability and low detection limits, GC has established itself in a multitude of fields (petrochemical industry, pharmaceutical sciences, biological sciences, and forensic analysis) for the identification and quantification of mixture components. Despite these well-defined advantages, conventional GC systems are large, expensive, power hungry and ill-suited for field applications. The emergence of microelectromechanical systems (MEMS) along with nanotechnology has enabled the miniaturization and performance enhancement of key GC components [21, 55, 78, 113, 117, 161-166].

Separation columns, being an integral part of the system, have also attracted significant attention and a number of prototype micro-GC (μGC) systems have also utilized silicon micromachined columns [91, 97, 167]. Typical MEMS-based separation columns have been designed with a fixed cross-sectional area, having either rectangular [19] or circular channel profiles [54], and are normally coated with polydimethylsiloxane based stationary phases [38]. Advancements in silicon micromachining techniques have enabled the introduction of novel column architectures in the last decade. Partially buried columns were introduced by A. Radadia *et al.* [34] to enable the uniform deposition of polymer based phases. Similarly, Agah *et al.* [33] introduced columns with suspended microchannels using low-mass oxynitride films to achieve high-efficiency separations. Moreover, in order to enhance key performance parameters like sample capacity, analysis time and separation efficiency, our group also previously introduced MEMS based narrow-width multicapillary [168] and semipacked columns having embedded micropillars [41, 169]. Additionally, innovative research work on deposition of non-traditional adsorbent based stationary phase coatings for rectangular microchannels has also been performed. This includes the integration of carbon nanotubes [40], self-assembled thiol monolayers [41, 168], silica nanoparticles [22] and MEMS compatible sputtered silica [25] thin-films inside the anisotropically etched channels.

As early as 1962, Purnell [170] suggested that gradual reduction in solvent-adsorbent interaction along the length of the column could effectively provide similar capabilities (shorter analysis times and improved sensitivity) as afforded by the programmed temperature or the programmed flow modes. This interaction could be minimized gradually by reducing either the stationary phase thickness or the column width. Although, effects of gradual reduction in stationary phase thickness have been theoretically studied and experimentally demonstrated [171], the effect of channel modulation on the separation process could not be materialized earlier due to fabrication difficulties. In this article, by employing a single lithography mask and a simple micromachining process, modulation in column width is achieved.

I. Theoretical Discussion

The efficiency of a chromatographic column is expressed in terms of either a theoretical plate number (N) or height-equivalent-to-a-theoretical-plate (HETP= $^{L}/_{N}$). As a general rule a high efficiency column has higher theoretical plates and less band-broadening (small HETP term). HETP could be further expanded to include the effects of diffusion in the mobile phase and mass-transfer in mobile and stationary phases. For the rectangular channels HETP is given by

$$HETP = \frac{2D_g}{\bar{u}} f_1 f_2 + \left[\frac{(1+9k+25.5\,k^2)}{105(k+1)^2}\ \frac{w^2}{D_g}\ \frac{f_1}{f_2} + \frac{2}{3}\frac{k}{(k+1)^2}\frac{(w+\mathrm{h})^2 d^2_f}{D_s \mathrm{h}^2}\right]\ \bar{\mathrm{u}} \quad (5.1)$$

where D_g and D_s are the binary diffusion coefficients in the mobile and stationary phase, $\bar{u}$ stands for the linear gas velocity, f_1 and f_2 are the Giddings-Golay and Martin-James gas compression coefficients respectively, k is the retention factor that is characteristic of a stationary phase, w stands for channel width and h for the channel height/depth [59].

To simplify the analysis, we ignore diffusion in the mobile phase (1st term) and also assume a very

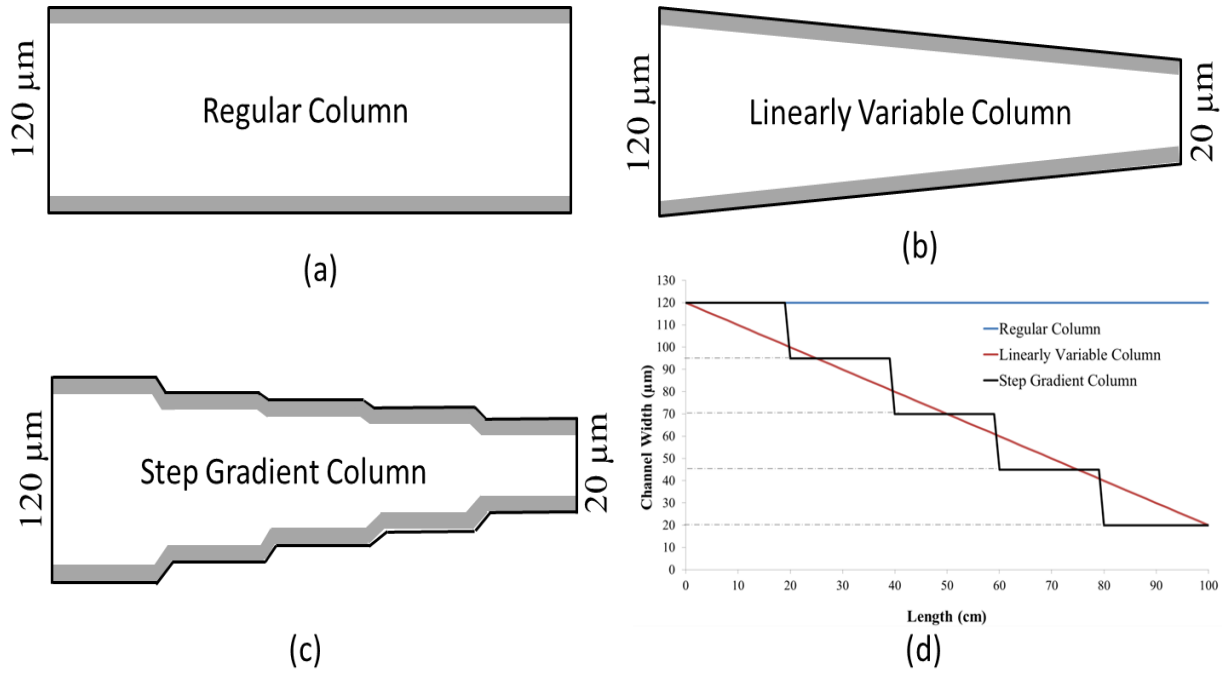

***Figure 5.2**: Channel profiles of 1 m long (a) regular, linearly variable (a) and step gradient columns. Figure (d) shows the plot for channel width versus channel length.*

thin stationary phase film (small d_f-term) therefore, we can neglect the contribution of band-broadening due to diffusion in the stationary phase (3rd term) in equation (1). The HETP becomes directly proportional to the square of column width

$$HETP \propto w^2 \qquad (5.2)$$

It is clear from equation (5.2) that columns with smaller width will provide efficient separations and column-width is one of the critical design parameters. Moreover, if the width of a column is gradually reduced along the length, then HETP will also decrease locally and effectively the overall HETP values will reduce. Therefore, in this article the modulation in width of the column is carried out and two new microfabricated width modulated column (µWMC) are introduced for the first time (Figure 5.2). The width of the linearly-variable-column (LVC) is modulated from 120 µm to 20 µm at 1 µm/cm (Figure 5.2b), and the step-gradient column (SGC) is modulated in 5 steps (120 µm, 95 µm, 70 µm, 45 µm and 20 µm) each with 20 cm length (Figure 5.2c). Moreover, for the step gradient column, the interconnections between the steps are gradually varied over the length of 700 µm. The separation capabilities of newly developed µWMCs are realized by utilizing our recently developed layer-by-layer (LbL) technique to get a highly-stable silica nanoparticle (SNP) stationary phase. Additionally, by shifting the stationary phase deposition step to occur after anodic bonding, multiple serially connected columns are coated

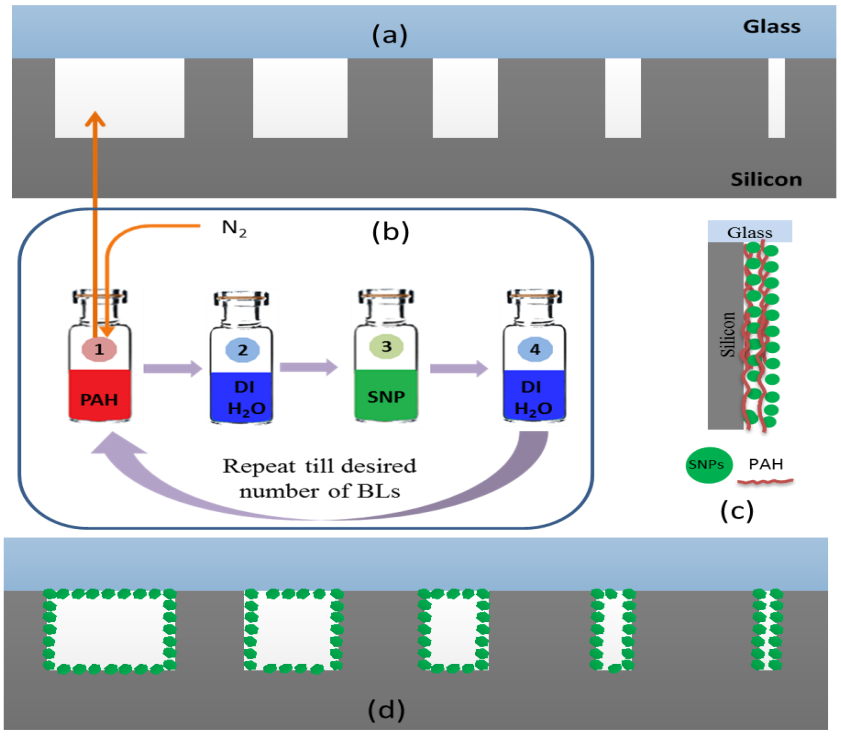

***Figure 5.3**: Process flow a) anisotropic etching followed by anodic bonding (b) LbL coating till 10 bilayers (BLs) using SNPs c) two BLs shown inside channel d) columns after calcination (500 °C) and silane coupling.*

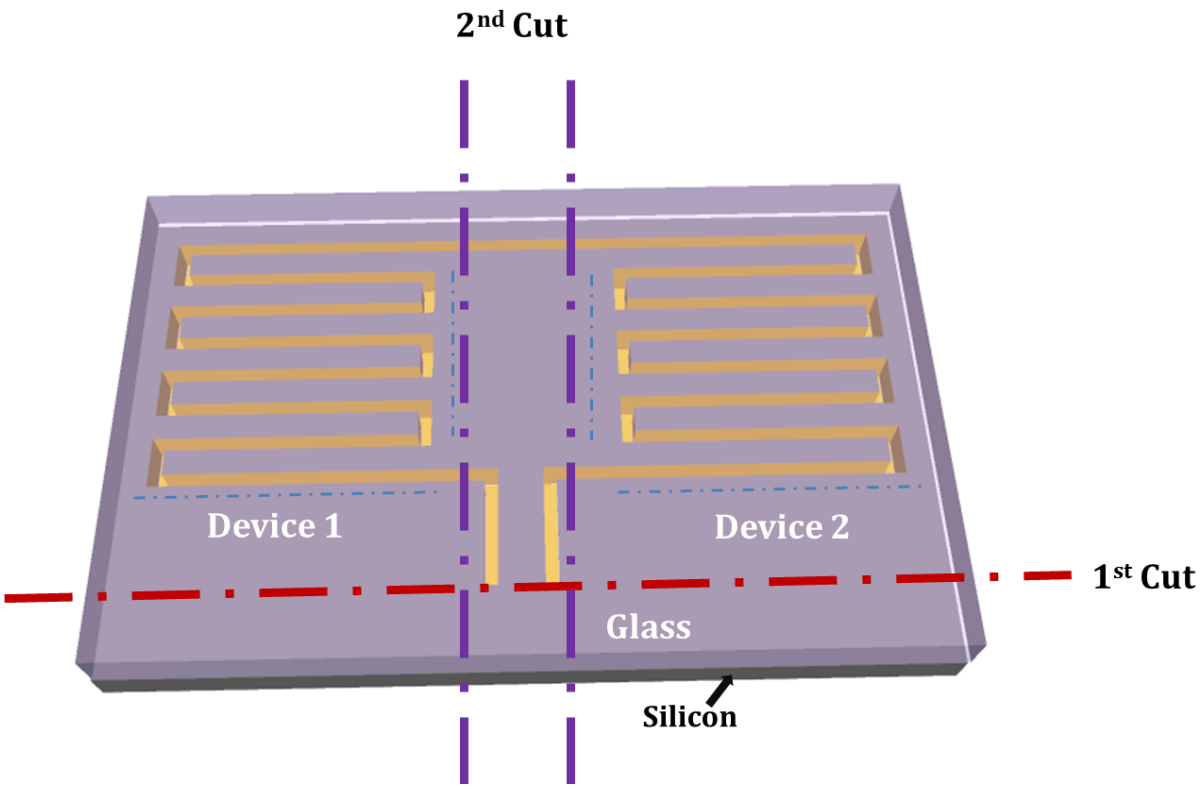

***Figure 5.4**: Schematic representation of newly developed method for serial stationary phase coating utilizing LbL method to enable complete coverage of microchannel.*

simultaneously providing high-throughput. The detailed fabrication process and chromatographic performance of our proposed µWMCs with SNPs coating is explained below.

II. Column Development

A. Fabrication

Figure 5.3 shows the single mask MEMS fabrication process for SNP coated columns on 4 inch, 500 µm thick single-side polished silicon and double side-polished Borofloat wafers. 1m-long, 250 µm-deep µWMCs and regular columns are realized using photolithography, deep reactive ion etching (DRIE) and anodic bonding. The fabrication of devices starts with the standard RCA cleaning and the priming of a silicon wafer. Afterwards, an 8 µm thick AZ9260 photoresist is patterned using a mask aligner followed by development in AZ 400K (Figure 5,3a). Next, the patterned wafer is hard baked for 4 minutes at 110 °C and then etched anisotropically using DRIE to get the desired channel dimensions. Following this, the etched silicon substrate is first cleaned with acetone and secondly by oxygen plasma. This is to ensure the removal of photoresist and the residual passivation polymer deposited during etching (Figure 5.3b). Following the cleaning steps, the etched wafer is sealed with a Borofloat glass wafer using an anodic bonding station at 400 °C and 1250 V for 45 minutes (Figure 5.3c). Subsequently, the bonded wafer is

diced to expose two microfluidic ports of a number of serially connected devices for the newly developed stationary phase coating technique, as shown in Figure 5.4.

B. Stationary Phase Coating

After the first dicing, the 25 cm-long deactivated fused silica capillary tubes (outer diameter 220 µm, inner diameter 100 µm) are attached to the microfluidic ports with epoxy. Next, dry nitrogen and deionized (DI) water are passed through the devices to remove any dirt gathered during dicing. The complete details of layer-by-layer (LbL) coating of SNPs can be found in an earlier report [22]. Briefly, the pH values of polyallylamine hydrochloride (PAH) solution (Sigma-Aldrich) and SNPs suspension (Nissan Chemical) are first adjusted to 7.0 (±0.1) and 9.0 (±0.1), respectively, by adding HCl and NaOH solutions respectively. The LbL coating starts by alternately passing a positively-charged long-chain inert polymeric aqueous solution (PAH) and negatively-charged SNPs suspension through a number of serially connected multiple devices for three minutes to form one bilayer. The electrostatic attraction of each solute to the oppositely-charged surface provides strong, rapid adsorption of a nanoscale layer of the solute onto the surface. Each PAH and SNP coating step is followed by a 3 minute DI water rinsing step. This removes

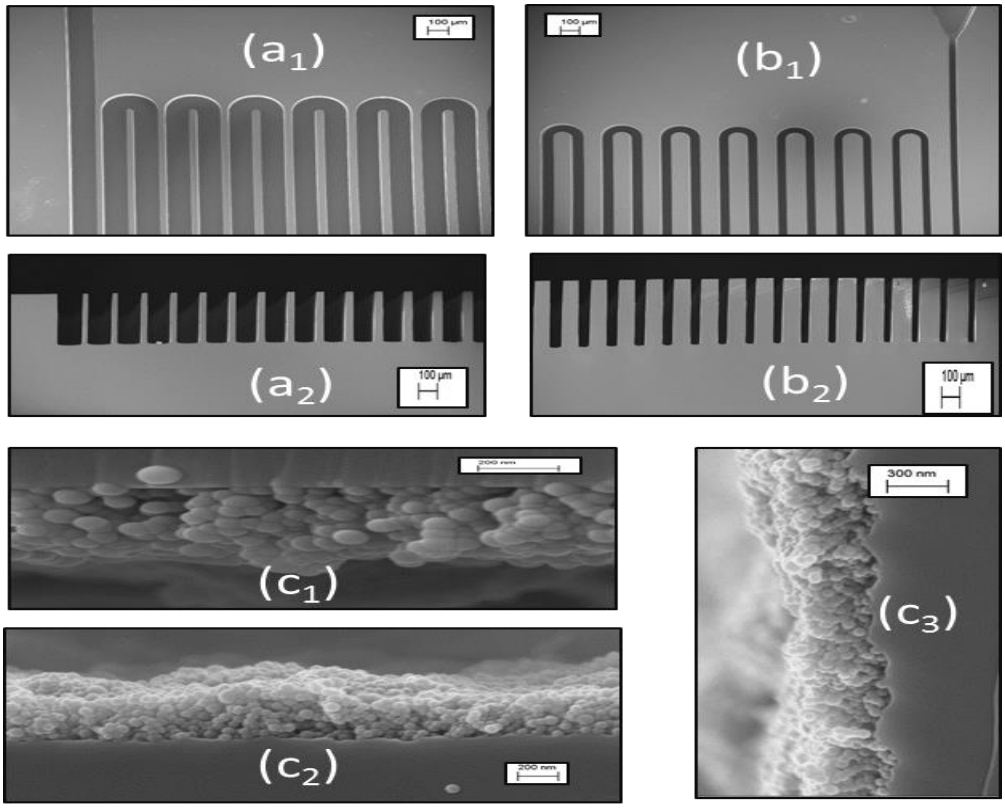

Figure 5.5: *Scanning electron micrographs of µWMC before bonding and SNPs coating (a-b), at 120 µm inlet (a1) top view (a2) cross sectional view and at 20µm inlet (b1) top view (b2) cross-sectional view, LbL SNPs coating after calcination and silane-coupling performed after bonding on (c1) glass surface (c2) bottom of the channel and along (c3) side-wall.*

any excess coating material deposited during the prior step that is not strongly bound by electrostatic attraction. In the present work, this process is terminated after 10 bilayers of PAH and SNPs. Similar to our earlier work for very narrow channel-width (20 µm) multicapillary columns [22], the original concentration of SNPs suspension is reduced to a third in order to achieve a uniform film thickness. At the end, the devices are thoroughly purged by passing DI water and dry nitrogen at low pressure for 15 minutes.

Next, the capillary tubes are removed and serially connected columns are diced into individual devices as shown in Figure 5.4. Calcination is performed afterwards at 500 °C for 8 hours to remove the PAH layer and fuse SNPs together, resulting in a stable and homogenous film. Following the calcination step, deactivated capillary tubes are fixed to the inlet and outlet ports of individual columns using epoxy. Before performing chromatographic separations, the surface of the SNPs is deactivated by filling each column with 10 mM chlorodimethyl octadecyl silane (CDOS) diluted in toluene for 12 hours.

III. Device Characterization

The characterization of µWMCs with a constant SNPs stationary phase film is performed using SEM (Figure 5.5). First, it is verified from the SEM images (top and cross-sectional views) that only the column width is modulated (Figure 5.5 a-b) without effectively changing the channel depth. It is pertinent to note that the effect of modulation in column depth on chromatographic separation could also be studied in the future and easily achieved by changing the DRIE etch parameters. Moreover, by employing the newly developed LbL SNPs coating after anodic bonding, a complete coverage of the microfluidic channel

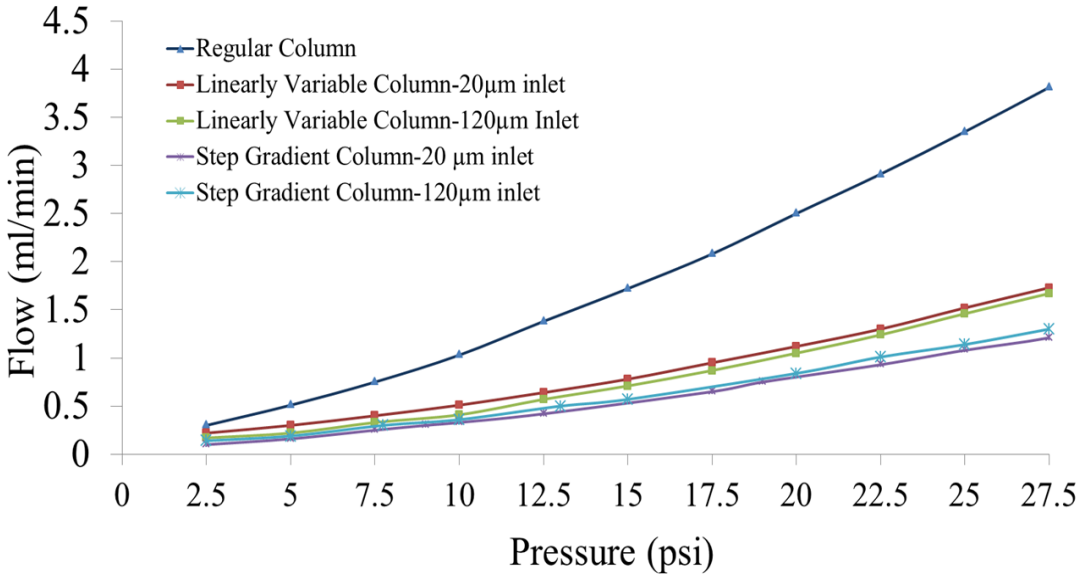

Figure 5.6: *Inlet pressure vs flow through different inlets of µWMC and regular column.*

including the glass surface is realized (Figure 5.5 C). This complete coverage of the separation channel results in improving the analyte-stationary phase interaction. The film thickness measured at different locations (top, bottom and sidewalls) inside the modulating microfluidic channel show that 10 BLs of SNPs yield roughly a constant film thickness in the range of 400~500 nm (Figure 5.5C). This is also consistent with our earlier reported LbL coating method [23] and demonstrates that the film thickness is proportional to the number of coating steps. The deviation in film thickness could be reduced further by utilizing nanoparticles with smaller average diameters for future studies.

IV. Results and discussion

A. Experimental Setup

The separation performance of the LVC, SGC and regular column is evaluated using a conventional GC oven (Agilent GC-7890A) equipped with an electronic pressure controller, a flame ionization detector (FID) and an autosampler (G-4513A). Both the injector and detector temperatures are maintained at 280 °C during GC testing. Ultra high purity nitrogen is used as a carrier gas for all experiments. Since nitrogen provides a higher theoretical plate number at a lower carrier gas velocity [112]. The chemicals used during the chromatographic testing are of HPLC standard and bought directly from Sigma-Aldrich. MEMS columns are attached to the inlet and detector ports using 25 cm-long deactivated (uncoated) fused silica capillary tubes.

After silane-coupling each SNPs functionalized column is first purged with dry nitrogen for 15 minutes. This is followed by column maturing in a GC oven under a constant pressure of 10 psi and an oven temperature of 140 °C until a flat baseline signal is observed. This step is necessary to drive-off contaminants from the column.

B. Separation results

Since the newly developed LVC and SGC (µWMCs) configurations have microfluidic ports with different dimensions (i.e. 20 µm and 120 µm), we can expect that the chromatographic response (retention times, flow rate and plate number) using each port as an inlet will be different. Therefore, both µWMCs cannot be considered bidirectional unlike regular columns. So the presented chromatographic parameters are first analyzed utilizing both inlets of µWMCs. As a first step, the flow rate through µWMCs and regular column is characterized against the applied inlet pressure (Figure 5.6) using a gas flow meter (ADM1000, Agilent Technologies). Due to a larger cross-sectional area (along the column length), the regular column presents a higher flow rate, while the SGC shows the minimum flow rate with the smallest cross-sectional area. Following the flow rate characterization, the separation performance (plate number/meter) of the columns is evaluated according to [112]

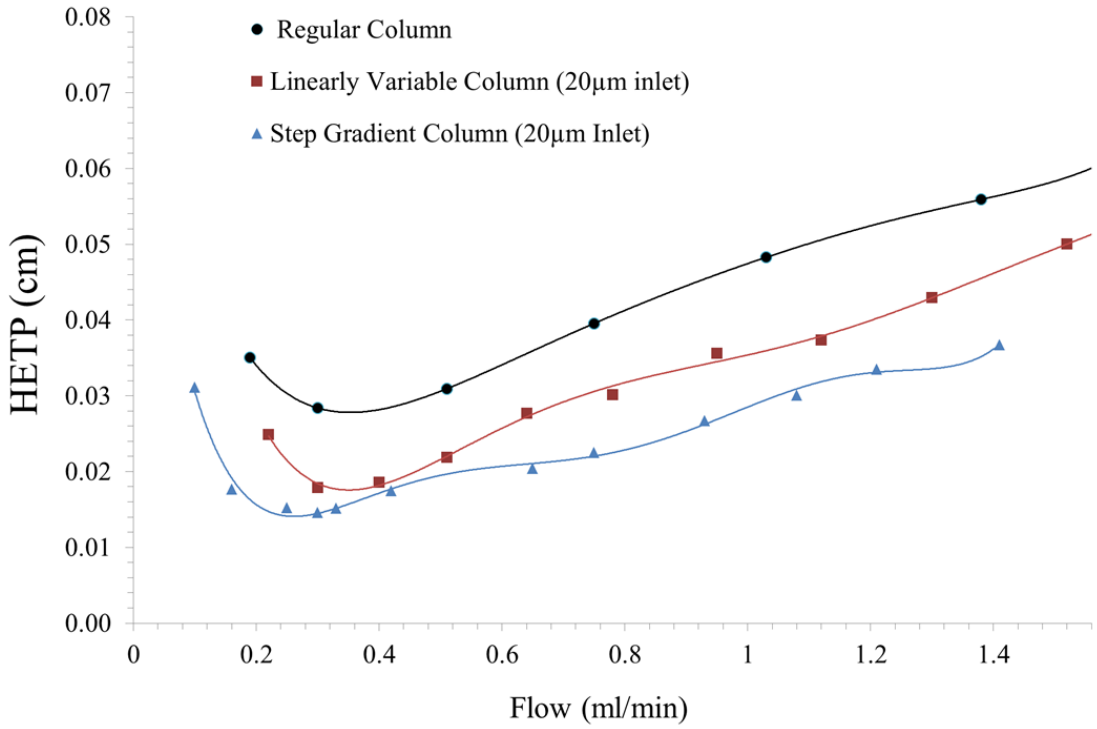

Figure 5.7: *Golay plots for different inlets of µWMC and regular column using nonane as a marker under isothermal conditions of 50 °C and 1µL sample injection.*

$$\mathbf{N = 5.54 \times \left(\frac{t_r}{w_{1/2}}\right)^2} \qquad (5.3)$$

where *N* is the plate number, t_r is the retention time and $w_{1/2}$ is the peak width at half height.

From Table 5.1, it is clear that the inlet selection for µWMCs plays an important role with a significant difference in the plate numbers and retention times. It is clearly demonstrated that the SGC provides a higher plate number (N_{max}=6859 plates/meter) compared to the LVC (N_{max}=5850 plates/meter). The higher plate numbers in the proposed µWMCs could be attributed to a gradual change in the width of the column and the stationary phase thickness. The sample molecules experience either a gradual reduction in solute-stationary phase interaction (using 120 µm as an inlet port) along the column length or get separated fast at the start of the column within the narrower column region when the injector is connected to a 20 µm column port. It has been shown (Table 5.1) that the later scenario provides an enhanced separation performance especially for the SGC. Furthermore, the LVC provides longer retention times than the SGC. Therefore, in order to achieve faster separations the SGC should be utilized but the LVC could provide a better separation resolution between different peaks. It can be further deduced that for both the µWMCs designs utilizing 20 µm ports as inlets provide better separation efficiencies. Therefore, all the

chromatographic results presented hereafter utilize 20 μm ports as column inlets.

For μWMCs the local plate height ($\overline{\mathbf{HETP}}$) will vary with position (length) down the column due to a change in interaction between the stationary phase and the solute, as the relative linear velocities change. Since, $\overline{\mathbf{HETP}}$ cannot be measured experimentally, the apparent plate height (HETP=L/N) is calculated. From the Golay plots (Figure 5.7), it is apparent that both LVC and SGC show superior performance compared to the regular columns (Nmax=3500 plates/m) for all flow rates.

Table 5. 1 *Retention times and plate numbers on μWMCs and regular columns at 0.3 ml/min flow rate using n-nonane as a probe.*

Column Type		**Retention time (min)**	**Maximum Plate Number (N_{max})**
Regular		1.054	3522
Linearly Variable	20 μm Inlet	1.041	5580
	120 μm Inlet	0.778	5496
Step Gradient	20 μm inlet	0.457	6859
	120 μm inlet	0.643	5784

In order to optimize the GC analysis, apart from the retention time and plate number, the resolution should also be characterized. Resolution, a characteristic of the separation of two adjacent peaks, is calculated according to [112]

$$\mathbf{R} = \mathbf{2} \times \left\{ \frac{\mathbf{t_{r_b}} - \mathbf{t_{r_a}}}{\mathbf{w_b} + \mathbf{w_a}} \right\} \qquad (5.4)$$

where $\boldsymbol{R}$ is the resolution, $\boldsymbol{t_{r_b}}$ and $\boldsymbol{t_{r_a}}$ are the retention times, $\boldsymbol{w_b}$ and $\boldsymbol{w_a}$ are peak widths at half heights of corresponding compounds a and b, respectively.

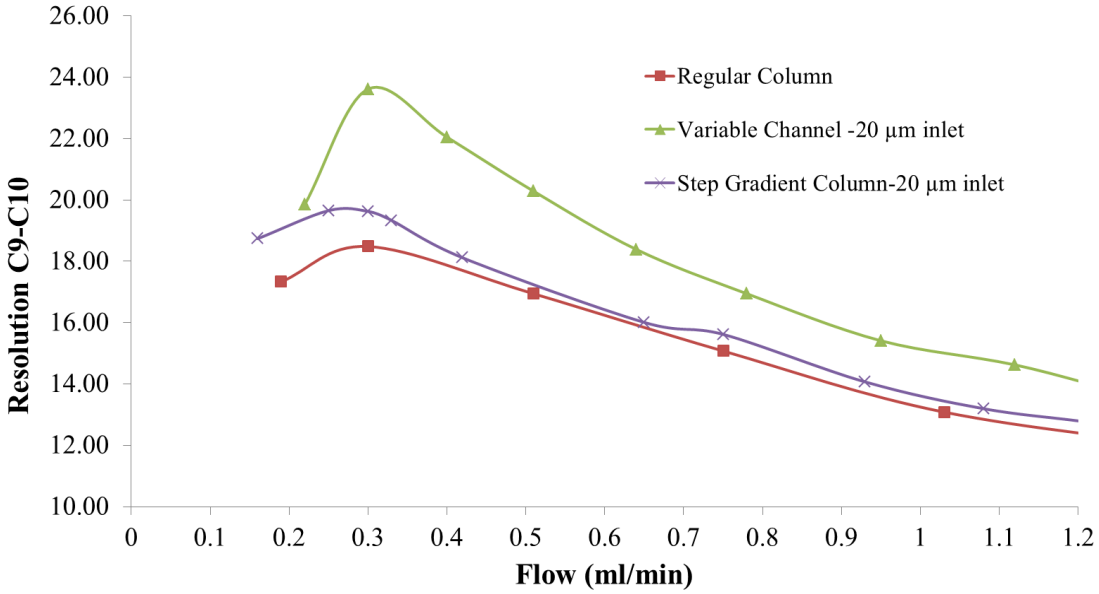

Figure 5.8: *Resolution between n-nonane and n-decane under isothermal conditions for different inlets of µWMC and regular column.*

Similar to HETP analysis, the LVC outperforms the fixed dimensional regular columns in terms of resolution between n-nonane and n-decane under isothermal conditions (Figure 5.8). The effect of peak resolution is further demonstrated from the separation of a custom-made hydrocarbon mixture with nine compounds. It is clear from the separation results (Figure 5.9) that under same flow rates the LVC is able to resolve all the nine compounds, while a regular microfabricated column is only able to resolve seven compounds in the test mixture. Moreover, it could also be concluded µWMCs are more suitable for the separation of compounds with lower boiling compounds. Additionally, we note that the SGC is only able to separate eight compounds in the sample test mixture (not shown).

V. Conclusion

Two unidirectional µWMCs are introduced for the first time and provide better resolution, plate numbers, retention times and chromatographic separations than a regular fixed dimensional column. Multiple serially-connected columns are coated using LbL self-assembly of SNPs to enable a constant stationary phase film thickness. Moreover, the effects of modulation in column depth (controlled by micromachining parameters) and film thickness could also be studied as a future study. Similarly, the length of the µWMCs could also be increased to study the effect of width modulation on the separation of lighter hydrocarbons.

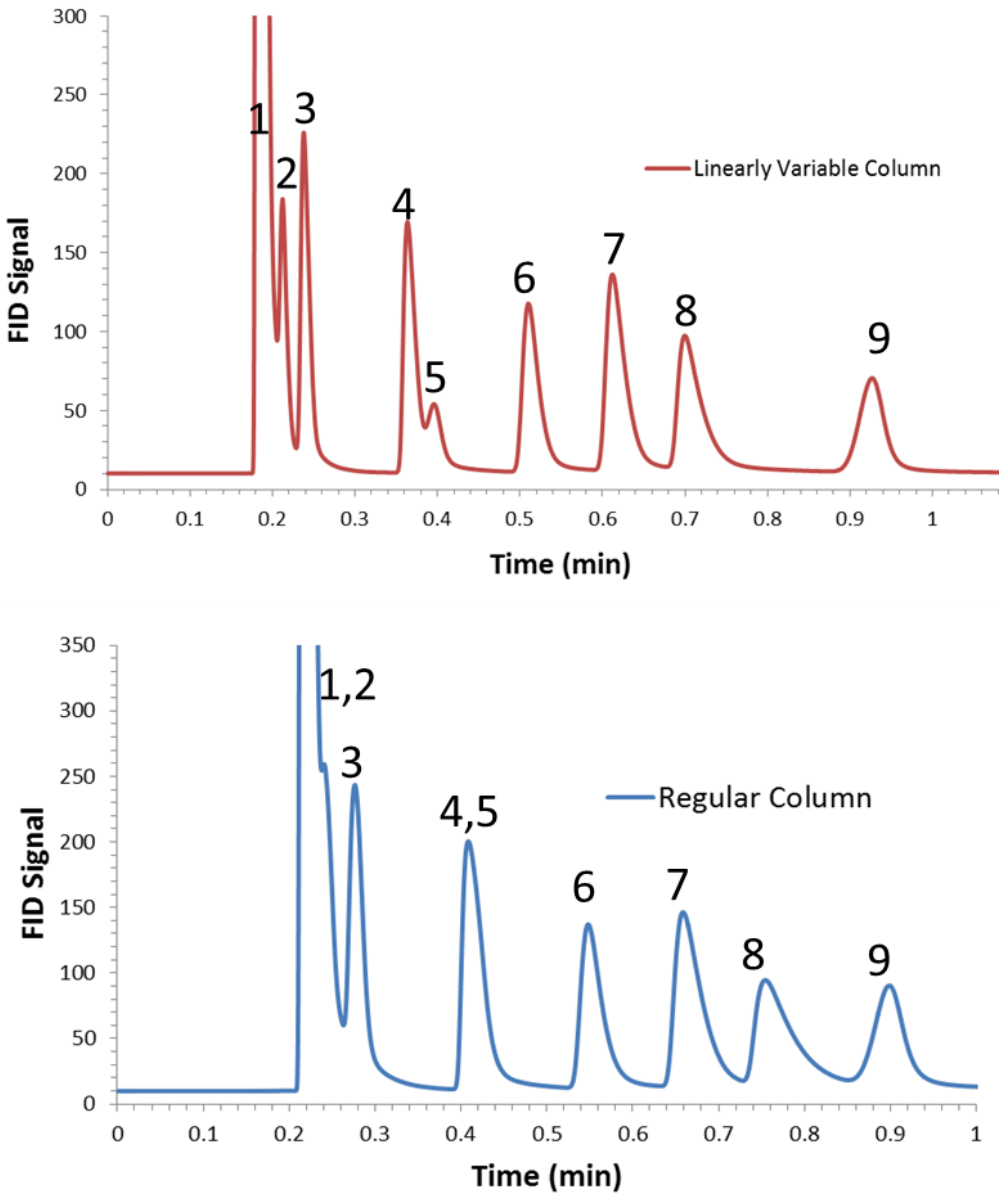

Figure 5.9: *GC separation results of a test mixture at 0.3 ml/min flow rate, 50 °C isothermal temperature and 100:1 split ratio. Compound identification in the order of elution (1) dichloromethane-solvent (2) n-hexane (3) benzene (4) toluene (5) tetrachloroethylene (6) chlorobenzene (7) ethylbenzene (8) p-xylene (9) n-nonane.*

CHAPTER 6: Semipacked Columns with Atomic Layer Deposited Alumina as a Stationary Phase

(Part of this chapter reproduced from [42] with permission from Sensors and Actuators: B Chemical)
H. Shakeel, G. W. Rice, and M. Agah, "Semipacked columns with atomic layer-deposited alumina as a stationary phase," Sensors and Actuators B: Chemical, vol. 203, pp. 641-646, 2014.

Gas chromatography (GC) is a reliable chemical analysis technique that is used to separate and identify the constituents of complex gas mixtures. GC has applications in a vast range of areas such as environment monitoring, food processing, pharmaceutical industry, biomedical science, forensic and trace analysis. Traditional bench-top GC instruments, though widely used, are bulky, expensive, time and energy intensive. The progressive innovations in microfabrication techniques coupled with nanotechnology have prompted a renewed interest in miniaturizing key GC components over the last decade [18, 21, 51, 55, 78, 91, 92, 113, 117, 163, 166, 172-176]. The development of new stationary phase coating techniques has been a continuous research area and the heart of micro gas chromatography (μGC) column performance [12, 22, 25, 40, 51, 106, 177]. Apart from the application of most common polymer based gas-liquid stationary phases [36-39, 51, 173] for μGC separation columns, there has also been considerable research efforts toward the development of MEMS-compatible methods for the integration of solid-adsorbent materials (monolayer-protected gold [23], carbon nanotubes [40], silica nanoparticles [22], gold nanoparticles [111], silica[25] and graphite [24]) into μGC columns. Although these adsorbent/gas-solid stationary phases have shown attractive features for the separation of complex mixtures, the application of these coating schemes for very narrow-width (<20 μm) and deep (>150 μm) rectangular microchannels has not been straightforward as summarized in Table 6.1 [12, 22, 25, 40]. The current adsorbent based coating schemes for these particular column designs mostly suffer from factors such as low-yield, chip-level coating, high processing temperatures and requiring elaborate experimentation. Moreover, these methods present a major hindrance towards the monolithic integration of different μGC components on a single chip. This warrants the need for developing wafer-level facile complimentary metal-oxide-semiconductor (CMOS) compatible coating techniques that produce mechanically and thermally stable, chemically inert and selective stationary phases.

ALD has emerged as a powerful tool for the growth of low-temperature thin-films on a variety of substrates for myriad applications [178, 179], generally as a gate oxide in CMOS technology. ALD enables conformal and homogeneous coatings of flat, very high-aspect-ratio (HAR) microchannels and even nanostructure surfaces with precision within a few angstroms. The use of ALD coatings for separation science has been very recently reported for ultra-thin-layer chromatography where the

Table 6. 1 *Summary of microfabricated GC columns with gas-solid stationary phases*

Authors	Column Geometry	Phase-Deposition	
		Method	*Limitations*
Reston [16] (1994)	Rectangular (30 µm deep, 100 µm wide, 0.9 m- long)	Evaporation of copper phthaocyanine film	Applicable to only shallow channel depth.
Stadermann [40] (2006)	Rectangular (100 µm deep, 100 µm wide, 50 cm- long)	Chemical vapor deposition of carbon nanotubes	Incomplete coverage of the channel and high process temperature.
Zareian-Jahromi [12] (2010) and Shakeel [23] (2013)	Rectangular (250 µm deep, 25 µm wide, 25 cm- long) Multicapillary (25 µm wide, 200 µm deep, 25 cm-long)	Self-assembly of thiol on electroplated gold surface	Extensive characterization, high-process temperature and chip-level processing.
J. Vial [25] (2011)	Rectangular and semipacked (100 -125 µm deep, 50-150 µm wide, 1m-long).	Wafer-level sputtered silica film deposition	High stationary phase film thickness variations and applicable to low-channel depth.
Wang and Shakeel [22] (2013)	Rectangular (250 µm deep, 150 µm wide, 1m-long). Multicapillary (200 µm deep, 20 µm wide, 25 cm-long).	Silica nanoparticles using layer-by-layer technique.	High-process temperature and chip-level processing.

enhancement of separation capabilities of silica support media using different ALD coatings was demonstrated [180]. The use of ALD-based films as a standalone separation media for µGC has not been reported to the best of our knowledge. Semipacked separation columns, having an ordered micro pillar array in the rectangular separation channel, are shown to reduce band-broadening, achieve high separation efficiency [25, 37, 39, 181] and improve sample capacity [182]. Previously semipacked columns have been coated with both polymeric [37, 39, 181] and adsorbent based stationary phases [25]. The gas-solid/adsorbent based coating of semipacked columns was limited by the 100 µm column depth [25] due to the poor step-coverage afforded by a sputtering process for the high-aspect-ratios microstructures. The novel wafer-level application presented here utilizes a silane functionalized aluminum oxide thin-film as a stationary phase medium for semipacked columns. ALD uses self-limiting gas phase chemical reactions for deposition, thus affording an alumina film with very high step-coverage of semipacked columns having aspect-ratios (depth: width) of 10:1. Since ALD has been successfully employed for coating micro/nano structures with aspect ratios of 1000 and beyond [183], our proposed coating technique could

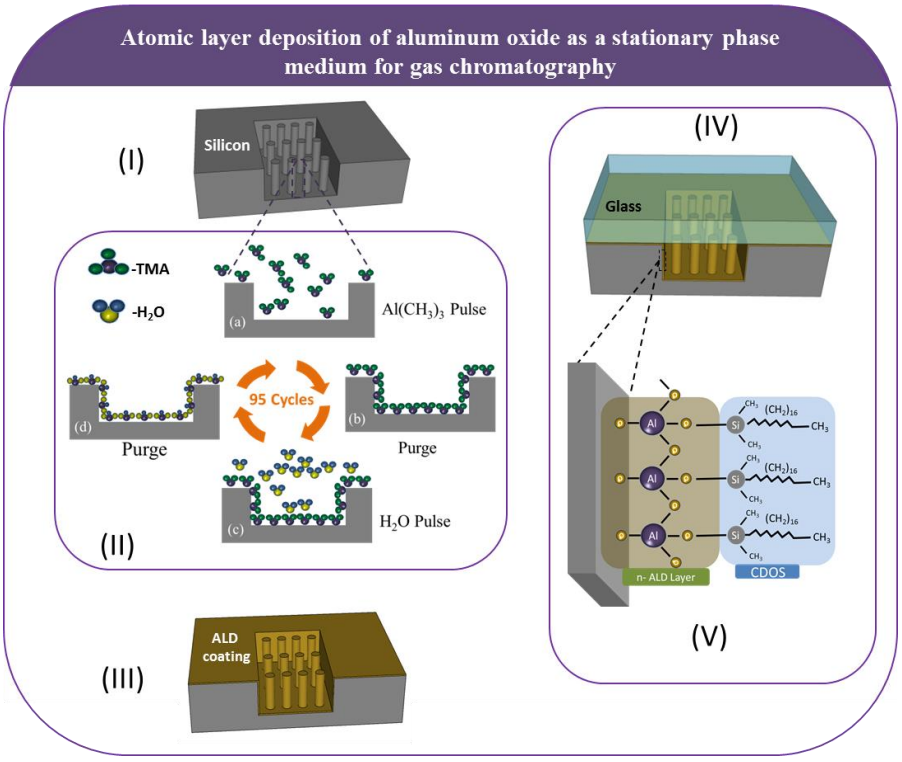

***Figure 6.1**: Schematic representation of ALD-based stationary phase coating. (I) anisotropically etched semipacked column, (II) and (III) atomic layer deposition of 10 nm alumina film and (II) 95 cycles with each cycle having four steps (a) TMA exposure (b) purge (c) H_2O exposure (d) purge, (IV) anodic bonding of ALD-coated wafer with glass substrate, (V) silane deactivation for 24 hours.*

be easily integrated to more challenging µGC columns with very narrow channel widths (5 µm or less). The detailed fabrication process and chromatographic analysis of our proposed scheme is explained below.

I. Experimental Procedures

The fabrication of microfabricated separation columns employs standard microelectromechanical systems (MEMS) processes for the lithographic, etching, ALD coating and anodic bonding of silicon-

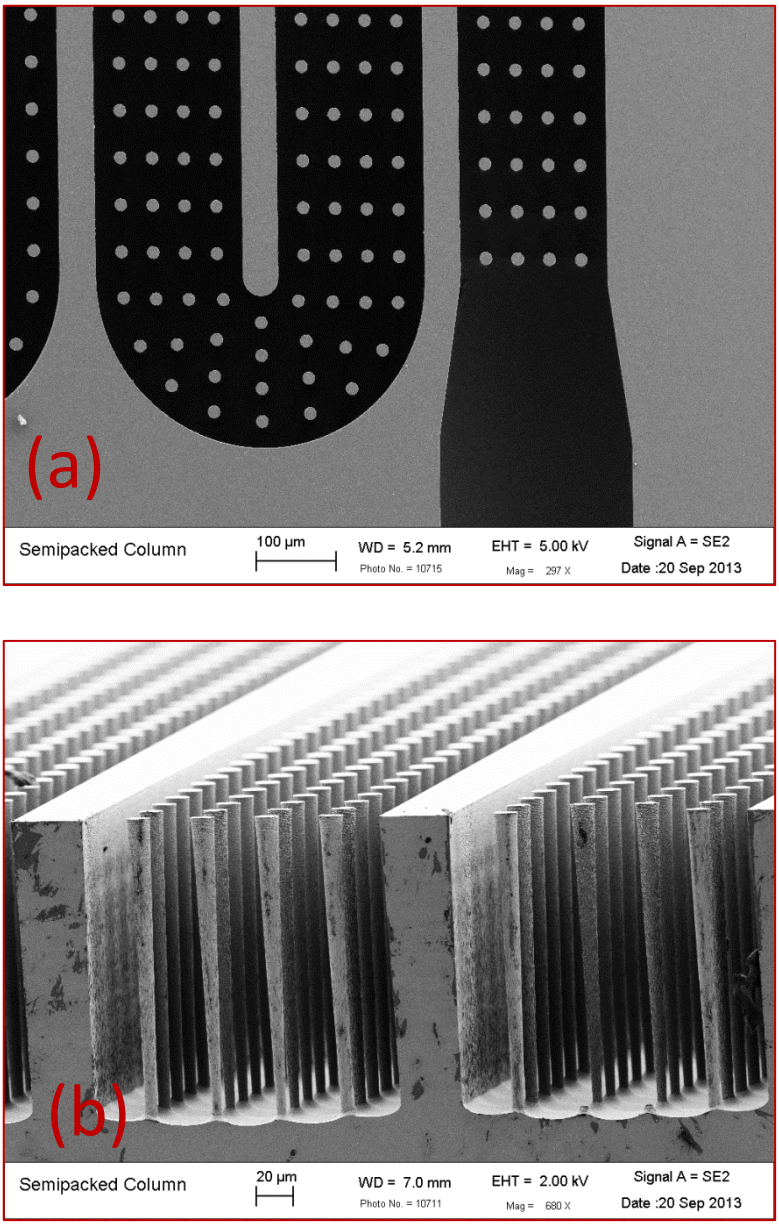

***Figure 6.2**: SEM micrographs of a 1m-long semipacked column with integrated 20 µm circular microposts and post spacing of 40 µm (a) top view and (b) cross-sectional view.*

glass chips.

A. Column Fabrication

The fabrication of the semipacked columns (1 m-long,190 µm wide by 180 µm deep channels, with 20 µm integrated circular micropillars with 40 µm post spacings) starts with a standard RCA cleaning of 4 inch, 500 µm thick n-type single side polished silicon wafers (University Wafers). After performing wafer priming using hexamethyldisilizane (HMDS), AZ9260 photoresist (AZ Electronic Materials) is spin coated at 2000 rpm to acquire an 8 µm thick resist layer. This is followed by soft-baking the resist-coated wafer at 110 °C for 1 minute. The wafer is then exposed for 50 seconds using a mask aligner (Karl Suss) to transfer features from a chrome mask on to the soft-baked resist-coated wafer. Following exposure, the features are developed in AZ400K developer (AZ Electronic Materials) and DI water (3:1). Afterwards, the developed wafer is hard-baked for 3 minutes at 110 °C. SF_6 and C_4F_8 are used to anisotropically etch the wafer (via a standard Bosch process) using an Alactel deep reactive ion etcher (DRIE). Following etching, the photoresist is first removed using acetone and the wafer is then placed in a piranha etch solution to remove any organic residue left during either the etching or photoresist removal steps (Figure. 6.1, step-I). SEM micrographs of a 1 m-long and 180 µm-deep microfluidic channel are shown in Figure 6.2 after anisotropic etching and photoresist removal.

B. ALD Coating

The ALD coating process for aluminum oxide using trimethylaluminum (TMA) and water as precursors is well established [179]. The successive reactions during aluminum oxide growth on the silicon surface

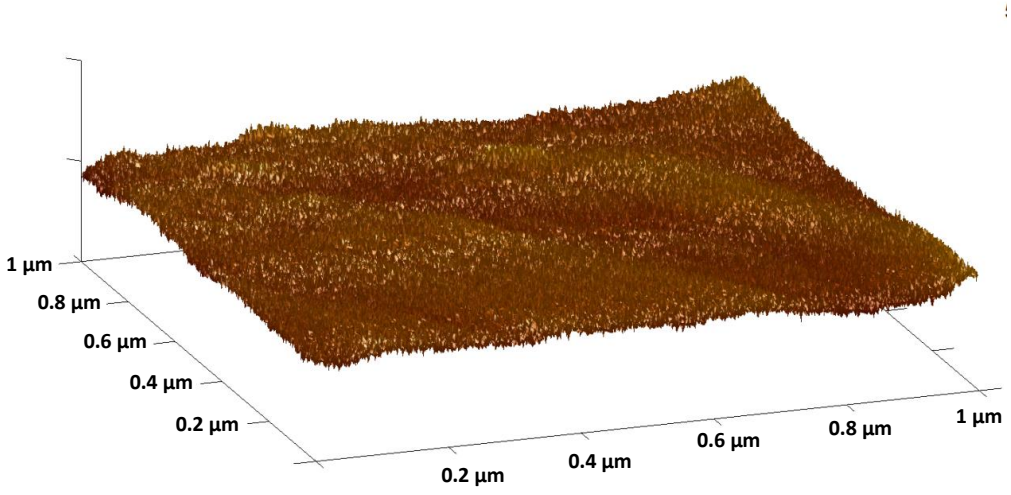

Figure 6.3: *AFM surface plot of a 10 nm aluminum oxide film coated on a flat silicon substrate. The scanned area is 1 µm x 1 µm and height scale is from 0 to 3 nm.*

from TMA and water is described by two sequential reactions as given below [184].

$$\text{(A)} \quad -Si-OH + Al(CH_3)_3 \longrightarrow -Si-O-Al(CH_3)_2 + CH_4$$

$$\text{(B)} \quad -Si-O-Al(CH_3)_2 + 2H_2O \longrightarrow -Si-O-AlO^*(OH) + 2CH_4$$

The asterick in reaction (B) represents an oxygen shared between adjacent aluminum atoms on the surface. During the first reaction (A), the surface silicon hydroxyl species react with TMA forming a dimethyl-terminated aluminum species and methane as a byproduct. The excess TMA will not react further with the surface, resulting in a self-limiting process. In the second reaction (B), two water molecules react with the dimethyl-terminated aluminum species, forming an oxide bridge between adjacent aluminum species and a terminal hydroxide on each aluminum atom as well. The terminal hydroxide then allows for the production of additional aluminum oxide monolayers by the same two step cycle.

Thin alumina film deposition on the etched silicon wafer was performed at 250 °C using a thermal ALD Cambridge NanoTech system (Savannah S100). TMA (Sigma-Aldrich) and water precursors (deionized water used from clean room) were used to deposit a 10 nm aluminum oxide film. Each ALD deposition cycle consists of a 15 ms sequential precursor gas exposure of either TMA or H_2O (20 sccm flow) followed by a 4 second purge (Figure 6.1, step-II) to provide a film thickness of 1.07 Å per cycle. The wafer was coated for approximately 16 minutes (95 cycles) to get the desired film thickness of 10 nm. The surface of the ALD-coated silicon was characterized using an atomic force microscope (Bruker Nanoscope V) with a silicon tip in a tapping mode. A 1 μm^2 area was scanned at a rate of 0.98 Hz and recorded using 512 scan lines. The 3-D surface plot of a 10 nm aluminum oxide film (Figure 6.3) gave a root mean square roughness of 0.264 nm, clearly demonstrating that the aluminum oxide film generates a highly smooth and uniform surface.

Although the thin-film deposition rate afforded by the available ALD system is very low, it could be improved further by employing a recently developed spatially separated ALD process [185]. It has been shown that the growth rates of as high as 1.2 nm/sec could be achieved for aluminum oxide thin films using this technique. Therefore, this modified ALD process could be integrated into MEMS fabrication of columns for high throughput stationary phase deposition.

C. Column bonding and functionalization

After performing the ALD coating, the etched silicon wafer was anodically bonded with a 700 µm thick and 4 inch wide double side polished Borofloat wafer (Coresix Precision Glass) at 1250V and 400 °C for 45 minutes (Figure 6.1, step-III). The wafer was then diced into individual devices for functionalization and chromatographic testing. In order to provide an interface between the GC injection port and detector,

220 µm outer diameter by 100 µm internal diameter fused silica capillary tubing (Polymicro Technologies) was attached to the column inlet and outlet ports using Epoxy 907 (Miller Stephenson). The surface of the ALD oxide film and the glass cover was finally functionalized by filling each column with 10 mM chlorodimethyloctadecylsilane (CDOS, Sigma Aldrich), in toluene solution [22] for 24 hours at room temperature (Fig 6.1, step-IV*)*.

Before performing chromatographic tests, each device was first purged for 30 minutes with nitrogen. This was followed by column temperature conditioning in the GC oven for approximately one hour (35 °C ramped at 2 °C/min to 150 °C) at a constant inlet pressure of 10 psi.

D. Chromatographic Instrumentation

A bench top 7890 series Agilent GC system equipped with a flame ionization detector (FID), an electronic pressure controller and an autosampler (7359A) unit was used for injection and detection purposes. Both the injector and detector temperatures were maintained at 280 °C. Ultrapure nitrogen (>99.99%) was purchased from Air Gas Ltd, USA and used as the carrier gas. Methane (99% grade, Matheson Trigas, Ohio) was used for calculating the gas velocities to generate Golay plots. All chromatographic test mixtures were prepared using standard HPLC grade chemicals (Sigma-Aldrich).

II. Results and Discussion

A. Column functionalization

Ideally a chromatographic peak should be symmetrical, or Gaussian, in shape. Asymmetric peaks, usually in the form of peak tailing, influence the column performance. A tailing factor (T_f) can be used to quantify the peak tailing [112] and is given by

$$T_f = \frac{a+b}{2a} \qquad (6.1)$$

where both a and b, measured at 5% of the peak height, represent the front and back half-widths respectively. A $T_f = 1$ represents a perfectly symmetric peak (a=b), whereas peak tailing (a<b) will yield values of $T_f > 1$.

Alumina as an adsorbent material has been successfully used for conventional gas-solid chromatographic separations [112, 186]. Although our ALD-based alumina coating (without any alkylsilane based treatment) clearly demonstrates separation capabilities, significant asymmetric peak shapes are observed as shown (Figure 6.4) and tailing factors (T_f) of 5.95 and 7.15 were calculated for n-nonane and n-decane peaks (7000 ppm diluted in n-hexane) respectively. This may be the result of unknown changes in the alumina structure from the ALD process that affects the equilibration of the solutes with the stationary

phase. Figure 6.4 also shows the separation profile for the same hydrocarbon mix on the atomic layer deposited alumina column after silane functionalization. The chromatographic performance of the alumina adsorbent is significantly enhanced using alkylsilane functionalization performed after anodic bonding of the cover glass wafer (tailing factor of 1). Organochloroalkylsilanes are some of the most popular column deactivating reagents in chromatography and provide very reproducible surface treatment methods for active sites, which in this case would be from the terminal hydroxide groups from the last ALD deposition as described in Section 2.2. We have previously utilized CDOS for functionalization of silica nanoparticles [22] and glass substrate surfaces [41] with promising results. There are marked

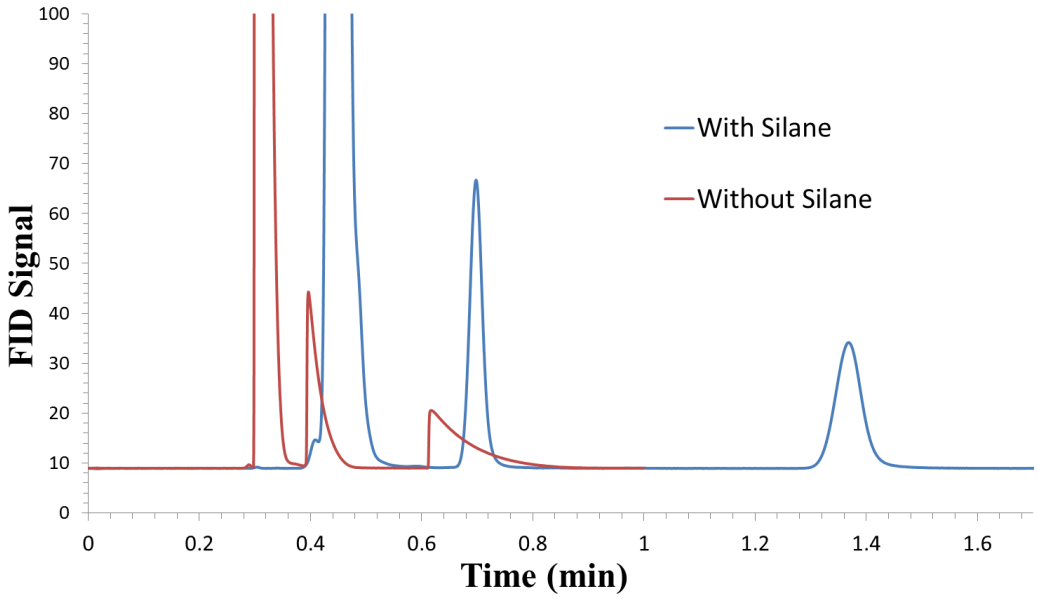

Figure 6.4: *Effect of silane functionalization on a ALD-coated semipacked column at 50 °C, 250:1 split ratio, 0.1µL injection volume and 10 psi column pressure (compound identification in the order of elution n-hexane (solvent), n-nonane and n-decane).*

improvements with respect to enhanced retention times and peak symmetry, most likely due to interactions with the hydrocarbon tail of the silane. No chromatographic separations were obtainable on bare silicon columns without ALD or silane treatment.

B. Column Performance

The primary performance criterion for GC columns is expressed by the number of theoretical plates (N) for a certain compound and is calculate from chromatogram [112] using following formula.

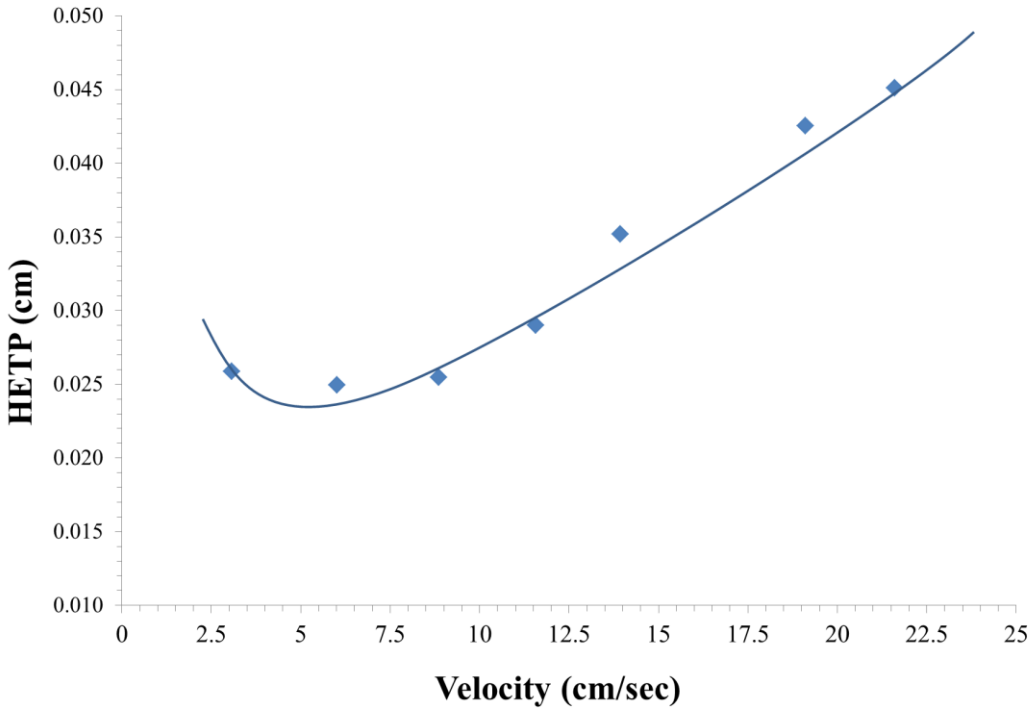

Figure 6.5: *HETP vs carrier gas velocity plots for an ALD treated semipacked column at 50 °C using n-decane as a probe and methane for calculating the carrier gas velocity.*

$$N = 5.546 \times \left(\frac{t_r}{w_{1/2}}\right)^2 \qquad (6.2)$$

where t_r is the retention time and $w_{1/2}$ is the peak width at half height. Another related parameter that takes into account the column length (L) for the comparison of different columns is the height-equivalent-to-a-theoretical-plate (HETP), where

$$HETP = \frac{L}{N} \qquad (6.3)$$

The ALD-coated/silane functionalized semipacked MEMS columns provided up to 4200 plates per meter using n-decane (diluted in dichloromethane) at 50 °C at an optimum inlet pressure of 7.5 psi (linear velocity of 8.15 cm/sec). Methane vapor was assumed to be unretained and used for calculating the carrier gas velocity at different inlet pressures to generate the Golay plots [112]. A typical Golay plot obtained from one of the silane treated ALD columns is shown in Figure 6.5. Typically, a meter long microfabricated column coated with gas-solid stationary phases (sputtered silica [25] or carbon nanotubes [40]) yields around 4000-5000 plates/meter. Thus, the performance of our newly developed phase for

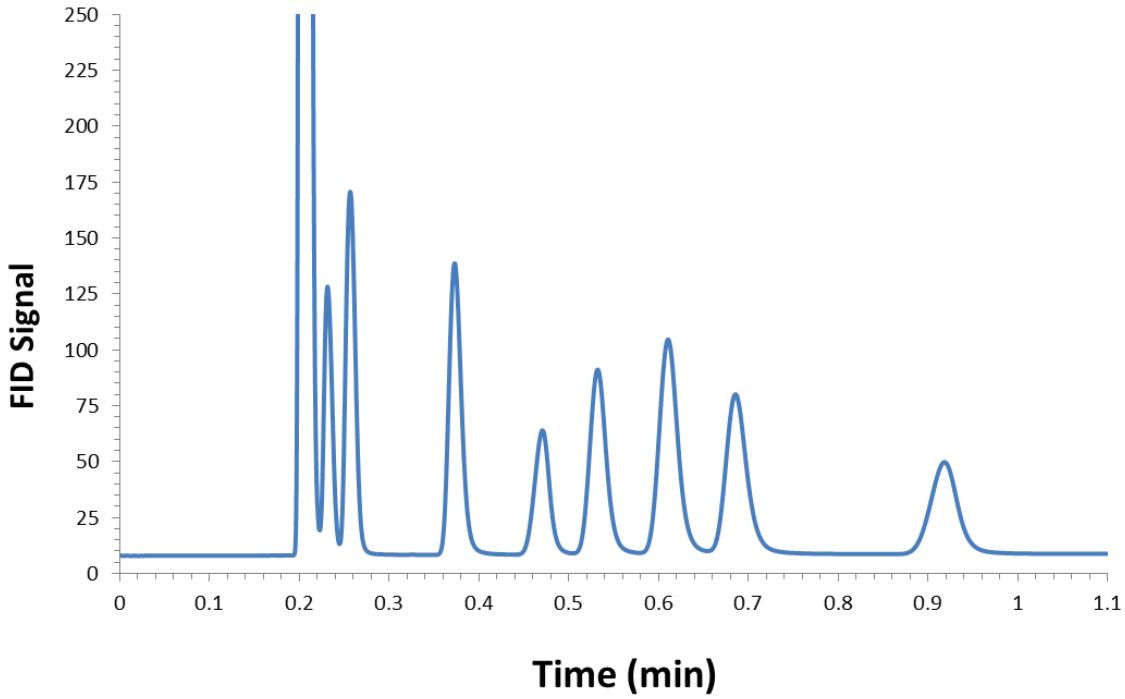

Figure 6.6: *Separation performance of an ALD-coated/silane functionalized semipacked MEMS column at 50 °C, 7.5 psi inlet pressure with split ratio of 75:1. Compound identification in order of elution 1.dichloromethane (solvent) 2. n-hexane (k'=0.23) 3. benzene (k'=0.38) 4. toluene (k'=1.01) 5. Tetrachloroethylene (k'=1.55) 6. chlorobenzene (k'=1.90) 7. Ethylbenzene (k'=2.34) 8. p-xylene (k'=2.75) 9. n-nonane (k'=4.00).*

micro GC columns is comparable to other non-conventional coatings; however, other types of non-conventional as well as conventional stationary phases cannot be readily applied to columns with very high aspect ratios and very small dimensions that can be achieved with the ALD process.

C. Chromatographic Separations

The separation capability of the new stationary phase was tested using a mixture containing eight compounds (n-hexane, benzene, toluene, tetrachloroethylene, chlorobenzene, ethylbenzene, p-xylene and n-nonane diluted in dichloromethane to a concentration of 15000 ppm. An autosampler was used to inject 0.3 µL of the mixture with a split ratio of 75:1. The column pressure and oven temperature were maintained at 7.5 psi and 50 °C respectively. The resulting chromatographic separation (Figure 6.6) provided good resolution and retention of the compounds, with the entire separation achieved in less than a minute at isothermal conditions. Capacity factors (k'), the ratio of the time spent in the stationary phase relative to the mobile phase, ranged from 0.23 for hexane to 4.0 for n-nonane, with the separation driven primarily by differences in boiling points as reflected by the order of elution.

It is important to note that this newly developed coating scheme has not been able to provide adequate separation abilities for active compounds like alcohols and is only able to separate mixtures with either straight chain alkanes or aromatic hydrocarbons. Similarly, the conventional gas capillary columns with alumina particles (stationary phase) have been utilized for the separation of alkanes, alkenes, alkynes and aromatic hydrocarbons with a maximum operating temperature of 200 °C [186]. Therefore, our proposed functionalized alumina thin film also shows similar separation capabilities as afforded by conventional alumina particles.

D. Stability and Repeatability

The long-term and thermal stability of this newly developed gas-solid stationary was also evaluated. Chlorobenzene and n-nonane (diluted in dichloromethane) were utilized as probes with multiple injections made using an autosampler unit. The deviations in the plate numbers (N) and the capacity factors (k') of each compound were calculated from the 1st, 25th, 50th and 75th injections as presented in Table 6.2. These results clearly demonstrate that after multiple injections the silane-functionalized alumina coating remains stable, with less than 8 % deviation in plate numbers and less than 3% deviations in k' values. Similarly, using the same compounds, the thermal stability of the ALD based stationary phase was also evaluated. The column was subjected to thermal cycles of 100 °C, 150 °C and 200 °C for 8 hours each under a constant inlet nitrogen pressure of 2.5 psi. After each thermal cycle, the column testing was carried out at 50 °C and 7.5 psi. The deviations in the N and k' values are shown in Table 6.3.

Table 6. 2 *Long-term stability of ALD based stationary phase with multiple injections (GC testing at 50 °C, 7.5psi).*

Injection	**Chlorobenzene**		**n-Nonane**	
	Plate Number (N)	*Capacity Factor (k')*	*Plate Number (N)*	*Capacity Factor (k')*
1st	3368	1.87	4380	3.77
25th	3508	1.85	4359	3.82
50th	3319	1.85	3962	3.89
75th	3886	1.85	3948	3.90
%RSD	7.3	0.64	5.7	1.6

The results show that the alumina based stationary phase remains stable up to 150 °C with small variations in retention times; however, there is some degeneration at 200 °C, and column performance deteriorates considerably if heated beyond temperatures of 200 °C. Given that highly effective separations can readily be performed at much lower temperatures on one meter columns as illustrated in Figure 6.6, this is not a critical disadvantage for MEMS based devices. The effect of variations in microfabrication

Table 6. 3 *Temperature stability test of ALD based stationary phase (GC testing at 50 °C, 7.5psi)*

Column heating for 8 hours @	**Chlorobenzene**		**n-Nonane**	
	Plate Number (N)	*Capacity Factor (k')*	*Plate Number (N)*	*Capacity Factor (k')*
Before Heating	3990	1.80	4343	3.92
100 °C	3930	1.82	4251	3.94
150 °C	3808	1.80	4308	3.91
200 °C	3128	1.65	4020	3.59
%RSD	10.7	4.3	3.4	4.3

processes on chromatographic efficiency was also considered. Three separation columns were fabricated on different wafers using identical fabrication techniques as discussed in the experimental section. A 15% variation (RSD) was observed in the plate number values (using n-decane) for the tested columns. This high chip-to-chip variation could be attributed to variations in the end connections.

III. Conclusion

In this initial report we describe for the first time the use of atomic layer deposited alumina with alkylsilane functionalization for gas chromatographic separations. The use of ALD ensures highly conformal film deposition inside complex column designs and affords good selectivity, separations and retention of different compounds. Compared to very recently reported methods for µGC columns that utilize sputtering systems for alumina deposition [106], our method achieves very symmetric peaks and separations. Moreover, our method is not limited by the column depth; thus improving column flow rate and the sample capacity by increasing the cross-sectional area of the microfluidic channel. For future work, it is envisioned that the selectivity of alumina films could be tuned further by using silanes with different functional groups. Since ALD is used for very thin film depositions, we envision that in range of 5~15 nm there will not be a significant change in the separation performance. The effect of film thickness will be studied more in the future. Moreover, the effect chamber temperature and other film-deposition conditions could also be studied in detail for further optimization.

CHAPTER 7: High Density Semipacked Separation Columns with Optimized Atomic Layer Deposited Phases

Microfabricated separation columns are produced using standard micromachining processes that selectively etch a silicon substrate; this is followed by sealing the etched silicon channels with a glass wafer. After which the sealed silicon microchannels are coated with either a polymer based liquid or solid-adsorbent thin films. The utilization of MEMS techniques for miniaturization of separation columns is an ongoing research area and dates back to 1979 when Terry and coworkers [7] fabricated 1.25 m-long, 200 µm-wide and 30-µm deep silicon columns. After wet etching, the columns were sealed with a glass wafer and coated with a liquid based stationary phase (OV-101). The condensation of stationary phase at corners and non-uniform film thickness lead to poor chromatographic performance. Following this in 1994, 90-cm long, 10-µm deep and 300-µm wide rectangular columns were fabricated by Reston and Co. [187]. Moreover, researchers at Sandia National Lab [188] developed separation columns with different channel dimensions from 10 µm to 80 µm-wide, 200 µm to 400 µm- deep and 10 cm to 100 cm-long using both wet and plasma etching techniques. These columns were etched anisotropically and channels with aspiral pattern were designed. Both static and dynamic coating techniques were used for coating OV1 based polymer stationary phases after performing anodic bonding. Although the film thickness was not uniform, columns were able to successfully separate a mixture of dimethyl methyl phosphate (DMMP) from toluene and xylene. Moreover, Agah and Co [189] introduced high performance rectangular separation columns with on-chip heaters and sensors for rapid temperature programming. In this report, 3 m-long, 150 µm-wide and 250 µm-deep etched-backed and dynamically coated columns were able to separate a complex 20 compound mixture in 5 minutes. Similarly, Reidy and coworkers [38] at the University of Michigan, Ann Arbor described an efficient procedure for statically coating rectangular silicon columns with dimethyl polysiloxane (PDMS). In this paper, the authors reported coating a 3 m-long separation column with a very thin (100 nm -200 nm) and uniform film to achieve high separation efficiency (12,500 theoretical plates). Although separation columns have been traditionally fabricated on a silicon wafer, Bhushan *et al.* [190] utilized a standardized LiGA (lithography, electroplating and molding) process to fabricate high-aspect-ratio nickel columns. In this study, 2 m-long, 50 µm-wide and 300 µm-deep metal columns were sealed using electroplating and statically coated with OV-1 polymer. Agah *et al.* [191] employed very innovative low-mass oxynitride films to realize 25 cm-long, 65 µm-semicircular buried separation columns. These columns provided 5000 plates/meter and showed better performance than a 50 µm fused silica capillary column. It is pertinent to mention that up until 2009 microfabricated columns were designed like an open channel configuration. For the first time

Amin *et al.* [192] utilized MEMS techniques and introduced multicapillary columns (MCCs) to improve the separation efficiency and sample capacity. Two and four channel polymer coated MCCs (25 µm-wide) were produced to achieve high separation efficiencies of 12,500 plates/meter. Similarly, Mark Shannon's group at the University of Illinois at Urbana Champaign also utilized MEMS fabrication techniques to realize partially buried columns [34] with a rounded channel profile. Meanwhile, the MEMS lab at Virginia Tech reported a unique microfabricated column design called "Semipacked Columns (SPCs)" [37]. In order to improve the sample capacity and velocity profile inside microchannels, the group skillfully integrated micropillars inside the fluidic channel. These new generation columns provided superior chromatographic performance (15,000 plates/m) and sample capacity compared to their open-rectangular counterparts.

Although the miniaturization of separation columns generates a number of benefits but it also presents a number of technical fabrication challenges. One of these challenges being to be able to achieve uniform and reproducible stationary phase coatings especially for very small column dimensions. Similar to conventional capillary columns, microcolumns were initially coated with liquid polymer based thin films. The use of nontraditional adsorbent based coating method for microfabricated columns was first reported by Stadermann *et al.* [40]. The authors integrated single-walled CNTs into a 50 cm-long, 100 µm x 100 µm square microfabricated column. The growth of CNTs was carried out in-situ using a standard chemical vapor deposition technique. CNTs based solid stationary phase coupled with integrated resistive heaters enabled the ultrafast separation of a four compound mixture in less than a second. Moreover, Amin *et al.* reported a new stationary phase deposition technique called monolayer-protected gold layer [12] for ultra-narrow single and multi-channel microfabricated columns. This method was based on seedless electroplating techniques followed by a simple thiol-functionalization. Although requiring manual gold removal steps, this technique presented promising separation results and produced columns with 20,000 plates/meter. Furthermore, Vial *et al.* employed MEMS compatible sputtering technique to deposit solid adsorbent materials like silica [25], graphite [24] and alumina [106] for open and semipacked columns. Additionally, our group integrated thin films (~500 nm) of silica nanoparticles (SNPs) inside both 1m-long single channel columns (150 µm-wide and 250µm-deep) and 25cm-long MCCs (20µm-wide and 220µm-deep) using a well-established layer-by-layer coating method. This highly stable and homogenous SNPs based stationary phase was able to separate a complex aromatic hydrocarbon mixture. Similarly, atomic layer deposition (ALD) based coating, recently developed by our group for SPCs (1m-long, 190µm-wide with 20µm-circular micropillars and 20µm-post spacing), also enables the realization of a highly reproducible, conformal, easy to use, mechanically and thermally stable separation films [42].

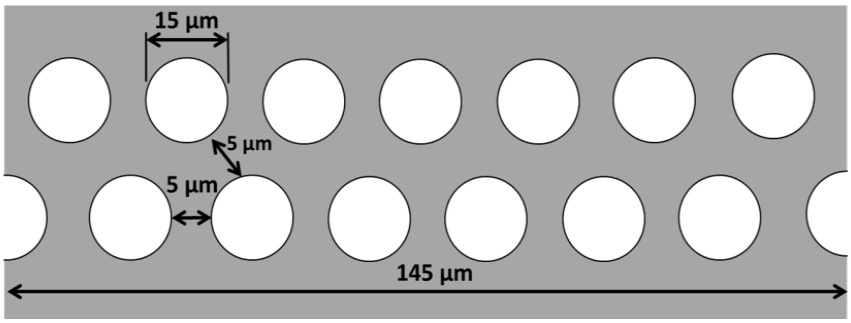

Figure 7.1: *Profile of 1m-long high density semipacked columns.*

There are a number of publications related to SPCs but due to limitation of coating techniques all of the reported designs either utilized very lightly packed columns (micro-pillar post spacing ≥20 µm) [39] or channels with shallow depths (≤ 100 µm) [25]. It has been well established (Van Deemter Equation) that the efficiency of separation columns can be enhanced by decreasing the column width. Therefore, the performance of SPCs could be further improved by reducing the effective channel width (reducing the micropillar diameters and spacing) provided a suitable stationary phase coating method exists. Due to the inherent properties of ALD, especially its highly conformal deposition, it holds a tremendous potential for coating the columns with very small features (below ≤ 10µm regime). In this report, we present high-density semipacked columns (HDSPCs), as shown in Figure 7.1, coated with optimized silane functionalized/ALD based stationary phases. The performance of ALD-based thin films is optimized using different deposition temperatures (100˚C, 150˚C, 250˚C and 300˚C) and thicknesses (10nm, 20nm, and 30nm).

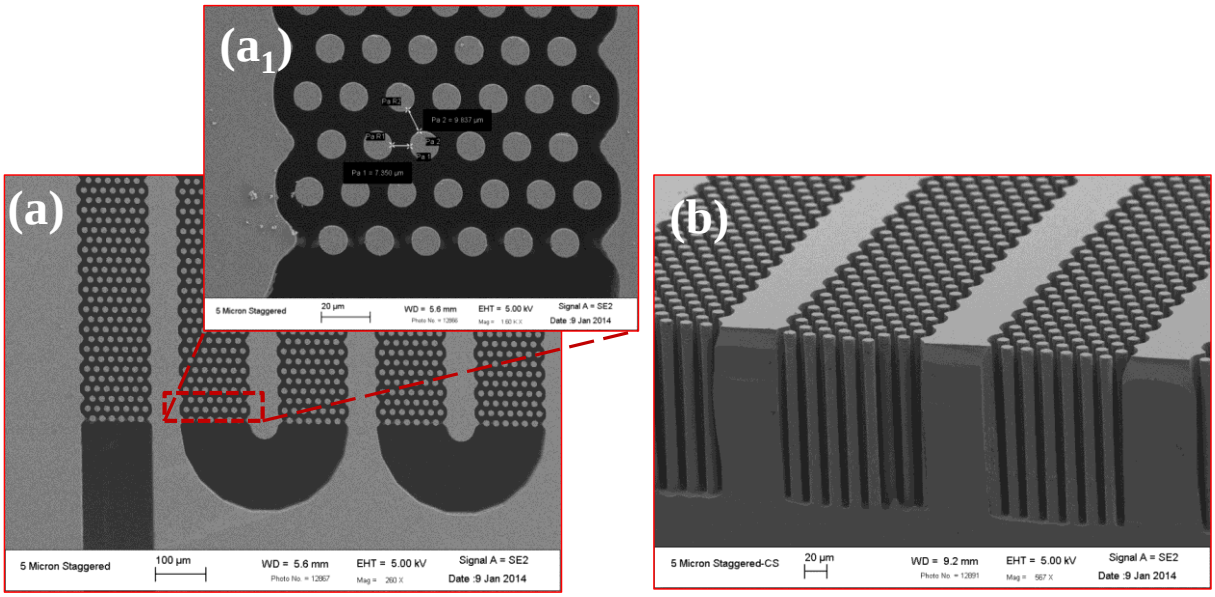

Figure 7.2: *SEM images of high density semipacked columns (a) top view, (b) cross-section.*

I. Fabrication

A. Column Fabrication

To demonstrate the wafer-level coating for our newly developed HDSPCs architecture, we developed 1m-long, 145µm-wide, 180µm-deep HDSPCs with 15µm circular posts and 5µm post-spacing using standard MEMS processes. The fabrication of these columns is similar to our recently published work [42] and performed on a 4 inch-wide and 100 µm-thick single side polished silicon wafer. The RCA cleaned wafer is first primed using HMDS followed by heating at 110˚C for 4 minutes. Afterwards AZ9260 photoresist is spin coated at 2000 rpm and the wafer is soft-baked at 110˚C for 90 seconds to get film thickness of 8µm. An ultra violet light source is used to transfer the pattern from the mask onto the spin-coated wafer using a mask aligner (MA-6). Afterwards the wafer is first developed in a diluted AZ400K solution and then hard-baked for 4 minutes at 110˚C. DRIE is used to etch the hard-baked wafer at -10˚C to produce columns with a highly anisotropic etch profile and depth of ~220 µm. In the next step, acetone is first used to clean the etched silicon wafer followed by an oxygen plasma cleaning step for 5 minutes. The use of oxygen plasma is twofold; first it removes the photoresist from the top silicon surface and finally it removes the passivation polymer inside the microchannels deposited during DRIE. It has been experimentally confirmed that the non-removal of this passivation polymer results in improper ALD-film deposition since the surface properties of the polymer are different from the silicon surface. Figure 7.2 shows the SEM images of a highly-packed etched silicon device after photoresist removal and plasma cleaning steps.

B. ALD Coating

The optimization of aluminum oxide film is carried out at different temperatures (Table 7.1) and thicknesses using trimethylaluminum (TMA) and water as precursors inside a thermal ALD chamber.

Table 7. 1 *Deposition conditions for 10 nm thick aluminum oxide film deposited at different temperatures using TMA and H_2O as precursors.*

10 nm aluminum oxide ALD film growth from H_2O and TMA at different temperatures				
Cycle	100 ˚C	150 ˚C	250 ˚C	300 ˚C
H_20 (s)	0.015			
Wait (s)	60	20	5	4
TMA (s)	0.015			
Deposition time (minutes)	200	32	17	13

Since the film deposition at lower temperatures takes a longer time, first the effect of change in chamber temperature is studied for a fixed film thickness (100 cycles and 10nm). It is important to note that the deposition rate for each recipe in Table 7.1 is around 1 Å/cycle. Each ALD deposition cycle consists of four steps, exposure of each precursor i.e. TMA and water for 15 ms (20 sccm flow) is followed by a purge cycle depending on the selected temperature. The increase in purge time for a low temperature (Table 7.1) is necessary to avoid the chemical vapor deposition of aluminum oxide film [178] which is due to the slow desorption rate of water at low temperatures. Figure 7.3 shows the graphical representation of a well-established ALD based aluminum oxide film deposition during each precursor exposure and purge cycles.

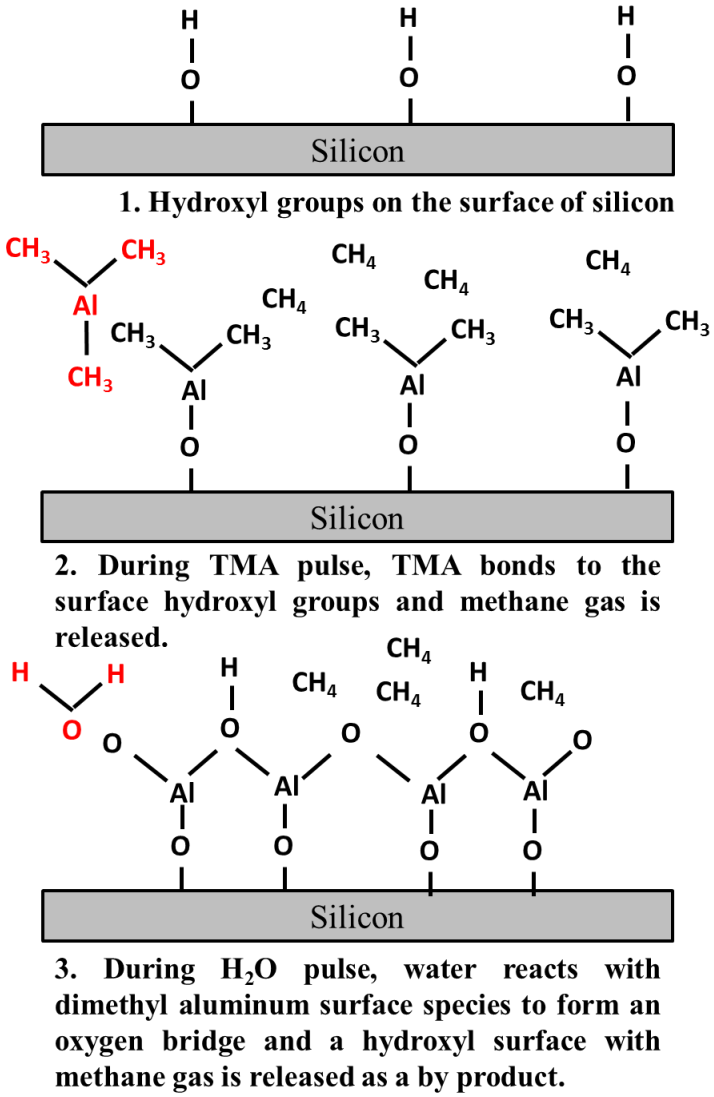

Figure 7.3: *Graphical representation of surface reactions during an ALD process using TMA and H_2O precursors.*

C. Anodic Bonding and Silane Coating

Following ALD coating, the etched silicon wafer is first diced into the individual devices and then separately bonded with a Borofloat™ wafer at 380˚C and 1250 V for 45 minutes using a custom-made anodic bonding station. Following this deactivated fused silica glass capillary tubing (200 µm outer-diameter, 100 µm internal-diameter and 25cm-long) is attached to the inlet and outlet ports of each column using a two port epoxy adhesive. As demonstrated previously, the surface of ALD-aluminum oxide is not sufficient for chromatographic separations. Therefore, each column is filled with a solution of 10mM chlorodimethyloctadecylsilane (CDOS) diluted in toluene for surface functionalization. In the next step, each column is sealed at both ends using septa and kept at room temperature for 15 hours. Before performing any chromatographic experiments, columns are purged with dry nitrogen for 45 minutes to remove silane solution. Afterwards each column is conditioned inside a GC oven for one hour from a room temperature to 150˚C (2˚C/min) with a constant nitrogen flow (7.5 psi).

II. Results and Discussion

The effect of aluminum oxide deposition conditions on the chromatographic separations is studied in detail by first varying the chamber temperature (100˚C, 150˚C, 250˚C and 300˚C) and then the film thickness (10 nm, 20 nm and 30 nm). As a first step, the film thickness is fixed to 10 nm while the deposition temperature is varied using conditions mentioned in Table 7.1. It is important to note that it takes longer to deposit ALD-based films at lower temperatures. Different chromatographic parameters (Golay plots, Van't Hoff plots, peak-to-peak resolution, Trenzahl number, separation factor, retention time, and peak widths) are extracted from the chromatogram to benchmark the performance of each deposited film using n-nonane and n-decane (diluted in dichloromethane) as probes. An unretained

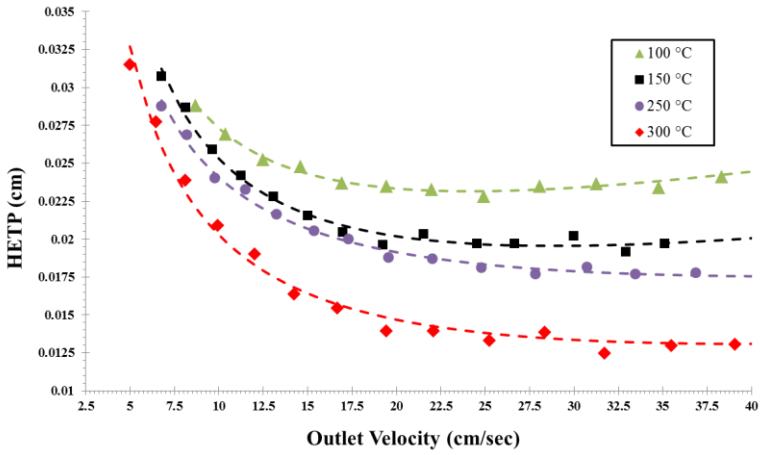

Figure 7.4: *Golay plots for HDSPCs with 10 nm ALD/silane functionalized film deposited at different temperatures. The error bars in the plot are smaller than symbols therefore they are omitted (sample size 3).*

methane gas vapor is used to measure the average carrier gas velocities and hold-up time (three sample points) against different inlet pressures for each ALD/silane functionalized column. Plate height (H) is considered to be the most important performance index for quantitative evaluation and optimization of a chromatographic system. H is given by L/N, where L is the length of a column and N is the plate number. Theoretically N is given by equation 1 and typically measured graphically from a chromatogram using equation 7.2 [1]

$$N = \frac{t_r^2}{\sigma^2} \qquad (7.1)$$

$$N = 5.546 \times \left(\frac{t_r}{w_{1/2}}\right)^2 \qquad (7.2)$$

Where, σ^2 represents the peak dispersion (band broadening), t_r is known as the retention time and $w_{1/2}$ is the peak width at the half height. The high packing density of HDSPCs result in the longer hold-up times compared to our previously reported lightly packed columns [42]. Therefore, the plate numbers (N) and plate height (H) cannot be true indicators of the column's separation power. Under this condition, a better approach to characterize the separation efficiency of the MEMS columns is to use the effective plate number ($N_{eff.}$) as the figure of merit [1]

$$N_{eff} = 5.546 \times \left(\frac{t_r - t_o}{w_{1/2}}\right)^2 \qquad (7.3)$$

$$H_{eff} = \frac{L}{N_{eff}} \qquad (7.4)$$

Where t_r is the retention time and $w_{1/2}$ is the peak-width at half height for n-decane diluted in dicholormethane. While t_o is the methane hold-up time. Figure 7.4 shows Golay plots of HDSPCs with aluminum oxide film deposited at different temperatures. From these plots it is clear that film deposited at

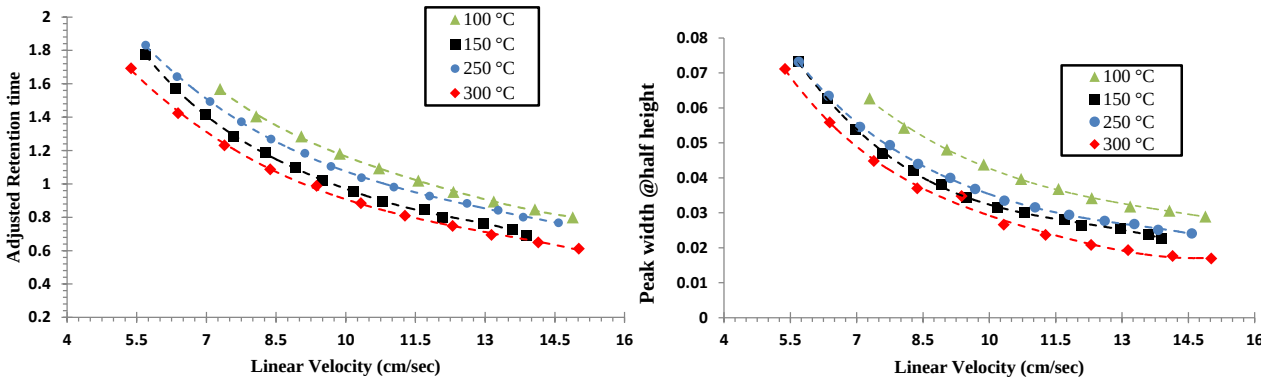

Figure 7.5: *Adjusted retention time and peak-width plots for HDSPCs with 10 nm ALD/silane functionalized film deposited at different temperatures.*

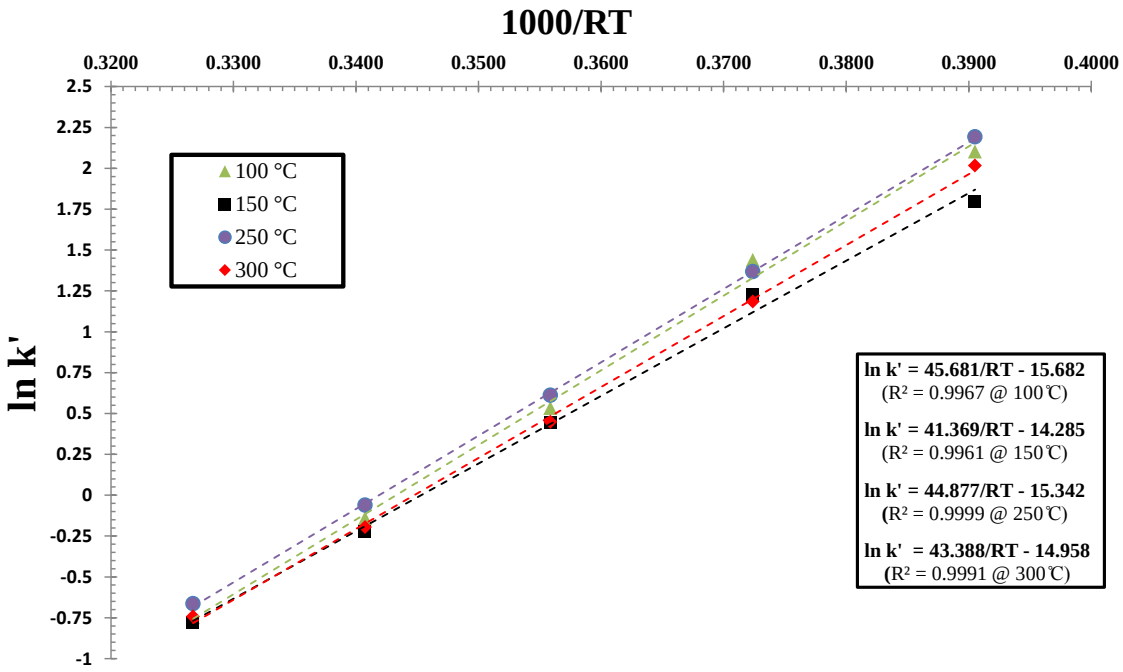

Figure 7.6: *Thermodynamic properties (Van't Hoff plots) of silane functionalized aluminum oxide films deposited at different temperatures using. n-decane is used as a probe with each column tested from 35˚°C to 80˚°C at 12 cm/sec. Methane vapor is used to calculate the dead times/capacity factors (k') corresponding to different temperatures with R= 8.314 J/K•mol. The error bars in the plot are smaller than symbols therefore they are omitted (sample size 3).*

300˚C provides the best performance (N_{eff}=8021 plates per meter) for the complete range of carrier gas velocities. A more insightful look into the plots presented in Figure 7.5 demonstrates that the adjusted retention time ($t_r - t_o$) for the films deposited at lower temperature is larger, while films deposited at higher temperatures provide narrower chromatographic peaks resulting in an overall high efficiency and peak-to-peak resolution. These results clearly demonstrate that the surface properties of films deposited at various temperatures is significantly different.

Thermodynamic properties of silane functionalized aluminum oxide films were also evaluated using Van't Hoff plots (Figure 7.6). The linear plots (R^2>0.99) are generated between 35˚C to 80˚C using n-decane (diluted in dichloromethane) as a probe and dead-time is calculated from an unretained methane vapor. From these plots, the standard adsorption heat ($|\Delta_r H^\theta|$) for silane functionalized ALD-films deposited at different temperatures is calculated, they range from 41.4-45.6 $k \bullet J/mol$. The results show that all these films show similar retention behavior and are thermodynamically very similar. These values are close to higher surface area CNTs ($|\Delta_r H^\theta|$=45.6 $k \bullet J/mol$) based coatings, deposited using chemical vapor deposition and also using n-decane as a probe [40]. Moreover, other chromatographic

Table 7. 2 *Different chromatographic parameters extracted from GC testing of HDSPCs with 10 nm aluminum oxide film grown at four different temperatures.*

Temperature	HETP ^{min} (cm)	N_{eff} (max) (plates/m)	Optimum Velocity (cm/sec)	Resolution ^{max} (C_9-C_{10})	Separation Factor (k_{n+1}/k_n)	Trenzahl Numbers (TZ)	ΔH (kJ/mol)
100 °C	0.022	4381	13.18	21.79	2.43-2.53	9.89	45.68
150 °C	0.019	5214	13.61	22.54	2.4-2.5	10.13	41.36
250 °C	0.017	5654	12.61	24.49	2.47-2.58	11.28	44.87
300 °C	0.012	8021	15.91	28.4	2.38-2.53	13.24	43.38

parameters such peak-to-peak resolution (R_S), separation factor and Trenzahl (TZ) number between the two adjacent hydrocarbon analytes (n-nonae and n-decane) are also evaluated [112]

$$R_S = 2 \times \left(\frac{t_{rb} - t_{rb}}{w_{rb} + w_{ra}}\right) \qquad (7.5)$$

$$TZ = \left(\frac{t_{rb} - t_{rb}}{w_{rb} + w_{ra}}\right) - 1 \qquad (7.6)$$

Where, t_{ra} and t_{rb} correspond to retention times and w_{ra} and w_{rb} represent the peak widths at the base of the corresponding compounds a and b. The TZ number gives valuable information regarding the number of peaks that can be included between the two consecutive homologous hydrocarbons (here n-nonae and n-decane). Table 7.2 shows the complete list of these extracted parameters (average values, sample size 3) for four different HDSPCs, each with a 10 nm film deposited at four different temperatures. It is clear from the results (Table 7.2) that the best chromatographic performance (N_{eff}, R_S and TZ) is achieved when ALD-film is deposited at higher temperature (300˚C). The deposition at 300˚C provides an additional advantage of taking the least time (~13 minutes). After the optimization of

Table 7. 3 *Different chromatographic parameters extracted from GC testing of HDSPCs with aluminum oxide film grown at 300˚C with three different thicknesses.*

Thickness (deposition time)	HETP ^{min} (cm)	N_{eff} (max) (plates/m)	Optimum Velocity (cm/sec)	Resolution ^{max} (C_9-C_{10})	Separation Factor (k_{n+1}/k_n)	Trenzahl Numbers (TZ)	ΔH (kJ/mol)
10 nm (13 min)	0.012	8021	15.91	28.4	2.38-2.53	13.24	43.38
20 nm (26 min)	0.018	5424	13.26	24.28	2.44-2.55	12.14	43.88
30 nm (39 min)	0.023	4347	13.51	21.86	2.58-2.60	10.96	43.81

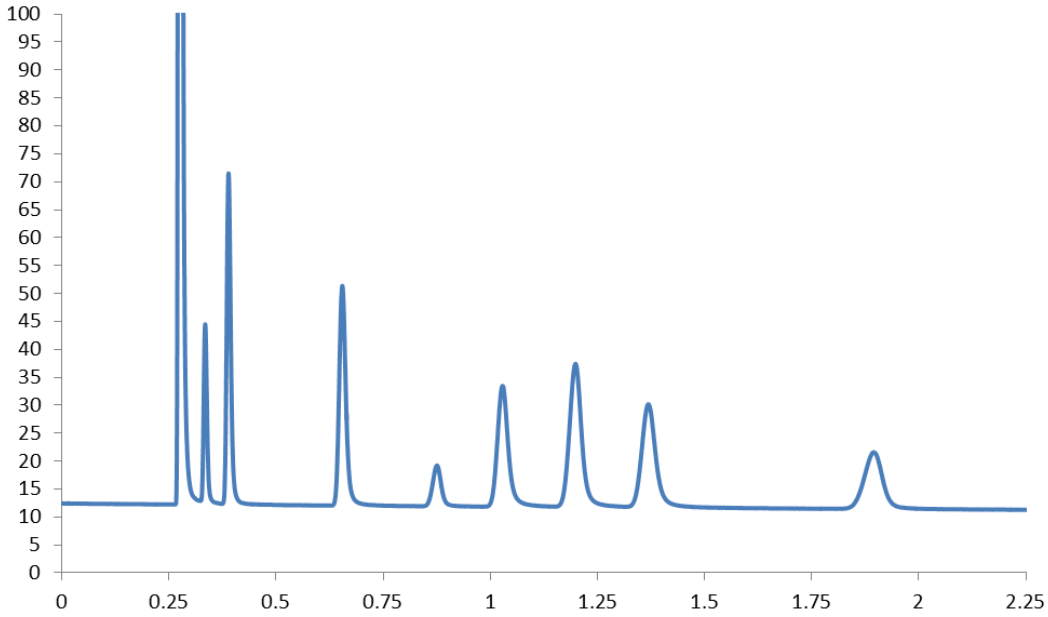

Figure 7.7: *Separation performance of an ALD-coated/silane functionalized HDSPCs at 50˚ C. Compound identification in order of elution 1.dichloromethane 2. n-hexane 3. benzene 4. toluene 5. tetrachloroethylene 6. chlorobenzene 7. ethylbenzene 8. p-xylene 9. n-nonane*

deposition temperature,the next step is the optimization in the film thickness (10 nm, 20 nm, and 30 nm) which is carried out using the same performance parameters. Table 7.3 shows the summary of these results and it is clearly demonstrated that 10 nm film deposited at 300˚ C shows the best overall chromatographic performance. Moreover, the kinetic, thermodynamic and retention behavior of 30 nm film deposited at 300˚C (taking 39 minutes to deposit) is very similar to the 10 nm film deposited at 100˚ C (240 minutes).

A test mixture containing a nine hydrocarbon mixture was prepared to test the separation capability of the HDSPCs with ALD enabled alumina stationary phase. HDSPC with ALD coating successfully separates this custom made test mixture at isothermal conditions (50˚C, 37.5 psi and 100:1 split ratio) as shown in Figure 7.7. The performance of our newly developed class of HDSPCs is significantly better than our previously presented results for lightly packed semi-packed columns [42].

III. Conclusion

This research allowed us to introduce a new generation of semi-packed columns with a high packing density. Our recently introduced high-yield ALD/silane functionalized coating scheme is integrated with these HDSPCs to provide the chromatographic separation capabilities. The coating is further optimized by varying both the deposition temperature (100˚C, 150˚C, 250˚C, and 300˚C) and the film thickness (10 nm, 20 nm, and 30 nm). The best chromatographic performance is generated by a 10 nm aluminum oxide

film deposited at 300˚C. Moreover, this optimized film also yields the highest peak-to-peak resolution and peak capacity.

CHAPTER 8: Conclusion and Future Research

I. Conclusion

The aim of this thesis was to integrate different microfabrication and nanotechnology based techniques in order to enhance key separation column performance parameters. During the course of this research new microfabrication techniques were developed to integrate thin gold films inside high-aspect ratio microcolumns. These self-patterning methods are independent of any gold removal steps and are readily applied to different column architectures like multicapillary and semipacked columns. The patterned gold film was further functionalized with thiol based coatings for chromatographic separations. Moreover, two new nanotechnology based stationary phases were also introduced. In collaboration with the Physics Department at Virginia Tech, first LbL method was employed to deposit highly stable, controllable and homogenous nanoparticles (silica and gold) based coatings inside open channels, multicapillary and semi-packed columns. The separation performance of SNPs was further enhanced using silane based surface functionalization. The scaling down of key column dimensions such as column width below 10 µm theoretically affords greater separation power. The key constraint for achieving high efficiencies is in achieving a uniform and reproducible stationary phase inside very narrow microstructures (<10 µm). Currently available polymer and solid adsorbent based methods are not compatible with these designs. Recently we have demonstrated a new stationary phase method based on atomic layer deposition (ALD) of metal oxide thin films for semipacked columns. The chromatographic testing of ALD based columns is performed using both liquid (10,000 ppm) [193] and gas phase samples [194]. The separation results

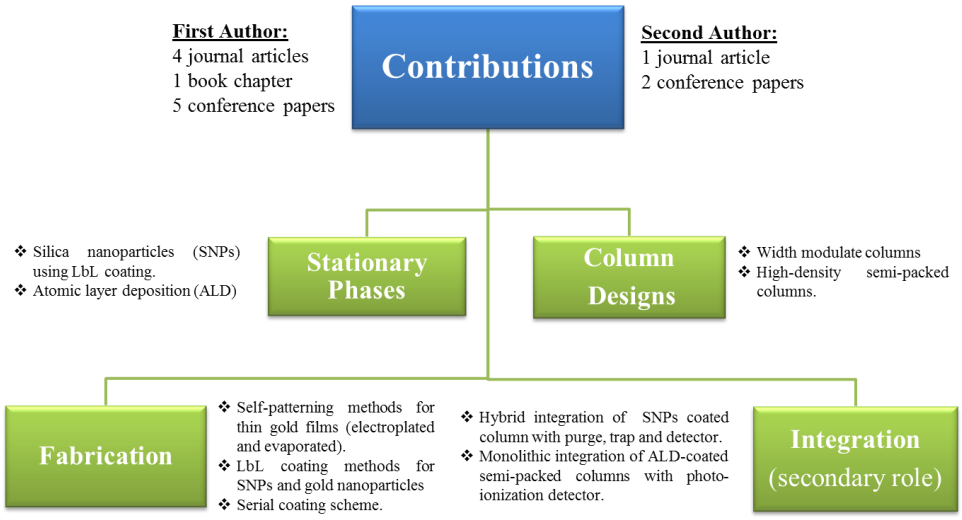

***Figure 8.1**: A breakdown of contribution of this research into development of new stationary phases, column designs, microfabrication techniques and integration.*

clearly demonstrate that the large variations in sample concentration does not affect the separation performance significantly. Additionally, two new high performance column designs were also introduced. The first of its kind width-modulated columns (linearly variable and step-gradient), coated with SNPs, were designed with variable width and provided better chromatographic performance compared to columns with fixed dimensions. One of the original contributions of this research is the development of highly packed semi-packed columns (5 µm post spacing) with optimized ALD/silane functionalized stationary phases. Moreover both kinetic and thermodynamic properties of these phases are studied. Additionally the standard Van Deemter equation was found to be valid for these high density semi-packed columns. The breakdown of this equation could be studied in future for columns with even smaller features. Figure 8.1 further categorizes these key contributions in terms of stationary phase development, column design, fabrication and integration.

II. Summary of Publications

a. Self-Patterned Gold Electroplated Multicapillary Gas Separation Columns with MPG Stationary Phases (Chapter 2).

This paper reports the development of two diverse self-patterned gold electro-deposition fabrication techniques for high-aspect-ratio microfluidic channels including multicapillary gas chromatography columns. First approach involves geometry dependent tuned electroplating conditions to self-pattern gold along the vertical sidewalls without any deposition on horizontal top and bottom surfaces, while the second method provides highly conformal gold deposition inside the three dimensional microchannels. Both reported approaches do not require a post-deposition patterning step, while affording at the same time excellent bonding and stationary phase coating yields. The ability of thiol to self-assemble on gold surface is also utilized to form monolayer-protected-gold (MPG) surfaces and is used as a stationary phase for micro gas chromatography. To evaluate chromatographic performance of both schemes, 250µm-deep, 30µm-wide, 25cm-long microfabricated multicapillary columns (µMCC) with 16 channels are functionalized by self-assembly of octadecanethiol ($C_{18}H_{37}SH$) to form the MPG surface. With about 7300 plates/m theoretical plates, these columns demonstrate the highest reported separation efficiency on 16 channels µMCCs and are capable of separating complex gas mixtures containing compounds with wide range of boiling points.

b. Improved Self-Assembled Thiol Stationary Phases in Microfluidic Gas Separation Columns (Chapter 3).

Semipacked columns (SPCs) with integrated micropillars have been characterized for high chromatographic efficiencies and fast separations. In this article, high-yield and stable alkane thiol based stationary phase coating methods are presented for SPCs. Briefly, a new three step (anisotropic,

O2 plasma, and isotropic) etching method is first developed in order to improve metal lift-off by producing a 3-dimensional undercutting profile inside deep etched SPCs. This innovative fabrication scheme is used for 1m-long, 220 µm-deep, 190 µm-wide SPCs with circular micropillars of 20 µm-diameters and 42 µm-post spacing. Two different thin gold film deposition techniques are utilized for microcolumns 1) a wafer-level physical vapor deposition, and 2) a device level layer-by-layer (LbL) self-assembly of gold nanoparticles (3.2 nm diameter). After gold film deposition and metal lift-off, the surface of the patterned gold layer is functionalized with a 2 mM octadecanethiol (C18H37SH) solution for chromatographic separations. Both kinetic (Golay plots) and thermodynamic (Van't Hoff plot) properties of thiol-functionalized gold phases are studied. The significance of SPCs, for faster analysis, is also validated by achieving baseline separation of a straight chain alkane mixture, containing high boilers (174˚C to 287˚C), within 45 seconds.

c. Highly Stable Surface Functionalization of Microgas Chromatography Columns Using Layer-by-Layer Self-Assembly of Silica Nanoparticles (Chapter 4).

In this journal article published in Analytical Chemistry, a controllable and high-yield surface functionalization of silicon microchannels using layer-by-layer (LbL) self-assembly of SiO_2 nanoparticles (SNPs) is presented. The application of SNPs (45 nm average diameter) coating as a stationary phase for chromatographic separation is also demonstrated with surface functionalization using chloroalkylsilanes. This method facilitates a simple, low-cost and parallel processing scheme that also provides homogenous and stable nanoparticle based stationary phases with ease of control over the coating thickness. The SNP-functionalized microfabricated columns with either single capillary channels (1 m-long, 150 µm-wide, 240 µm-deep) or very narrow multicapillary channels (25 cm-long, 30 µm-wide, 240 µm-deep, 16 parallel channels) successfully separated a multicomponent gas mixture with a wide range of boiling points with high reproducibility.

d. Width-modulated Microfluidic Columns for Gas Separations (Chapter 5).

Microgas chromatography separation columns typically employ channels with fixed cross sections. In this paper, we demonstrate a new class of unidirectional microfabricated width-modulated columns (µWMC) that afford improved chromatographic efficiency, resolution, and retention times compared with corresponding constant width (120 µm) bidirectional columns. Two new µWMCs architectures are introduced: a linearly variable column (LVC) and a step gradient column (SGC). The width of a 1-m long, 250-µm-deep LVC is gradually reduced from 120 to 20 µm at 1 µm/cm. While that of a 1-m-long SGC is modulated in five steps (120, 95, 70, 45, and 20 µm) each with a length of 20 cm. The effect of inlet selection (120 or 20 µm) on chromatographic performance is also evaluated. Moreover, with our improved fabrication process, multiple serially connected devices are simultaneously coated

for the first time with highly stable silica nanoparticles utilizing layer-by-layer technique enabling constant film thickness.

e. Semipacked columns with atomic layer deposited alumina as a stationary phase (Chapter 6).

This paper describes a new approach for utilizing atomic layer deposited metal oxides as a gas-solid stationary phase medium for microfabricated gas chromatography columns. After atomic layer deposition (ALD) of aluminum oxide, a chloroalkylsilane is utilized to functionalize the oxide surface to improve peak symmetry and retention times. Semipacked columns (1m-long, 190 µm-wide with 20 µm-embedded circular micropillars) were utilized for validation of this newly developed approach. The inherent properties of atomic layer deposition provide an easy route to coat any microfabricated column architecture.

In conclusion table 8.1 lists different types of bonds associated with each nanotechnology enabled stationary phase. Moreover, the adsorption forces that bind gas phase molecules to a particular surface is also presented. Although in most cases adsorption is based on Van der Waals forces but for thiol based polar stationary phase (6 M1H) [41] the adsorption forces are different. Moreover, the separation of analytes for this phase is based on the polarities of compounds rather than their volatilites.

Table 8. 1 *Different types of bonds associated with the presented stationary phases and the corresponding forces.*

Type		Bond	Adsorption forces
Thiol-gold	Octadecane (C_{18}) thiol	dative bond	Van der Waals forces
	6-Mercapto-1-Hexanol thiol (6M1H)		Dipole-dipole and hydrogen bonding for polar solutes.
SNPs- Silane		covalent bond	Van der Waals forces
ALD-Silane		covalent bond	

III. Future Outlook

This research work primarily dealt with the introduction of new column designs, fabrication methodologies and novel coatings for MEMS based separation columns. The chromatographic evaluation of these columns was carried out using standard and simple hydrocarbon mixtures containing straight chain alkanes, aromatic hydrocarbons, and simple polar compounds. There is a critical requirement for developing new stationary phase surfaces to separate different classes of compounds such as (fatty acid

methyl esters, chiral, and semi-volatile organic compounds) and inert gases (helium, argon, oxygen, and nitrogen). This work can take advantage of already developed MPG, LbL and ALD based coatings methods to engineer the surface properties of these films using different thiol and/or silane chemistries. Moreover, the work on LbL coating could also be extended in future to CNTs and graphene nano-sheet based coatings. Microfabricated separation columns are typically designed with fixed cross-sections. As demonstrated in Chapter 5, open channel WMCs were introduced to enhance chromatographic efficiency and resolution. In the future, an in-depth study could be carried out to optimize critical column dimensions (maximum and minimum widths, length and channel depth) using detail chromatographic analysis. Similarly, a new class of microcolumns could also be designed by combining modulating channels with embedded micropillars. After detailed optimization of ALD based aluminum oxide coating (thickness and deposition temperature) as presented in Chapter 7, other available oxide (tantalum pentoxide, hafnium oxide etc) and nitride based thin films could also be deposited using ALD to provide chemical selectivity. Similarly, plasma based ALD systems could also be employed for deposition instead of utilizing thermal ALD systems. HDSPCs (Chapter 7) are introduced with a minimum feature size of 5 µm, given the availability of an electron beam lithography system the minimum feature size could be reduced to further enhance the separation performance.

References

[1] H. M. McNair and J. M. Miller, "Basic Gas Chromatography," Second ed NJ: Wiley, 2009.

[2] V. P. Zhdanov, V. N. Sidelnikov, and A. A. Vlasov, "Dependence of the efficiency of a multicapillary column on the liquid phase loading method," *Journal of Chromatography A*, vol. 928, pp. 201-207, 2001.

[3] V. N. Sidelnikov, Y. V. Patrushev, and O. A. Nikolaeva, "Express gas chromatography on multicapillary columns and its potential," *Catalysis in Industry*, vol. 2, pp. 206-216, 2010.

[4] G. M. Gross, D. A. Nelson, J. W. Grate, and R. E. Synovec, "Monolayer-Protected Gold Nanoparticles as a Stationary Phase for Open Tubular Gas Chromatography," *Analytical Chemistry*, vol. 75, pp. 4558-4564, 2003.

[5] Z. A. Khan, R. Kumar, W. S. Mohammed, G. L. Hornyak, and J. Dutta, "Optical thin film filters of colloidal gold and silica nanoparticles prepared by a layer-by-layer self-assembly method," *Journal of Materials Science*, vol. 46, pp. 6877-6882, Nov 2011.

[6] C. M. Hussain, C. Saridara, and S. Mitra, "Self-Assembly of Carbon Nanotubes via Ethanol Chemical Vapor Deposition for the Synthesis of Gas Chromatography Columns," *Analytical Chemistry*, vol. 82, pp. 5184-5188, 2010.

[7] S. C. Terry, J. H. Jerman, and J. B. Angell, "A gas chromatographic air analyzer fabricated on a silicon wafer," *Electron Devices, IEEE Transactions on*, vol. 26, pp. 1880-1886, 1979.

[8] A. D. Radadia, A. Salehi-Khojin, R. I. Masel, and M. A. Shannon, "The fabrication of all-silicon micro gas chromatography columns using gold diffusion eutectic bonding," *Journal of Micromechanics and Microengineering*, vol. 20, p. 015002, 2010.

[9] A. C. Lewis, J. F. Hamilton, C. N. Rhodes, J. Halliday, K. D. Bartle, P. Homewood, R. J. P. Grenfell, B. Goody, A. M. Harling, P. Brewer, G. Vargha, and M. J. T. Milton, "Microfabricated planar glass gas chromatography with photoionization detection," *Journal of Chromatography A*, vol. 1217, pp. 768-774, 2010.

[10] M. J. Madou, *Fundamentals of microfabrication: the science of miniaturization*: CRC press, 2002.

[11] E. Steinsland, M. Nese, A. Hanneborg, R. W. Bernstein, H. Sandmo, and G. Kittilsland, "Boron etch-stop in TMAH solutions," *Sensors and Actuators A: Physical*, vol. 54, pp. 728-732, 1996.

[12] M. A. Zareian-Jahromi and M. Agah, "Microfabricated Gas Chromatography Columns With Monolayer-Protected Gold Stationary Phases," *Microelectromechanical Systems, Journal of*, vol. 19, pp. 294-304, 2010.

[13] T. M. H. Lee, D. H. Y. Lee, C. Y. N. Liaw, A. I. K. Lao, and I. M. Hsing, "Detailed characterization of anodic bonding process between glass and thin-film coated silicon substrates," *Sensors and Actuators A: Physical*, vol. 86, pp. 103-107, 2000.

[14] A. d. Mello, "FOCUS On-chip chromatography: the last twenty years," *Lab on a Chip*, vol. 2, pp. 48N-54N, 2002.

[15] A. Manz, Y. Miyahara, J. Miura, Y. Watanabe, H. Miyagi, and K. Sato, "Design of an open-tubular column liquid chromatograph using silicon chip technology," *Sensors and Actuators B: Chemical*, vol. 1, pp. 249-255, 1990.

[16] R. R. Reston and E. S. Kolesar, "Silicon-micromachined gas chromatography system used to separate and detect ammonia and nitrogen dioxide. I. Design, fabrication, and integration of the gas chromatography system," *Microelectromechanical Systems, Journal of*, vol. 3, pp. 134-146, 1994.

[17] U. Lehmann, O. Krusemark, J. Müller, A. Vogel, and D. Binz, "Micro machined gas chromatograph based on a plasma polymerised stationary phase," in *Micro Total Analysis Systems 2000*, A. Berg, W. Olthuis, and P. Bergveld, Eds., ed: Springer Netherlands, 2000, pp. 167-170.

[18] P. R. Lewis, R. P. Manginell, D. R. Adkins, R. J. Kottenstette, D. R. Wheeler, S. S. Sokolowski, D. E. Trudell, J. E. Byrnes, M. Okandan, J. M. Bauer, R. G. Manley, and C. Frye-Mason, "Recent advancements in the gas-phase MicroChemLab," *Sensors Journal, IEEE*, vol. 6, pp. 784-795, 2006.

[19] M. Agah, J. A. Potkay, G. Lambertus, R. Sacks, and K. D. Wise, "High-performance temperature-programmed microfabricated gas chromatography columns," *Microelectromechanical Systems, Journal of*, vol. 14, pp. 1039-1050, 2005.

[20] Y. Qin and Y. B. Gianchandani, "iGC2 : an architecture for micro gas chromatographs utilizing integrated bi-directional pumps and multi-stage preconcentrators," *Journal of Micromechanics and Microengineering*, vol. 24, p. 065011, 2014.

[21] H. Shakeel, W. Dong, R. Heflin, and M. Agah, "Width-modulated microgas chromatography separation columns with silica nanoparticles stationary phase," in *Sensors, 2013 IEEE*, 2013, pp. 1-4.

[22] D. Wang, H. Shakeel, J. Lovette, G. W. Rice, J. R. Heflin, and M. Agah, "Highly Stable Surface Functionalization of Microgas Chromatography Columns Using Layer-by-Layer Self-Assembly of Silica Nanoparticles," *Analytical Chemistry*, vol. 85, pp. 8135-8141, 2013/09/03 2013.
[23] H. Shakeel and M. Agah, "Self-Patterned Gold-Electroplated Multicapillary Gas Separation Columns With MPG Stationary Phases," *Microelectromechanical Systems, Journal of*, vol. 22, pp. 62-70, 2013.
[24] R. Haudebourg, J. Vial, D. Thiebaut, K. Danaie, J. Breviere, P. Sassiat, I. Azzouz, and B. Bourlon, "Temperature-Programmed Sputtered Micromachined Gas Chromatography Columns: An Approach to Fast Separations in Oilfield Applications," *Analytical Chemistry*, vol. 85, pp. 114-120, 2012.
[25] J. Vial, D. Thiébaut, F. Marty, P. Guibal, R. Haudebourg, K. Nachef, K. Danaie, and B. Bourlon, "Silica sputtering as a novel collective stationary phase deposition for microelectromechanical system gas chromatography column: Feasibility and first separations," *Journal of Chromatography A*, vol. 1218, pp. 3262-3266, 2011.
[26] K. Nachef, F. Marty, E. Donzier, B. Bourlon, K. Danaie, and T. Bourouina, "Micro gas chromatography sample injector for the analysis of natural gas," *Microelectromechanical Systems, Journal of*, vol. 21, pp. 730-738, 2012.
[27] S. Narayanan, G. Rice, and M. Agah, "A micro-discharge photoionization detector for micro-gas chromatography," *Microchimica Acta*, vol. 181, pp. 493-499, 2014.
[28] E. Covington, F. I. Bohrer, C. Xu, E. T. Zellers, and C. Kurdak, "Densely integrated array of chemiresistor vapor sensors with electron-beam patterned monolayer-protected gold nanoparticle interface films," *Lab on a Chip*, vol. 10, pp. 3058-3060, 2010.
[29] N. K. Gupta, S. An, and Y. B. Gianchandani, "A Si-micromachined 48-stage Knudsen pump for on-chip vacuum," *Journal of Micromechanics and Microengineering*, vol. 22, p. 105026, 2012.
[30] Q. Yutao and Y. B. Gianchandani, "A micro gas chromatograph with integrated bi-directional pump for quantitative analyses," in *Micro Electro Mechanical Systems (MEMS), 2014 IEEE 27th International Conference on*, 2014, pp. 294-297.
[31] A. Garg, M. Akbar, E. Vejerano, S. Narayanan, L. Nazhandali, L. C. Marr, and M. Agah, "Zebra GC: A mini gas chromatography system for trace-level determination of hazardous air pollutants," *Sensors and Actuators B: Chemical, http://dx.doi.org/10.1016/j.snb.2014.12.136*.
[32] A. D. Radadia, A. Salehi-Khojin, R. I. Masel, and M. A. Shannon, "The effect of microcolumn geometry on the performance of micro-gas chromatography columns for chip scale gas analyzers," *Sensors and Actuators B: Chemical*, vol. 150, pp. 456-464, 2010.
[33] M. Agah and K. D. Wise, "Low-Mass PECVD Oxynitride Gas Chromatographic Columns," *Microelectromechanical Systems, Journal of*, vol. 16, pp. 853-860, 2007.
[34] A. D. Radadia, R. D. Morgan, R. I. Masel, and M. A. Shannon, "Partially Buried Microcolumns for Micro Gas Analyzers," *Analytical Chemistry*, vol. 81, pp. 3471-3477, 2009.
[35] X. Yan, J. Yang, Q. Wang, and Y. Liu, "Theoretical tools for predicting optimal cross-sectional shapes in micro-gas chromatography," *Journal of Separation Science*, vol. 36, pp. 1537-1544, 2013.
[36] B. Alfeeli, M. A. Zareian-Jahromi, and M. Agah, "Micro Preconcentrator with Seedless Electroplated Gold As Self-Heating Adsorbent," presented at the 8th IEEE Conference on Sensors, Chirstchurch, New Zealand, 2009.
[37] S. Ali, M. Ashraf-Khorassani, L. T. Taylor, and M. Agah, "MEMS-based semi-packed gas chromatography columns," *Sensors and Actuators B: Chemical*, vol. 141, pp. 309-315, 2009.
[38] S. Reidy, G. Lambertus, J. Reece, and R. Sacks, "High-Performance, Static-Coated Silicon Microfabricated Columns for Gas Chromatography," *Analytical Chemistry*, vol. 78, pp. 2623-2630, 2006.
[39] B. Alfeeli, S. Narayanan, D. Moodie, P. Zellner, M. McMillan, D. Hirtenstein, G. Rice, and M. Agah, "Interchannel Mixing Minimization in Semi-Packed Micro Gas Chromatography Columns," *Sensors Journal, IEEE*, vol. 13, pp. 4312-4319, 2013.
[40] M. Stadermann, A. D. McBrady, B. Dick, V. R. Reid, A. Noy, R. E. Synovec, and O. Bakajin, "Ultrafast Gas Chromatography on Single-Wall Carbon Nanotube Stationary Phases in Microfabricated Channels," *Analytical Chemistry*, vol. 78, pp. 5639-5644, 2006.
[41] H. Shakeel, G. Rice, and M. Agah, "First reconfigurable MEMS separation columns for micro gas chromatography," in *Micro Electro Mechanical Systems (MEMS), 2012 IEEE 25th International Conference on*, 2012, pp. 823-826.
[42] H. Shakeel, G. W. Rice, and M. Agah, "Semipacked columns with atomic layer-deposited alumina as a stationary phase," *Sensors and Actuators B: Chemical*, vol. 203, pp. 641-646, 2014.
[43] H. Shakeel and M. Agah, "High-Performance Multicapillary Gas Separation Columns with MPG Stationary Phases," in *IEEE Sensors*, 2011, pp. 1909-1912.

[44] H. Zareie, B. Alfeeli, M. A. Zareian-Jahromi, and M. Agah, "Self-patterned gold electroplated multicapillary separation columns," in *IEEE Sensors,*, 2010, pp. 1526-1529.
[45] P. R. Lewis, P. Manginell, D. R. Adkins, R. J. Kottenstette, D. R. Wheeler, S. S. Sokolowski, D. E. Trudell, J. E. Byrnes, M. Okandan, J. M. Bauer, R. G. Manley, and C. Frye-Mason, "Recent advancements in the gas-phase MicroChemLab," *Sensors Journal, IEEE,* vol. 6, pp. 784-795, 2006.
[46] E. S. Kolesar, Jr. and R. R. Reston, "Silicon-micromachined gas chromatography system used to separate and detect ammonia and nitrogen dioxide. II. Evaluation, analysis, and theoretical modeling of the gas chromatography system," *Microelectromechanical Systems, Journal of,* vol. 3, pp. 147-154, 1994.
[47] N. Hong-seok, P. J. Hesketh, and G. C. Frye-Mason, "Parylene gas chromatographic column for rapid thermal cycling," *Microelectromechanical Systems, Journal of,* vol. 11, pp. 718-725, 2002.
[48] M. Li, E. B. Myers, H. X. Tang, S. J. Aldridge, H. C. McCaig, J. J. Whiting, R. J. Simonson, N. S. Lewis, and M. L. Roukes, "Nanoelectromechanical Resonator Arrays for Ultrafast, Gas-Phase Chromatographic Chemical Analysis," *Nano Letters,* vol. 10, pp. 3899-3903, 2010.
[49] B. Alfeeli, S. Narayanan, M. McMillan, D. Hirtenstein, G. Rice, and M. Agah, "The Effect of Pillar Array in Semi-packed Micro Gas Chromatography," in *IEEE Sensors*, 2011, pp. 1097-1100.
[50] A. Bhushan, D. Yemane, D. Trudell, E. Overton, and J. Goettert, "Fabrication of micro-gas chromatograph columns for fast chromatography," *Microsystem Technologies,* vol. 13, pp. 361-368, 2007.
[51] A. D. Radadia, R. I. Masel, M. A. Shannon, J. P. Jerrell, and K. R. Cadwallader, "Micromachined GC Columns for Fast Separation of Organophosphonate and Organosulfur Compounds," *Analytical Chemistry*, vol. 80, pp. 4087-4094, 2008.
[52] S. Sreedharan Nair, B. Alfeeli, and M. Agah, "Two-Port Static Coated Micro Gas Chromatography Column with an Embedded Thermal Conductivity Detector," *Sensors Journal, IEEE,* vol. 12, pp. 1893-1900, 2012.
[53] R. Manginell, J. Bauer, M. Moorman, L. Sanchez, J. Anderson, J. Whiting, D. Porter, D. Copic, and K. Achyuthan, "A Monolithically-Integrated μGC Chemical Sensor System," *Sensors,* vol. 11, pp. 6517-6532, 2011.
[54] J. A. Potkay, G. R. Lambertus, R. D. Sacks, and K. D. Wise, "A Low-Power Pressure- and Temperature-Programmable Micro Gas Chromatography Column," *Microelectromechanical Systems, Journal of,* vol. 16, pp. 1071-1079, 2007.
[55] B. C. Kaanta, H. Chen, and X. Zhang, "A monolithically fabricated gas chromatography separation column with an integrated high sensitivity thermal conductivity detector," *Journal of Micromechanics and Microengineering,* vol. 20, p. 055016, 2010.
[56] M. Nishino, Y. Takemori, S. Matsuoka, M. Kanai, T. Nishimoto, M. Ueda, and K. Komori, "Development of μGC (micro gas chromatography) with high performance micromachined chip column," *IEEJ Transactions on Electrical and Electronic Engineering,* vol. 4, pp. 358-364, 2009.
[57] K. Reddy, Y. Guo, J. Liu, W. Lee, M. K. Khaing Oo, and X. Fan, "On-chip Fabry–Pérot interferometric sensors for micro-gas chromatography detection," *Sensors and Actuators B: Chemical,* vol. 159, pp. 60-65, 2011.
[58] T. Nakai, S. Nishiyama, M. Shuzo, J.-J. Delaunay, and I. Yamada, "Micro-fabricated semi-packed column for gas chromatography by using functionalized parylene as a stationary phase," *Journal of Micromechanics and Microengineering,* vol. 19, p. 065032, 2009.
[59] G. E. Spangler, "Relationships for modeling the performance of rectangular gas chromatographic columns," *Journal of Microcolumn Separations,* vol. 13, pp. 285-292, 2001.
[60] M. van Deursen, M. van Lieshout, R. Derks, H.-G. Janssen, and C. Cramers, "Theoretical Design Considerations for Multi-capillary Columns in Fast Gas Chromatography," *Journal of High Resolution Chromatography,* vol. 22, pp. 119-122, 1999.
[61] Y. Patrushev, O. Nikolaeva, and V. Sidelnikov, "Multicapillary columns with a porous layer based on the divinylbenzene copolymer," *Russian Journal of Physical Chemistry A, Focus on Chemistry,* vol. 84, pp. 871-875, 2010.
[62] V. Sidelnikov, Y. Patrushev, and O. Nikolaeva, "Express gas chromatography on multicapillary columns and its potential," *Catalysis in Industry,* vol. 2, pp. 206-216, 2010.
[63] B. R. Rosenkranz and J. B. Bettmer, "Rapid separation of elemental species by multicapillary GC," *Analytical and Bioanalytical Chemistry,* vol. 373, pp. 461-465, 2002.
[64] A. de Mello, "On-chip chromatography: the last twenty years," *Lab on a Chip,* vol. 2, pp. 48N-54N, 2002.
[65] A. Bhushan, D. Yemane, E. B. Overton, J. Goettert, and M. C. Murphy, "Fabrication and Preliminary Results for LiGA Fabricated Nickel Micro Gas Chromatograph Columns," *Microelectromechanical Systems, Journal of,* vol. 16, pp. 383-393, 2007.
[66] M. Schlesinger and M. Paunovic, *Modern Electroplating*, Fourth ed. NY: John Wiley & Sons, 2000.

[67] J. J. Kelly, P. E. Bradley, and D. Landolt, "Additive Effects during Pulsed Deposition of Cu-Co Nanostructures," *Journal of The Electrochemical Society*, vol. 147, pp. 2975-2980, 2000.
[68] S. K. Griffiths, R. H. Nilson, A. Ting, R. W. Bradshaw, W. D. Bonivert, and J. M. Hruby, "Modeling electrodeposition for LIGA microdevice fabrication," *Microsystem Technologies*, vol. 4, pp. 98-101, 1998.
[69] S. K. Griffiths, R. H. Nilson, R. W. Bradshaw, A. Ting, W. D. Bonivert, J. T. Hachman, and J. M. Hruby, "Transport limitations in electrodeposition for LIGA microdevice fabrication," in *SPIE*, Santa Clara, CA, USA, 1998, pp. 364-375.
[70] H. Yang, R. Chein, T. Tsai, J. Chang, and J. Wu, "High-aspect-ratio microstructural posts electroforming modeling and fabrication in LIGA process," *Microsystem Technologies*, vol. 12, pp. 187-192, 2006.
[71] T. Fujita, S. Nakamichi, S. Ioku, K. Maenaka, and Y. Takayama, "Seedlayer-less gold electroplating on silicon surface for MEMS applications," *Sensors and Actuators A: Physical*, vol. 135, pp. 50-57, 2007.
[72] A. Ulman, "Formation and Structure of Self-Assembled Monolayers," *Chemical Reviews*, vol. 96, pp. 1533-1554, 1996.
[73] G. M. Gross, J. W. Grate, and R. E. Synovec, "Development and evaluation of gold-centered monolayer protected nanoparticle stationary phases for gas chromatography," *Journal of Chromatography A*, vol. 1060, pp. 225-236, 2004.
[74] T. Sukaew, H. Chang, G. Serrano, and E. T. Zellers, "Multi-stage preconcentrator/focuser module designed to enable trace level determinations of trichloroethylene in indoor air with a microfabricated gas chromatograph," *Analyst*, vol. 136, pp. 1664-1674, 2011.
[75] M. Akbar and M. Agah, "A Microfabricated Propofol Trap for Breath-Based Anesthesia Depth Monitoring," *IEEE Journal of Microelectromechanical Systems*, vol. 22, pp. 443-451, 2013.
[76] T. Wei-Cheng, S. W. Pang, L. Chia-Jung, and E. T. Zellers, "Microfabricated preconcentrator-focuser for a microscale gas chromatograph," *IEEE Journal of Microelectromechanical Systems*, vol. 12, pp. 264-272, 2003.
[77] I. Gràcia, P. Ivanov, F. Blanco, N. Sabaté, X. Vilanova, X. Correig, L. Fonseca, E. Figueras, J. Santander, and C. Cané, "Sub-ppm gas sensor detection via spiral μ-preconcentrator," *Sensors and Actuators B: Chemical*, vol. 132, pp. 149-154, 2008.
[78] M. Akbar, D. Wang, R. Goodman, A. Hoover, G. Rice, J. R. Heflin, and M. Agah, "Improved performance of micro-fabricated preconcentrators using silica nanoparticles as a surface template," *Journal of Chromatography A*, vol. 1322, pp. 1-7, 2013.
[79] G. Serrano, T. Sukaew, and E. T. Zellers, "Hybrid preconcentrator/focuser module for determinations of explosive marker compounds with a micro-scale gas chromatograph," *Journal of Chromatography A*, vol. 1279, pp. 76-85, 2013.
[80] B. Alfeeli, D. Cho, M. Ashraf-Khorassani, L. T. Taylor, and M. Agah, "MEMS-based multi-inlet/outlet preconcentrator coated by inkjet printing of polymer adsorbents," *Sensors and Actuators B: Chemical*, vol. 133, pp. 24-32, 2008.
[81] G. Serrano, S. M. Reidy, and E. T. Zellers, "Assessing the reliability of wall-coated microfabricated gas chromatographic separation columns," *Sensors and Actuators B: Chemical*, vol. 141, pp. 217-226, 2009.
[82] D. Gaddes, J. Westland, F. L. Dorman, and S. Tadigadapa, "Improved micromachined column design and fluidic interconnects for programmed high-temperature gas chromatography separations," *Journal of Chromatography A*, vol. 1349, pp. 96-104, 2014.
[83] H. Hao-Chieh and K. Hanseup, "Miniature circulatory column system for gas chromatography," in *Micro Electro Mechanical Systems (MEMS), 2014 IEEE 27th International Conference on*, 2014, pp. 1007-1010.
[84] A. Bhushan, D. Yemane, E. B. Overton, J. Goettert, and M. C. Murphy, "Fabrication and Preliminary Results for LiGA Fabricated Nickel Micro Gas Chromatograph Columns," *IEEE Journal of Microelectromechanical Systems*, vol. 16, pp. 383-393, 2007.
[85] M. Agah, J. A. Potkay, G. Lambertus, R. Sacks, and K. D. Wise, "High-performance temperature-programmed microfabricated gas chromatography columns," *IEEE Journal of Microelectromechanical Systems*, vol. 14, pp. 1039-1050, 2005.
[86] M. Agah, G. R. Lambertus, R. Sacks, and K. Wise, "High-Speed MEMS-Based Gas Chromatography," *IEEE Journal of Microelectromechanical Systems*, vol. 15, pp. 1371-1378, 2006.
[87] S. Narayanan and M. Agah, "Fabrication and Characterization of a Suspended TCD Integrated With a Gas Separation Column," *Microelectromechanical Systems, Journal of*, vol. 22, pp. 1166-1173, 2013.
[88] F. I. Bohrer, E. Covington, C. a. Kurdak, and E. T. Zellers, "Characterization of Dense Arrays of Chemiresistor Vapor Sensors with Submicrometer Features and Patterned Nanoparticle Interface Layers," *Analytical Chemistry*, vol. 83, pp. 3687-3695, 2011.

[89] S. Zampolli, I. Elmi, J. Stürmann, S. Nicoletti, L. Dori, and G. C. Cardinali, "Selectivity enhancement of metal oxide gas sensors using a micromachined gas chromatographic column," *Sensors and Actuators B: Chemical*, vol. 105, pp. 400-406, 2005.

[90] K. Reddy, L. Jing, M. K. K. Oo, and F. Xudong, "Integrated Separation Columns and Fabry-Perot Sensors for Microgas Chromatography Systems," *IEEE Journal of Microelectromechanical Systems*, vol. 22, pp. 1174-1179, 2013.

[91] S. Zampolli, I. Elmi, F. Mancarella, P. Betti, E. Dalcanale, G. C. Cardinali, and M. Severi, "Real-time monitoring of sub-ppb concentrations of aromatic volatiles with a MEMS-enabled miniaturized gas-chromatograph," *Sensors and Actuators B: Chemical*, vol. 141, pp. 322-328, 2009.

[92] S. K. Kim, H. Chang, and E. T. Zellers, "Microfabricated Gas Chromatograph for the Selective Determination of Trichloroethylene Vapor at Sub-Parts-Per-Billion Concentrations in Complex Mixtures," *Analytical Chemistry*, vol. 83, pp. 7198-7206, 2011/09/15 2011.

[93] Y. Qin and Y. B. Gianchandani, "iGC2: an architecture for micro gas chromatographs utilizing integrated bi-directional pumps and multi-stage preconcentrators," *Journal of Micromechanics and Microengineering*, vol. 24, p. 065011, 2014.

[94] R.-S. Jian, L.-Y. Sung, and C.-J. Lu, "Measuring real-time concentration trends of individual VOC in an elementary school using a sub-ppb detection μGC and a single GC–MS analysis," *Chemosphere*, vol. 99, pp. 261-266, 2014.

[95] J. Liu, J. H. Seo, Y. Li, D. Chen, K. Kurabayashi, and X. Fan, "Smart multi-channel two-dimensional micro-gas chromatography for rapid workplace hazardous volatile organic compounds measurement," *Lab on a Chip*, vol. 13, pp. 818-825, 2013.

[96] M. Akbar, S. Narayanan, M. Restaino, and M. Agah, "A purge and trap integrated microGC platform for chemical identification in aqueous samples," *Analyst*, vol. 139, pp. 3384-3392, 2014.

[97] R. P. Manginell, J. M. Bauer, M. W. Moorman, L. J. Sanchez, J. M. Anderson, J. J. Whiting, D. A. Porter, D. Copic, and K. E. Achyuthan, "A monolithically-integrated μGC chemical sensor system," *Sensors*, vol. 11, pp. 6517-6532, 2011.

[98] C. Chen, F. Tsow, K. D. Campbell, R. Iglesias, E. Forzani, and N. Tao, "A wireless hybrid chemical sensor for detection of environmental volatile organic compounds," *IEEE Sensors Journal*, vol. 13, p. 1748, 2013.

[99] J. Sun, D. Cui, X. Chen, L. Zhang, H. Cai, and H. Li, "Fabrication and characterization of microelectromechanical systems-based gas chromatography column with embedded micro-posts for separation of environmental carcinogens," *Journal of Chromatography A*, vol. 1291, pp. 122-128, 2013.

[100] V. Lindroos, S. Franssila, M. Tilli, M. Paulasto-Krockel, A. Lehto, T. Motooka, and V.-M. Airaksinen, *Handbook of silicon based MEMS materials and technologies*: Elsevier, 2009.

[101] H. Shakeel and M. Agah, "Self-Patterned Gold-Electroplated Multicapillary Gas Separation Columns With MPG Stationary Phases," *IEEE Journal of Microelectromechanical Systems*, vol. 22, pp. 62-70, 2013.

[102] B. Alfeeli, S. Narayanan, D. Moodie, P. Zellner, M. McMillan, D. Hirtenstein, G. Rice, and M. Agah, "Inter-channel Mixing Minimization in Semi-packed Micro Gas Chromatography Columns," *IEEE Sensors Journal*, vol. PP, pp. 1-1, 2013.

[103] M. A. Zareian-Jahromi and M. Agah, "Microfabricated Gas Chromatography Columns With Monolayer-Protected Gold Stationary Phases," *IEEE Journal of Microelectromechanical Systems*, vol. 19, pp. 294-304, 2010.

[104] M. Agah and K. D. Wise, "Low-Mass PECVD Oxynitride Gas Chromatographic Columns," *IEEE Journal of Microelectromechanical Systems*, vol. 16, pp. 853-860, 2007.

[105] H. Shakeel, D. Wang, J. R. Heflin, and M. Agah, "Width-Modulated Microfluidic Columns for Gas Separations," *IEEE Sensors Journal*, vol. 14, pp. 3352-3357, 2014.

[106] R. Haudebourg, Z. Matouk, E. Zoghlami, I. Azzouz, K. Danaie, P. Sassiat, D. Thiebaut, and J. Vial, "Sputtered alumina as a novel stationary phase for micro machined gas chromatography columns," *Analytical and Bioanalytical Chemistry*, vol. 406, pp. 1245-1247, 2014.

[107] J. Sun, D. Cui, F. Guan, X. Chen, and L. Zhang, "High resolution microfabricated gas chromatography column with porous silicon acting as support," *Sensors and Actuators B: Chemical*, vol. 201, pp. 19-24, 2014.

[108] Y. Li, X. Du, Y. Wang, H. Tai, D. Qiu, Q. Lin, and Y. Jiang, "Improvement of column efficiency in MEMS-Based gas chromatography column," *RSC Advances*, vol. 4, pp. 3742-3747, 2014.

[109] D. Wang, H. Shakeel, J. Lovette, G. W. Rice, J. R. Heflin, and M. Agah, "Highly Stable Surface Functionalization of Microgas Chromatography Columns Using Layer-by-Layer Self-Assembly of Silica Nanoparticles," *Analytical Chemistry*, 2013.

[110] M. Akbar, D. Wang, H. Shakeel, J. R. Heflin, and M. Agah, "A MEMS enabled integrated microGC platform for on-site monitoring of water organic compounds," in *IEEE Transducers* Barcelona, Spain, 2013, pp. 2759-2762.

[111] B. Alfeeli, S. Ali, V. Jain, R. Montazami, J. Heflin, and M. Agah, "MEMS-based gas chromatography columns with nano-structured stationary phases," in *Sensors, 2008 IEEE*, 2008, pp. 728-731.

[112] H. M. McNair and J. M. Miller, *Basic gas chromatography*: John Wiley & Sons, 2011.

[113] K. Reddy, Y. Guo, J. Liu, W. Lee, M. K. Khaing Oo, and X. Fan, "Rapid, sensitive, and multiplexed on-chip optical sensors for micro-gas chromatography," *Lab on a Chip*, vol. 12, pp. 901-905, 2012.

[114] R.-S. Jian, R.-X. Huang, and C.-J. Lu, "A micro GC detector array based on chemiresistors employing various surface functionalized monolayer-protected gold nanoparticles," *Talanta*, vol. 88, pp. 160-167, 2012.

[115] H. Shakeel, G. Rice, and M. Agah, "First reconfigurable MEMS separation columns for micro gas chromatography," in *25th IEEE International Conference on Micro Electro Mechanical Systems (MEMS)*, , Paris, France, 2012, pp. 823-826.

[116] S. Narayanan, B. Alfeeli, and M. Agah, "Two-Port Static Coated Micro Gas Chromatography Column With an Embedded Thermal Conductivity Detector," *IEEE Sensors Journal*, vol. 12, pp. 1893-1900, 2012.

[117] G. Serrano, D. Paul, S.-J. Kim, K. Kurabayashi, and E. T. Zellers, "Comprehensive Two-Dimensional Gas Chromatographic Separations with a Microfabricated Thermal Modulator," *Analytical Chemistry*, vol. 84, pp. 6973-6980, 2012.

[118] J. A. Potkay, G. R. Lambertus, R. D. Sacks, and K. D. Wise, "A Low-Power Pressure- and Temperature-Programmable Micro Gas Chromatography Column," *IEEE Journal of Microelectromechanical Systems*, vol. 16, pp. 1071-1079, 2007.

[119] P. R. Lewis, R. P. Manginell, D. R. Adkins, R. J. Kottenstette, D. R. Wheeler, S. S. Sokolowski, D. E. Trudell, J. E. Byrnes, M. Okandan, J. M. Bauer, R. G. Manley, and C. Frye-Mason, "Recent advancements in the gas-phase MicroChemLab," *IEEE Sensors Journal*, vol. 6, pp. 784-795, 2006.

[120] M. A. Zareian-Jahromi, M. Ashraf-Khorassani, L. T. Taylor, and M. Agah, "Design, Modeling, and Fabrication of MEMS-Based Multicapillary Gas Chromatographic Columns," *IEEE Journal of Microelectromechanical Systems*, vol. 18, pp. 28-37, 2009.

[121] M. Mittermuller and D. A. Volmer, "Micro- and nanostructures and their application in gas chromatography," *Analyst*, vol. 137, pp. 3195-3201, 2012.

[122] E. Guihen, "Nanoparticles in modern separation science," *TrAC Trends in Analytical Chemistry*, vol. 46, pp. 1-14, 2013.

[123] L.-M. Yuan, C.-X. Ren, LiLi, P. Ai, Z.-H. Yan, M. Zi, and Z.-Y. Li, "Single-Walled Carbon Nanotubes Used as Stationary Phase in GC," *Analytical Chemistry*, vol. 78, pp. 6384-6390, 2006.

[124] A. V. Herrera-Herrera, M. Á. González-Curbelo, J. Hernández-Borges, and M. Á. Rodríguez-Delgado, "Carbon nanotubes applications in separation science: A review," *Analytica Chimica Acta*, vol. 734, pp. 1-30, 2012.

[125] K. D. Bartle and P. Myers, "History of gas chromatography," *TrAC Trends in Analytical Chemistry*, vol. 21, pp. 547-557, 2002.

[126] G. Decher and J. D. Hong, "Buildup of ultrathin multilayer films by a self-assembly process .1. Consecutive adsorption of anionic and cationic bipolar amphiphiles on charged surfaces," *Makromolekulare Chemie-Macromolecular Symposia*, vol. 46, pp. 321-327, Jun 1991.

[127] G. Decher, J. D. Hong, and J. Schmitt, "Buildup of ultrathin multilayer films by a self-assembly process .3. Consecutively alternating adsorption of anionic and cationic polyelectrolytes on charged surfaces," *Thin Solid Films*, vol. 210, pp. 831-835, Apr 1992.

[128] T. Zeng, R. Claus, F. Zhang, W. Du, and K. L. Cooper, "Ultrathin film actuators fabricated by layer-by-layer molecular self-assembly," *Smart Materials & Structures*, vol. 10, pp. 780-785, Aug 2001.

[129] R. Montazami, S. Liu, Y. Liu, D. Wang, Q. Zhang, and J. R. Heflin, "Thickness dependence of curvature, strain, and response time in ionic electroactive polymer actuators fabricated via layer-by-layer assembly," *Journal of Applied Physics*, vol. 109, p. 104301, 2011.

[130] T. Fukushima, K. Asaka, A. Kosaka, and T. Aida, "Fully plastic actuator through layer-by-layer casting with ionic-liquid-based bucky gel," *Angewandte Chemie-International Edition*, vol. 44, pp. 2410-2413, 2005.

[131] S. Liu, R. Montazami, Y. Liu, V. Jain, M. Lin, X. Zhou, J. R. Heflin, and Q. M. Zhang, "Influence of the conductor network composites on the electromechanical performance of ionic polymer conductor network composite actuators," *Sensors and Actuators A: Physical*, vol. 157, pp. 267-275, 2010.

[132] N. Raoufi, F. Surre, T. Sun, M. Rajarajan, and K. T. V. Grattan, "Wavelength dependent pH optical sensor using the layer-by-layer technique," *Sensors and Actuators B: Chemical*, vol. 169, pp. 374-381, Jul 2012.

[133] J. H. Kim, S. H. Kim, and S. Shiratori, "Fabrication of nanoporous and hetero structure thin film via a layer-by-layer self assembly method for a gas sensor," *Sensors and Actuators B: Chemical*, vol. 102, pp. 241-247, Sep 2004.

[134] B. Z. Wang, X. Y. Du, M. Q. Wang, W. L. Gong, and J. Anzai, "A facile preparation of H2O2 sensors using layer-by-layer deposited thin films composed of poly(ethyleneimine) and carboxymethyl cellulose as matrices for immobilizing hemin," *Electroanalysis*, vol. 20, pp. 1028-1031, May 2008.

[135] G. A. Evtugyn and T. Hianik, "Layer-by-Layer Polyelectrolyte Assembles Involving DNA as a Platform for DNA Sensors," *Current Analytical Chemistry*, vol. 7, pp. 8-34, Jan 2011.

[136] P. Sun, Y. D. Jiang, G. Z. Xie, X. S. Du, X. Li, and J. Hu, "Layer-by-layer assembly carbon nanotubes thin film based gas sensors for ammonia detection," *Science China-Information Sciences*, vol. 54, pp. 2680-2686, Dec 2011.

[137] L. L. Cui, T. Pu, Y. Liu, and X. Q. He, "Layer-by-layer construction of graphene/cobalt phthalocyanine composite film on activated GCE for application as a nitrite sensor," *Electrochimica Acta*, vol. 88, pp. 559-564, Jan 2013.

[138] I. Del Villar, I. R. Matias, F. J. Arregui, and P. Lalanne, "Optimization of sensitivity in long period fiber gratings with overlay deposition," *Optics Express*, vol. 13, pp. 56-69, Jan 10 2005.

[139] Z. Wang, J. R. Heflin, K. Van Cott, R. H. Stolen, S. Ramachandran, and S. Ghalmi, "Biosensors employing ionic self-assembled multilayers adsorbed on long-period fiber gratings," *Sensors and Actuators B: Chemical*, vol. 139, pp. 618-623, Jun 4 2009.

[140] A. Marletta, F. A. Castro, C. A. M. Borges, O. N. Oliveira, R. M. Faria, and F. E. G. Guimaraes, "Enhanced optical properties of layer-by-layer films of poly(p-phenylenevinylene) alternated with a long chain counterion and converted at low temperatures," *Macromolecules*, vol. 35, pp. 9105-9109, Nov 2002.

[141] H. H. Yu, D. S. Jiang, X. F. Li, D. S. Yu, and L. D. Zhou, "Reflection-enhancing coatings from layer-by-layer self-assembled polyelectrolyte/colloidal TiO2 multilayers," in *Advanced Materials and Devices for Sensing and Imaging II*. vol. 5633, A. Wang, Y. Zhang, and Y. Ishii, Eds., ed, 2005, pp. 470-473.

[142] S. Wang, L. Zhao, X. Zhang, Z. Shi, Z. Cui, and Y. Yang, "Electric-field-induced layer-by-layer fabrication of inorganic-organic hybrid second-order nonlinear optical films," *Journal of Colloid and Interface Science*, vol. 336, pp. 470-476, Aug 15 2009.

[143] J. R. Heflin, M. T. Guzy, P. J. Neyman, K. J. Gaskins, C. Brands, Z. Wang, H. W. Gibson, R. M. Davis, and K. E. Van Cott, "Efficient, Thermally Stable, Second Order Nonlinear Optical Response in Organic Hybrid Covalent/Ionic Self-Assembled Films," *Langmuir*, vol. 22, pp. 5723-5727, 2006.

[144] R. Montazami, V. Jain, and J. R. Heflin, "High contrast asymmetric solid state electrochromic devices based on layer-by-layer deposition of polyaniline and poly(aniline sulfonic acid)," *Electrochimica Acta*, vol. 56, pp. 990-994, Dec 2010.

[145] V. Jain, R. Sahoo, S. P. Mishra, J. Sinha, R. Montazami, H. M. Yochum, J. R. Heflin, and A. Kumar, "Synthesis and Characterization of Regioregular Water-Soluble 3,4-Propylenedioxythiophene Derivative and Its Application in the Fabrication of High-Contrast Solid-State Electrochromic Devices," *Macromolecules*, vol. 42, pp. 135-140, 2008.

[146] K. Shinbo, K. Kato, F. Kaneko, K. Onishi, R. C. Advincula, and X. W. Fan, "Fabrication and electrochromic properties of layer-by-layer self-assembled ultrathin films containing water-soluble phthalocyanine," *Molecular Crystals and Liquid Crystals*, vol. 407, pp. 493-500, 2003.

[147] V. Jain, M. Khiterer, R. Montazami, H. M. Yochum, K. J. Shea, and J. R. Heflin, "High-Contrast Solid-State Electrochromic Devices of Viologen-Bridged Polysilsesquioxane Nanoparticles Fabricated by Layer-by-Layer Assembly," *ACS Applied Materials & Interfaces*, vol. 1, pp. 83-89, Jan 2009.

[148] D. J. Schmidt, E. M. Pridgen, P. T. Hammond, and J. C. Love, "Layer-by-Layer Assembly of a pH-Responsive and Electrochromic Thin Film," *Journal of Chemical Education*, vol. 87, pp. 208-211, Feb 2010.

[149] C. H. B. Silva, N. A. Galiote, F. Huguenin, E. Teixeira-Neto, V. R. L. Constantino, and M. L. A. Temperini, "Spectroscopic, morphological and electrochromic characterization of layer-by-layer hybrid films of polyaniline and hexaniobate nanoscrolls," *Journal of Materials Chemistry*, vol. 22, pp. 14052-14060, 2012.

[150] D. M. DeLongchamp and P. T. Hammond, "Multiple-color electrochromism from layer-by-layer-assembled polyaniline/Prussian Blue nanocomposite thin films," *Chemistry of Materials*, vol. 16, pp. 4799-4805, Nov 16 2004.

[151] A. D. Taylor, M. Michel, R. C. Sekol, J. M. Kizuka, N. A. Kotov, and L. T. Thompson, "Fuel Cell Membrane Electrode Assemblies Fabricated by Layer-by-Layer Electrostatic Self-Assembly Techniques," *Advanced Functional Materials*, vol. 18, pp. 3003-3009, 2008.

[152] X. Li, F. Gittleson, M. Carmo, R. C. Sekol, and A. D. Taylor, "Scalable Fabrication of Multifunctional Freestanding Carbon Nanotube/Polymer Composite Thin Films for Energy Conversion," *ACS Nano*, vol. 6, pp. 1347-1356, 2012.

[153] B.-S. Kong, J. Geng, and H.-T. Jung, "Layer-by-layer assembly of graphene and gold nanoparticles by vacuum filtration and spontaneous reduction of gold ions," *Chemical Communications (Cambridge, United Kingdom)*, vol. 0, pp. 2174-2176, 2009.

[154] F. Wang, S. Peters, J. Guzda, R. H. Blunk, and A. P. Angelopoulos, "Silica Nanoparticle Layer-by-Layer Assembly on Gold," *Langmuir*, vol. 25, pp. 4384-4392, 2009.

[155] Y. Lvov, K. Ariga, M. Onda, I. Ichinose, and T. Kunitake, "Alternate Assembly of Ordered Multilayers of SiO2 and Other Nanoparticles and Polyions," *Langmuir*, vol. 13, pp. 6195-6203, 1997.

[156] J. Y. Kim, J. P. DeRocher, P. Mao, J. Han, R. E. Cohen, and M. F. Rubner, "Formation of Nanoparticle-Containing Multilayers in Nanochannels via Layer-by-Layer Assembly," *Chemistry of Materials*, vol. 22, pp. 6409-6415, 2010.

[157] J. P. DeRocher, P. Mao, J. Han, M. F. Rubner, and R. E. Cohen, "Layer-by-Layer Assembly of Polyelectrolytes in Nanofluidic Devices," *Macromolecules*, vol. 43, pp. 2430-2437, 2010.

[158] B. Rosenkranz and J. Bettmer, "Rapid separation of elemental species by multicapillary GC," *Analytical and Bioanalytical Chemistry*, vol. 373, pp. 461-465, 2002.

[159] S. E. Yancey, W. Zhong, J. R. Heflin, and A. L. Ritter, "The influence of void space on antireflection coatings of silica nanoparticle self-assembled films," *Journal of Applied Physics*, vol. 99, p. 034313, 2006.

[160] F. Ç. Cebeci, Z. Wu, L. Zhai, R. E. Cohen, and M. F. Rubner, "Nanoporosity-Driven Superhydrophilicity: A Means to Create Multifunctional Antifogging Coatings," *Langmuir*, vol. 22, pp. 2856-2862, 2006.

[161] R. Haudebourg, J. Vial, D. Thiebaut, K. Danaie, J. Breviere, P. Sassiat, I. Azzouz, and B. Bourlon, "Temperature-Programmed Sputtered Micromachined Gas Chromatography Columns: An Approach to Fast Separations in Oilfield Applications," *Analytical Chemistry*, vol. 85, pp. 114-120, 2013.

[162] S. Narayanan, B. Alfeeli, and M. Agah, "Two-Port Static Coated Micro Gas Chromatography Column With an Embedded Thermal Conductivity Detector," *Sensors Journal, IEEE*, vol. 12, pp. 1893-1900, 2012.

[163] S. Narayanan, G. Rice, and M. Agah, "A micro-discharge photoionization detector for micro-gas chromatography," *Microchimica Acta*, pp. 1-7, 2013.

[164] L. K. Wright and E. T. Zellers, "A nanoparticle-coated chemiresistor array as a microscale gas chromatograph detector for explosive marker compounds: flow rate and temperature effects," *Analyst*, vol. 138, pp. 6860-6868, 2013.

[165] M. Akbar, S. Narayanan, M. Restaino, and M. Agah, "Purge and trap integrated microGC platform for chemical identification in aqueous samples," *Analyst*, vol. DOI: 10.1039/c4an00254g, 2014.

[166] M. Akbar and M. Agah, "A Microfabricated Propofol Trap for Breath-Based Anesthesia Depth Monitoring," *Microelectromechanical Systems, Journal of*, vol. 22, pp. 443-451, 2013.

[167] C.-J. Lu, W. H. Steinecker, W.-C. Tian, M. C. Oborny, J. M. Nichols, M. Agah, J. A. Potkay, H. K. Chan, J. Driscoll, and R. D. Sacks, "First-generation hybrid MEMS gas chromatograph," *Lab on a Chip*, vol. 5, pp. 1123-1131, 2005.

[168] H. Shakeel and M. Agah, "Self-Patterned Gold-Electroplated Multicapillary Gas Separation Columns With MPG Stationary Phases," *Journal of Microelectromechanical Systems*, vol. 22, pp. 62-70, 2013.

[169] B. Alfeeli, S. Narayanan, D. Moodie, P. Zellner, M. McMillan, D. Hirtenstein, G. Rice, and M. Agah, "Interchannel Mixing Minimization in Semi-Packed Micro Gas Chromatography Columns," *IEEE Sensors Journal*, vol. 13, pp. 4312-4319, 2013.

[170] H. Purnell, *"Gas Chromatography"*. New York: John Wiley and Sons, 1962.

[171] D. C. Locke and C. E. Meloan, "Gradient Loaded Columns in Gas Chromatography," *Analytical Chemistry*, vol. 36, pp. 2234-2243, 1964.

[172] E. H. M. Camara, P. Breuil, D. Briand, N. F. de Rooij, and C. Pijolat, "A micro gas preconcentrator with improved performance for pollution monitoring and explosives detection," *Analytica Chimica Acta*, vol. 688, pp. 175-182, 2011.

[173] S. I. Shopova, I. M. White, Y. Sun, H. Zhu, X. Fan, G. Frye-Mason, A. Thompson, and S.-j. Ja, "On-Column Micro Gas Chromatography Detection with Capillary-Based Optical Ring Resonators," *Analytical Chemistry*, vol. 80, pp. 2232-2238, 2008.

[174] T. Wei-Cheng, H. K. L. Chan, L. Chia-Jung, S. W. Pang, and E. T. Zellers, "Multiple-stage microfabricated preconcentrator-focuser for micro gas chromatography system," *Journal of Microelectromechanical Systems*, vol. 14, pp. 498-507, 2005.

[175] H. Shakeel and M. Agah, "Semipacked separation columns with monolayer protected gold stationary phases for microgas chromatography," in *Sensors, 2012 IEEE*, 2012, pp. 2007-2010.
[176] S. N. Muhammad Akbar, Michael Restaino and Masoud Agah "Purge and trap integrated microGC platform for chemical identification in aqueous samples," *Analyst,* vol. 19, pp. 3384 - 3392, 2014.
[177] I. Azzouz, J. Vial, D. Thiébaut, R. Haudebourg, K. Danaie, P. Sassiat, and J. Breviere, "Review of stationary phases for microelectromechanical systems in gas chromatography: feasibility and separations," *Analytical and Bioanalytical Chemistry,* vol. 406, pp. 981-994, 2014.
[178] S. M. George, "Atomic Layer Deposition: An Overview," *Chemical Reviews (Washington, DC, United States),* vol. 110, pp. 111-131, 2009.
[179] R. L. Puurunen, "Surface chemistry of atomic layer deposition: A case study for the trimethylaluminum/water process," *Journal of Applied Physics,* vol. 97, pp. -, 2005.
[180] S. R. Jim, A. Foroughi-Abari, K. M. Krause, P. Li, M. Kupsta, M. T. Taschuk, K. C. Cadien, and M. J. Brett, "Ultrathin-layer chromatography nanostructures modified by atomic layer deposition," *Journal of Chromatography A,* vol. 1299, pp. 118-125, 2013.
[181] T. Nakai, S. Nishiyama, M. Shuzo, J. Delaunay, and I. Yamada, "Micro-fabricated semi-packed column for gas chromatography by using functionalized parylene as a stationary phase," *Journal of Micromechanics and Microengineering,* vol. 19, p. 065032, 2009.
[182] S. A. Ali, "Semi-packed micro gas chromatography columns," Virginia Polytechnic Institute and State University, 2008.
[183] J. W. Elam, *In Atomic Layer Deposition of Nanostructured Materials,Pinna, N.; Knez, M.; Eds,Wiley VCH, 2012,p227-249*.
[184] N. M. Dawson, "Atomic Layer Deposition Of Aluminum Oxide," University of California, 2010.
[185] P. Poodt, A. Lankhorst, F. Roozeboom, K. Spee, D. Maas, and A. Vermeer, "High-Speed Spatial Atomic-Layer Deposition of Aluminum Oxide Layers for Solar Cell Passivation," *Advanced Materials (Weinheim, Germany),* vol. 22, pp. 3564-3567, 2010.
[186] E. B. M. A. Mohd, *Advanced Gas Chromatography - Progress in Agricultural, Biomedical and Industrial Applications, Intech, 2012 pp-34*.
[187] R. R. Reston and E. S. Kolesar, "Silicon-micromachined gas chromatography system used to separate and detect ammonia and nitrogen dioxide. Design, fabrication, and integration of the gas chromatography system," *Journal of Microelectromechanical Systems,* vol. 3, pp. 134-146, 1994.
[188] C. M. Matzke, R. J. Kottenstette, S. A. Casalnuovo, G. C. Frye-Mason, M. L. Hudson, D. Y. Sasaki, R. P. Manginell, and C. C. Wong, "Microfabricated silicon gas chromatographic microchannels: fabrication and performance," 1998, pp. 262-268.
[189] M. Agah, J. A. Potkay, G. Lambertus, R. Sacks, and K. D. Wise, "High-performance temperature-programmed microfabricated gas chromatography columns," *Journal of Microelectromechanical Systems,* vol. 14, pp. 1039-1050, 2005.
[190] A. Bhushan, D. Yemane, E. B. Overton, J. Goettert, and M. C. Murphy, "Fabrication and Preliminary Results for LiGA Fabricated Nickel Micro Gas Chromatograph Columns," *Journal of Microelectromechanical Systems,* vol. 16, pp. 383-393, 2007.
[191] M. Agah and K. D. Wise, "Low-Mass PECVD Oxynitride Gas Chromatographic Columns," *Journal of Microelectromechanical Systems,* vol. 16, pp. 853-860, 2007.
[192] M. A. Zareian-Jahromi, M. Ashraf-Khorassani, L. T. Taylor, and M. Agah, "Design, Modeling, and Fabrication of MEMS-Based Multicapillary Gas Chromatographic Columns," *Journal of Microelectromechanical Systems,* vol. 18, pp. 28-37, 2009.
[193] H. Shakeel, G. Rice, and M. Agah, "Semipacked columns with atomic layer deposited alumina as a stationary phase " *Sensors and Actuators B: Chemical,* vol. 203, pp. 641-646, 2014.
[194] M. Akbar, H. Shakeel, and M. Agah, "GC-on-chip: integrated column and photoionization detector," *Lab on a Chip, DOI: 10.1039/c4lc01461h,* 2015.

Appendix I: List of publications

Book Chapter

Hamza Shakeel and Masoud Agah "Chip Based GC", in Volume 3 Gas Chromatography, Sub- and Supercritical Chromatography, Wiley VCH, Editors: Jared l. Anderson, Verónica Pino (in press).

Journal Publications

1. **H.Shakeel**, G.W Rice and M. Agah, "Semipacked columns with atomic layer deposited alumina as a stationary phase", Sensors and Actuators B: Chemical, vol. 203, November 2014, pp 641-646.
2. **H.Shakeel**, D. Wang, J. R. Heflin and M. Agah "Width-modulated microfluidic columns for gas separations", IEEE Sensors Journal, Vol. 14 issue 10, October 2014, pp 3352 - 3357.
3. D.Wang*, **H.Shakeel***, J. Lovette G.W Rice, J.R Heflin and M. Agah "Highly stable surface functionalization of microgas chromatography columns using layer-by-layer self-assembly of silica nanoparticles", ACS, Analytical Chemistry, vol. 85, September 2013, pp. 8135-8141 (*equal contribution).
4. **H.Shakeel** and M. Agah "Self-patterned gold electroplated multicapillary gas separation columns with MPG stationary phases", IEEE Journal Of Microelectromechanical Systems, vol. 22, no. 1, February 2013, pp. 62-70.

Conference Proceedings

1. M. Akbar, **H. Shakeel**, and M. Agah, "An Integrated Chromatography Chip for Rapid Gas Separation and Detection", IEEE MEMS 2015, January 2015, Estoril, Portugal, (poster presentation).
2. **H.Shakeel**, D. Wang, J. R. Heflin and M. Agah, "Width-modulated microgas chromatography separation columns with silica nanoparticles stationary phase" IEEE Sensors 2013, November 2013, Baltimore, USA, pp. 8-11.
3. M. Akbar, D. Wang, **H. Shakeel**, J.R Heflin and M. Agah "A MEMS enabled integrated microgc platform for on-site monitoring of water organic compounds", IEEE Transducer, June 2013, Barcelona, Spain, pp. 2759-2762.
4. **H. Shakeel**, and M, Agah, "Semipacked separation columns with monolayer protected gold stationary phases for microgas chromatography," IEEE Sensors 2012, October 2012, Taipei, Taiwan, pp. 2007-2010.
5. D. Wang*, **H. Shakeel***, R. Montazami, G. Rice, R. Heflin and M. Agah, "Highly stable surface functionalization of high-aspect-ratio microgas chromatography columns using layer-by-layer self-

assembly of SiO2¬ nanoparticles", Solid-State Sensors, Actuators, and Microsystems Workshop (Hilton Head '12), June 2012, Hilton Head Island, SC, pp. 201-204.

6. **H. Shakeel**, G. Rice and M. Agah, "First reconfigurable MEMS separation columns for micro gas chromatography", IEEE MEMS 2012, January 2012, Paris, France, pp. 823-826.

7. **H. Shakeel**, and M. Agah, "High-performance multicapillary gas separation columns with mpg stationary phases," IEEE Sensors, October 2011, Limerick, Ireland, pp. 1909-1912.

Appendix II: Attribution

This research work has been a collaborative effort between our group headed by Dr Masoud Agah (Associate Professor, Electrical Engineering Department, Virginia Tech) and research groups lead by Dr Randy Heflin (Professor, Department of Physics, Virginia Tech) and Dr Gary Rice (Associate Professor and Dean, Department of Chemistry, College of William and Marry). All of these chapters have been written by the author of this dissertation (Hamza Shakeel), while all three professors have provided valuable technical feedback and editorial comments during manuscript submission. Dr Masoud Agah has served as a principal investigator through the course of this project. A brief description about the contribution of different students/professors from these groups is worth to mention and listed below.

Chapter 3: Improved Self-Assembled Thiol Stationary Phases in Microfluidic Gas Separation Columns

Dr Dong Wang (currently a post-doc at Electrical Engineering department, Virginia Tech) from Dr Randy Heflin's group coated gold-nanoparticle inside semi-packed columns.

Chapter 4: Highly Stable Surface Functionalization of Microgas Chromatography Columns Using Layer-by-Layer Self-Assembly of Silica Nanoparticles

Dr Dong Wang (Dr Heflin's group) developed and optimized the LbL process for coating SNPs inside microcolumns. Students from Dr Rice's group generated chromatographic results, specifically Figure 4.6 and part of Figure 4.8.

Chapter 5: Width-modulated Microfluidic Columns for Gas Separations

Dr Dong Wang from Dr Randy Heflin's group coated these columns with SNPs coating.

Chapter 6: Semipacked Columns with Atomic Layer Deposited Alumina as a Stationary Phase

Dr Gary Rice helped shape technical discussion for the journal article and also provided valuable editorial comments.